ENGINEERED NANOPARTICLES AS CONTRAST AGENTS: UPTAKE AND CLEARANCE STUDIES

By

DEBAMITRA DUTTA

A DISSERTATION PRESENTED TO THE GRADUATE SCHOOL
OF THE UNIVERSITY OF FLORIDA IN PARTIAL FULFILLMENT
OF THE REQUIREMENTS FOR THE DEGREE OF
DOCTOR OF PHILOSOPHY

UNIVERSITY OF FLORIDA

2009

To my loving husband, my best friend and guarding angel, and my affectionate parents and siblings. Without their encouragement and support,
I would have never been able to pursue my dreams.

ACKNOWLEDGMENTS

There were so many people who have been with me on this long journey towards my doctoral degree that it actually makes me nostalgic while writing this section as I retrace my footsteps back to the early days of Graduate School. Firstly, I would like to express my sincere gratitude to my advisor and mentor Dr Brij Moudgil, who gave me the opportunity to work in some great research environments, at PERC, UF and at PNNL, WA to deal with some of the most challenging scientific problems of our times. Apart from my PhD research work, I have had the opportunity to participate in industrial advisory board meetings, conferences and leadership councils that have shaped me as a consummate research professional. I am grateful to Dr. Swadeshmukul Santra for mentoring me during the early days in PERC and initiating me into the field of bioimaging. His mentorship essentially set the tone for my PhD research and his inputs have been invaluable to my dissertation. I have also had an opportunity to publish a number of journal papers and two book chapters due to his constant encouragement. I am also greatly thankful to Dr. Justin Teeguarden for his invaluable mentorship during the second phase of my PhD research work at PNNL. I benefited immensely from these research interactions and thank him for his inputs in my work. It helped the transition to particokinetic studies of this research work much easier, which would have been difficult, if not impossible without his mentorship.

I would like to sincerely thank the members of my PhD Committee, Drs. Hassan El-Shall, Christopher Batich, Henry Hess and Steve Roberts for their valuable inputs during the various stages of my research work. It is a matter of great pride for me to have such accomplished researchers and experts evaluate my candidature for the PhD degree. At every point along this program, they were far less just committee members, and much more my valued mentors who helped to show me directions to get things done in a more effective manner.

I gratefully acknowledge all nanotoxicology team members at UF, especially Drs Scott Brown, David Barber, Nancy Denslow, David Moraga, Scott Wasdo, Kevin Powers, and Maria Palazuelos who helped lay the foundation for this interdisciplinary research work. Further, I also acknowledge the members of EBI at PNNL, Drs. Joel Pounds, S.K. Sundaram, Tom Weber and Brian Riley, for their invaluable help for my research at Richland. My heartfelt appreciation is extended to all past & present Moudgil and El-Shall group members who have helped me during this research work: Drs. Madhavan Esayanur, Ayman El-Midany, Suresh Yeruva, Georgios Pyrgiotakis, Parvesh Sharma, Vijay Krishna, Marie Kissinger, Kyoung-Ho Bu, Stephen Tedeschi and Rhye Hamey. Special thanks to Amit Singh, Ajoy Saha and Paul Carpinone for their help. Special appreciations for all PERC and PNNL staff members without whose invaluable help, it would be very difficult to complete this work in time: Gary Scheiffele, Gill Brubaker, Greg Norton, Jo-Anne Standridge, Donna Jackson, Sophie Leone, Jamie Anders and James Newman at UF and Vichaya Sukwarotwat, Jeff Creim, Jolen Soelberg, Teresa Luders, Terry Curry, Angela Woodstock, Andrea Busby and Barbara Goodwin at PNNL. I am also grateful to National Science Foundation (NSF) Grant (EEC-94-02989), NIRT (EEC-0506560), Particle Engineering Research Center (PERC) and its industrial collaborators for financial support.

I acknowledge my friends in Gainesville and Richland. It would not have been possible for me to come to Gainesville for the short trips from Richland without Sanchii, Bhuvan, Nima, Shruti and their hospitality. I also acknowledge my extended family, TCPC members and all other close friends who helped me to remain motivated. Finally, as I do not believe in acknowledging my very own, that’s why this dissertation is dedicated to the people who walked with me every step of this long and difficult journey, my husband, parents and siblings. We made it together so far and there’s so much more to travel to pursue all my dreams.

TABLE OF CONTENTS

page

LIST OF TABLES

LIST OF FIGURES

Abstract of Dissertation Presented to the Graduate School
of the University of Florida in Partial Fulfillment of the
Requirements for the Degree of Doctor of Philosophy

ENGINEERED NANOPARTICLES AS CONTRAST AGENTS: UPTAKE AND CLEARANCE STUDIES

By

DEBAMITRA DUTTA

May 2009

Chair: Brij Moudgil
Major: Materials Science and Engineering

Nanoparticle (NP) based probes have shown tremendous potential as contrast agents. However, an added therapeutic modality on NPs can help in cancer detection and therapy. The objective of this work is to develop engineered NPs as contrast agents and conduct their uptake and clearance studies. Effect of physicochemical parameters (size, composition and surface charge) of NPs in A549 cells and rat blood was studied. 100 and 190 nm fluorescent silica nanoparticles (FSNPs), 15 nm silica coated quantum dots (QDS) and gold speckled silica coated quantum dots (QDSG) and 15 nm gold NPs were synthesized using microemulsion and sol gel techniques. NPs were characterized for size, shape, surface charge, absorbance and fluorescence. Effect of two different FSNP-surface functionalizations: folate conjugation and amine modification was studied using A549 cells. Confocal microscopy and uptake studies showed folated NPs were uptaken more aggressively than aminated FSNPs and cell viability was quantified using lactate dehydrogenase assay after FSNP uptake.

Fluorescence from QD core and hyperthermic property of gold speckles on QDSG was utilized to image and kill cancer (A549) cells. Synthesis protocol was established for QDSG NPs with optimal fluorescence and absorbance properties. Excess gold speckles could quench the QD-core fluorescence. Increased silica shell thickness between QD-core and gold speckles

prevented quenching. Bioimaging capability of QDSG was demonstrated in A549 cells and daphnia.

Gold NPs with three different surface charges: bare gold G- (negative), amine-modified gold G+, (positive) and pegylated-gold GP (neutral) NPs, QDS and QDSG were used for rat clearance studies. Blood samples collected at selected time points were analyzed for gold and cadmium using Inductively Coupled Plasma Mass Spectroscopy. A one-compartmental model was generated to calculate half-life of NPs in rat blood. Half-life of QDS, QDSG and GP NPs were determined to be 12.5±9.7, 14±6.5 and 640±15.5 minutes, respectively. G+ and G- NPs were cleared rapidly (<5 minutes), QDSG and QDS NPs were cleared fast while PEG groups on GP led to delayed clearance and large half-life. Preliminary one-dimensional gel electrophoresis qualitatively showed that amount of adsorbed proteins on NPs were G+ and G- > QDS and QDSG > GP and correlated directly with blood clearance behavior.

CHAPTER 1
INTRODUCTION AND SCIENTIFIC BACKGROUND

The field of nanotechnology has attracted a lot of attention over the last decade (De *et al.* 2008, Eijkel & van den Berg 2006, Grodzinski *et al.* 2006, Hiremath & Hota 1999, Juang & Bogy 2005, Nayak & Lyon 2005, Safarik & Safarikova 2002, Salata 2005) and can be easily recognized as one of the most critical research endeavors of the early 21st century. It deals with research and technology development at an atomic, molecular and macromolecular scale by controlled manipulations. The prefix 'nano' is derived from the Greek word for dwarf as a nanometer (nm) is one thousand millionth of a meter (10^{-9} m). Literally, 'nanotechnology' refers to a field of applied science and technology that deals with structures, devices and systems with length scales ranging between 1 and 100 nm and possess novel properties characteristic of its dimensions. Firstly, nanomaterials with the same mass have a relatively larger surface area as compared to its larger counterparts. This generally leads to an increased chemical activity due to the high surface energy. Secondly, the quantum size effects begin to dominate the material properties as the size is reduced to nanoscale dimensions, thus resulting in enhanced physical, chemical and biological properties. Therefore it is not surprising that research on nanotechnology has made a profound impact (Romig 2004) in various areas such as materials and manufacturing, energy, electronics, medicine and healthcare, biotechnology, information technology and national security (Cohen 2001, Eijkel & van den Berg 2006, Grodzinski *et al.* 2006, Juang & Bogy 2005, Nayak & Lyon 2005, Salata 2005, Silva 2004). By some estimates (Nel *et al.* 2006), nanotechnology is expected to far exceed the impact of the Industrial Revolution and projected to become a $1 trillion market by 2015 AD.

1.1 Historical Perspective

Contrary to popular belief, the first mention towards the concept of nanotechnology occurred in 1867 by James Clerk Maxwell, who proposed the concept of a tiny entity known as "Maxwell's Demon" that can deal with individual molecules (Ivanitsky *et al*. 1998). Initial experiments of nanoparticle observations and size measurement were reported in the first decade of the 20th century – mostly from Richard Adolf Zsigmondy's study of 10 nm gold sols and other nanosized materials (Zsigmondy 1916). Subsequently, in the 1920's Irving Langmuir and Katherine B.Blodgett's introduced the concept of 'monolayer' or one molecule-thick layer of material (Blodgett & Langmuir 1932, Blodgett *et al.* 1932, Langmuir & Blodgett 1935). First surface force measurements by Derjaguin occurred in the early 1950s (Derjaguin *et al.* 1992), followed by a number of other research breakthroughs that served as the scientific basis to lay down the foundation for modern nanotechnology .

Late physicist and Nobel laureate Richard P. Feynman's classic lecture titled "there's plenty of room at the bottom" on December 29th 1959 at the annual meeting of the American Physical Society is considered an important landmark in the history of nanotechnology. It dealt with the future possibility and potential problems of manipulating and controlling things at the atomic scale (Feynman 1959). He visualized nanotechnology as the means to mimic nature and build nanosized objects, atom by atom and molecule by molecule. He envisioned the possibility of using various sets of building tools as operating sets to manipulate the individual atoms and molecules up or down, tailoring it to specific applications.

The term 'nanotechnology' was actually coined in 1974, by the Japanese researcher Norio Taniguchi (Taniguchi 1974) to mean "precision machining with tolerances of a micrometer or less". Twelve years later in 1986, Eric Drexler's book on 'Engines of Creation' and subsequent controversial study on 'Nanosystems' (discussion on the possibility of nanotechnology to

successfully replicate assemblers and lead to an exponential growth of productivity and personal wealth) is credited for creating public consciousness on nanotechnology (Drexler 1987).

In recognition to the reality of Feynman's vision in 1998, the National Science and Technology Council (NSTC) of White House created an interagency working group on nanoscience, engineering and technology. In January 2000, President Clinton in his State of the Union address, announced the $ 497 million federal National Nanotechnology Initiative for the fiscal year 2001 budget. This initiative to form a broad-based coalition between academic institutions, private sectors, and local state and federal government actually laid the foundation towards establishing Feynman's nanotech dream. Since then, there have been innumerable related inventions and discoveries that is a testament to Feynman's extraordinary vision on the future of nanotechnology (Bhushan 2007).

Today, it is envisioned that there shall be four generations of nanotechnology advancements. Currently, we have the first phase of passive nanostructural material developments to perform a single task, which shall be followed by the second phase of introducing active nanostructures for multi-tasking. The third generation is expected to feature novel interactive nanosystems followed by the development of the first integrated nanosystem functioning much like a biological cell with hierarchical nature (Nel *et al.* 2006).

The use of materials with nanometric dimensions is not new. Commonly encountered in nature, some of the life-dependent biological molecules include proteins, enzymes and DNA. Silver and gold nanoparticles (NPs) have been used to color ceramic glazes and stained glass since the 10th century AD (Eichelbaum *et al.* 2007). Nanomaterials can be classified into three groups: natural, anthropogenic and engineered. The natural sources of NPs include forest fires and volcanic eruptions. Other biological moieties like viruses, magnetite (found in cells and

animals) and ferritin (protein storing excess iron in the body) is also a part of this group. The anthropogenic NPs are by-products of industrial activities like polishing, simple combustion processes and internal combustion engines, power plants and welding fumes that release NPs into the environment. Even a simple process of food preparation like frying and grilling can be a source of NPs. The last group of artificially generated or 'engineered' nanomaterials refers to intentionally designed structures that exploit the technologically favorable properties that result as a consequence of particle size reduction. (Köhler & Fritzsche 2007).

1.2 Engineered Nanomaterials

Over the years, biological molecules occurring inside organisms and forming the basic units of life, served as a model for the development of 'engineered nanomaterials'. Generally engineered nanomaterials are designed with specific physical and chemical properties to meet the requirements of a particular application (Decker 2006). They have some remarkable differences from their naturally occurring counterparts that are generally polydispersed in nature and possess chemically complex behavior. For example, nanosized natural products of combustion processes may exhibit inconsistent composition, particle size and shape, and solubility characteristics. In contrast, the engineered structures are monodispersed and precisely regulated to have novel properties observable only at nanoscale dimensions. Today, engineered nanomaterials have presented numerous new opportunities for completely new applications in the healthcare and automobile industries as well as shown a lot of potential to increase the performance of traditional products like cosmetics and food products. It is expected that there will be an exponential growth in the use of engineered submicroscopic scale materials over the next decade. However, with the ever-increasing scope of nanoparticle (NP) applications over the last decade, the risk of exposure for human beings and the environment has become higher (Oberdorster *et al.* 1996, Oberdorster *et al.* 2005c). In contrast to the many efforts at exploiting the desirable

properties of NPs to improve human health, till very lately, there existed few systematic investigations into the specific properties of NPs that cause toxicity in living systems. This remains a challenge (Hett 2004, Nel *et al.* 2006) for the future growth of scope of nanotechnology, especially for its biological applications.

1.3 Nanobiotechnology

As the integration of nanotechnology into the physical and biological sciences continues to flourish, it is becoming increasingly evident that nanotechnology as applied to medicine, will lead to significant advances in the diagnosis and treatment of various diseases (Holm *et al.* 2002). The ultimate aim of medicine is to improve the quality of existence and it is anticipated that the use of engineered nanostructures and devices will help to monitor, control, construct, repair, defend and actually enhance human life. The use of particulates for nanomedicine will lead to a better understanding of the intricate mechanisms associated with various diseases. Certain applications in medicine that have been shown to make use of engineered nanostructures are: disease diagnostics, drug delivery, sensors, gene therapy, development of biocompatible prostheses and implants, and treatments for cancer and other diseases. As a result of the size-dependent properties and dimensional similarity of nanomaterials to biomacromolecules, they are ideal for use in the physiological environment, giving rise to the new field of nanobiotechnology.

Nanobiotechnology is a young and rapidly evolving sub-field at the cross-road of two interdisciplinary areas - biotechnology and nanoscience. It pertains to the utilization of biological systems to design functional nanostructures from organic and inorganic materials (Decker 2006). The topical areas of the field are still being defined towards a better understanding of living systems, developing new tools for medicine and better solutions for healthcare. Nanobiotechnology is expected to produce major advances in diagnostics, therapeutics and

prevent life-threatening diseases like cancer and other neurodegenerative diseases like Parkinson's and alzheimer's in the next decade (Goodsell 2004). Some of the vast and diverse array of nanosized devices developed includes nanovectors for targeted delivery of cancer drugs and imaging contrast agents for the early detection of pre-cancerous and malignant lesions and polyps from biological fluids. These and many other similar nanodevices can provide the essential breakthrough in the fight against cancer in the near future (Kim *et al.* 2006). Consequently, it is not surprising that two years ago in 2006 there were nearly 250 nanotechnology-based medical products commercially available in the market and many more were waiting in the pipeline (Dobrovolskaia *et al*. 2008, Powers 2006).

1.4 Cancer Nanotechnology

Despite nearly a quarter century of outstanding progress in fundamental cancer biology, there have been very little advances in the clinic regarding tumor detection. Two major roadblocks (Santra *et al.* 2005b) that account for this discrepancy are: (a) non-availability of efficacious instrumentation for tumor detection at the very onset and (b) severe limitations of existing contrast agents for imaging applications. The scope of this thesis is limited to the latter problem and deals with the development of novel nanoparticle based contrast agents for optical imaging of cancer. The ultimate goal is to detect lesions at the very onset of transformational events that leads towards malignancy. This may be possible through non-invasive routine screening from blood samples followed by more detailed molecular imaging of the contour profile of the growing lesions. Currently existing clinical cancer imaging technologies do not possess sufficient spatial resolution to identify lesions at the very onset (Sokolov *et al.* 2003a) . Most imaging technologies require contrast agents, equipped with signal-amplifying components attached to a molecular recognition and targeting ligand such as antibodies. Unfortunately, most contrast agents are somewhat limited to detecting abnormalities at the microscopic level. In

order to combat the formidable challenge of early cancer detection, it is important to identify suitable cancer biomarkers, understand their evolution over time and deploy new contrast agents, especially engineered for early diagnosis.

It is possible that nanotechnology (Ferrari 2005, Gao *et al.* 2004, Santra *et al.* 2005b, Wang *et al*. 2008, Wu *et al.* 2003), if properly integrated following thorough research on their environmental implications and health effects, could provide extraordinary opportunities to meet the challenges of bioimaging. Nanotechnology research is underway to establish suitable nanoparticle based contrast agents to detect lesions at the very onset by identifying molecular expressions in the microenvironment (Brigger *et al*. 2002, Rosi & Mirkin 2005, Sahoo & Labhasetwar 2003). There is a strong possibility of combining existing optical imaging technologies with the sophisticated nanoparticle- based contrast agents for high-resolution in vivo cancer imaging (Rosi & Mirkin 2005).

1.5 Optical Imaging

[The following section has been reproduced from Santra & Dutta, 2007, with permission].

Optical imaging is a sensitive, non-invasive, non-ionizing and relatively inexpensive technique that has shown a lot of potential for diagnostic imaging. Two major components associated with an optical imaging system are the imaging component and the optical contrast-enhancing component (i.e. contrast agent). Recent advances in optical imaging have utilized sophisticated laser technology, highly sensitive charged-coupled device (CCD) technology and powerful mathematical modeling of light propagation through the biological systems, and all these developments have formed a solid basis for the imaging component. Molecular fluorescent probes have been successfully used as optical contrast agents for imaging a variety of cancer tissues in the past (Bremer *et al*. 2003, Licha & Olbrich 2005). However, as mentioned before, the sensitivity of the contrast agent is a major obstacle in obtaining high-resolution image. Again,

in vivo deep tissue optical imaging has been limited because of the low penetration depth of the light in the ultraviolet (UV) and visible spectral range (the approximate tissue penetration depth is about 1-2 mm). Near infrared (NIR) light in the spectral range between 650 nm and 900 nm is however capable of penetrating much deeper (up to several centimeters) into the tissue and skull (Bremer *et al.* 2003, Licha *et al.* 2002). This is due to the relatively low absorption of tissue components (water and hemoglobin) in the NIR spectral range. Therefore, the development of NIR based optical imaging system is attracting tremendous attention in recent years.

For developing optical based imaging system, it is important to understand how light interacts with the biological tissues. Upon interacting with light in the UV and visible spectrum, all biological tissues autofluoresce to a certain extent. The autofluorescence originates from the fluorescent molecules of tissues such as nicotinamide, flavins, collagen, and elastin (Bornhop *et al.* 2001). Simply, a tissue can interact with light photons by absorption, scattering and reflection. Since biological tissue represents a complex system in terms of light propagation, it is expected that the optical image would be somewhat distorted.

1.6 Optical Imaging Techniques

[The following section has been reproduced from Santra & Dutta, 2007, with permission].

Optical based imaging methods such as confocal imaging, multiphoton imaging and many other techniques have been traditionally used to image fluorescence events that originate in vivo from surface and subsurface region. In recent years, advanced imaging technologies that use photographic systems with continuous or intensity-modulated light and tomographic systems has shown a great potential for deep tissue imaging. With the aid of highly sensitive contrast agents such as NPs (Santra & Dutta 2007), it may be possible to transfer optical imaging technology to human application.

1.7 Optical Contrast Agents

[The following section has been reproduced from Santra & Dutta, 2007, with permission].

The purpose of using an optical contrast agent in the biological system is to enhance the optical contrast by virtue of their contrast enhancing properties for applications like fluorescence and scattering. Tissue contrast agents, for example, are capable of reducing the background signal and improving the image resolution. Fluorescent molecular contrast agents, mostly organic fluorescent compounds, possess high extinction coefficient and quantum yield and have potential in drastically suppressing tissue autofluorescence and hence background signal. The effective delivery (loading) of these contrast agents to the target tissue has also been realized to be an important factor for achieving better image contrast, other than its intrinsic fluorescent characteristics (extinction coefficients and quantum yield) (Santra & Dutta 2007, Santra *et al.* 2005b). The concentration of contrast agent per unit volume of target tissue would determine the signal strength. Therefore, higher loading of contrast agent is always desirable for better image resolution and hence in obtaining a sharp marginal contrast between the normal and the diseased tissue.

A number of important features of an ideal contrast agent (Santra & Dutta 2007, Santra *et al.* 2005b) should be kept in mind prior to using or developing new contrast agents for diagnostic cancer imaging. Firstly, contrast agents should have minimum toxicity so that they can be administered safely. Secondly, contrast agents should have high extinction coefficient for effective absorption and high quantum yield for obtaining strong fluorescence signal. Thirdly, they should be photostable and should not have any photo-sensitizing effects (i.e. cause damage to cellular DNA and hence cell death; also termed as photosensitized cell death). Fourthly, contrast agents should be hydrophilic so that an aqueous based formulation can be easily made. Fifthly, contrast agents should preferably have an excitation and emission band maxima in the

NIR range (650 nm to 900 nm) for deep tissue imaging. Lastly, for cancer imaging, contrast agents should be attachable to appropriate cancer specific delivery systems for example antibodies, peptides and folates for targeting.

Organic fluorescent contrast agents, although studied extensively for a variety of bioimaging applications (Haugland 2003) starting from cellular to tissues to whole animal fluorescence imaging have several limitations for them to be considered as robust contrast agents (Santra *et al.* 2006). Firstly, organic fluorescent contrast agents (dyes) rapidly undergo degradation through photobleaching. As a result, fluorescence signal fades away when exposed to excitation light source (particularly when laser is used for the excitation), limiting sensitive detection of the target. Secondly, fluorescent dyes are usually hydrophobic. In order to make aqueous based formulation, chemical modifications like the use of sodium salt are often required that sometimes compromises with their spectral characteristics. Thirdly, only a handful of fluorescent compounds possess low toxicity. Lastly, a very limited number of fluorescent dyes have excitation and emission band in the NIR spectral range.

1.8 Nanoparticle Based Optical Contrast Agents

[The following section has been reproduced from Santra & Dutta, 2007, with permission].

Nanoparticle (NP) based contrast agents present a whole new class of robust nanometer size (between 1 nm and 100 nm) particulate materials that has strong potential for optical imaging of cancer. There are several advantages of using NPs for bioimaging applications.

Firstly, the sensitivity of the optical imaging could be greatly improved using nanoparticle based contrast agents. A classic example is the fluorescent quantum dots (QDs) and their applications in cancer imaging (Ben-Ari 2003, Gao *et al.* 2004, Medintz *et al.* 2005, Michalet *et al.* 2005, Stroh *et al.* 2005). The QDs are usually made of crystalline cadmium sulfide (CdS) and cadmium selenide (CdSe) based semiconductor particulate materials. They are small (<5 nm in

size) and bright having a broad excitation band but a narrow emission band. Dye doped NPs such as dye doped silica (He *et al.* 2004, He *et al.* 2002, Santra *et al.* 2005c, Santra *et al.* 2001a, Santra *et al.* 2004b), dye doped polymer particles (Pan *et al.* 2004, Stsiapura *et al.* 2004), present another class of materials for sensitive cancer detection. In dye doped NPs, each particle carries thousands of dye molecules, thus greatly enhancing the fluorescence signal (Santra *et al.* 2006, Santra *et al.* 2001a, Santra *et al*. 2001b, Sonvico *et al.* 2005). Dye doped NPs are usually smaller (about two to three orders of magnitude) than cells, which make them suitable for cellular application. Another well-studied particles are gold NPs (Copland *et al.* 2004, El-Sayed *et al.* 2005, Sokolov *et al.* 2003b, Sonvico *et al.* 2005) that have also been used for the sensitive cancer cell imaging. Gold NPs possess a strong surface plasmon band that originates from the efficient light scattering by the nanosize gold particles.

Secondly, NP based contrast agents have better photostability in comparison to the traditional organic dye based contrast agents. This has tremendous potential for sensitive and real-time monitoring of cancer progression like monitoring cancer growth and metastasis. Photostable NPs will allow non-invasive imaging of cancer tissue multiple times for monitoring tumor growth and also the effect of cancer drugs during cancer therapy. For example, QDs are extremely photostable. The effective surface passivation of QDs with a wide bandgap material such as zinc sulfide (ZnS) or zinc selenide (ZnSe) makes them photostable. In dye doped NPs, dye molecules remain encapsulated by the particle-matrix that protects them from photobleaching. This is because of the fact that particle-matrix is capable of somewhat preventing the penetration of oxygen molecules that cause dye degradation. Usually, QDs are more photostable than the dye doped NPs. Gold NPs efficiently scatter light and do not fade away via photobleaching process.

Lastly, multiple imaging modalities (Santra *et al.* 2005a) can be integrated into NP based contrast agents (also called as multifunctional NPs), making them suitable for imaging using multiple modalities such as fluorescence, X-ray and MRI. This would have great importance for in vivo cancer imaging applications (Weissleder 2002, Weissleder *et al.* 1999). Once labeled with the multimodal contrast agents, tumors could be imaged non-invasively using a CT scan or MRI for the pre-surgical assessment. During the surgical procedure tumor tissue could be directly visualized in real-time by the optical property of the contrast agent (Santra *et al.* 2005a). This mode of tumor visualization would provide direct guidance to surgeons for the effective tumor resection, enabling them to demarcate the boundary between the tumor and normal tissues. NP surface is usually modified to obtain multiple functional groups to improve aqueous dispersibility, specific targeting and biocompatibility(Gao *et al.* 2004, Levy *et al.* 2002, Pellegrino *et al.* 2005, Qhobosheane *et al.* 2001, Santra *et al*. 2005c, Santra *et al.* 2001a, Santra *et al.* 2004a, Santra *et al.* 2004b, Santra *et al*. 2005d, Santra *et al.* 2005e, Santra *et al.* 2001b, Wang *et al*. 2005, Yang *et al.* 2004b).

A robust NP design is the key step for the synthesis of highly sensitive optical contrast agents. In a typical NP based optical contrast agent design, the optical core is encapsulated by an intermediate coating followed by an outermost layer containing appropriate functional groups for bioconjugation. NPs based contrast agents have strong potential for early cancer diagnosis since they are bright and photostable. In the following sections a variety of NP based contrast agents are discussed in considerable details.

1.8.1 Fluorescent Silica Nanoparticles (FSNPs)

Amorphous silica or silicon dioxide NPs produced via Stober's sol-gel method (Qhobosheane *et al.* 2001, Santra *et al.* 2005c, Stober *et al.* 1968) or by the microemulsion technique (He *et al.* 2004, Santra *et al*. 2001a, Santra *et al.* 2004a, Santra *et al.* 2004b, Santra *et*

al. 2001b) have recently found applications in bioimaging applications. Unlike many other nanostructures, silica is not inherently fluorescent and hence cannot be exploited for sensitive imaging applications by itself. However, fluorescent dye molecules can be incorporated (dye doped) into the silica NPs to make them fluorescent (Santra *et al.* 2005c, Santra *et al.* 2001a, Santra *et al.* 2004a, Santra *et al*. 2001b). Another approach that has also been reported is to attach fluorescent dye molecules via covalent binding into the silica matrix.

For optical imaging applications (Santra *et al.* 2001b), it is preferable that dye molecules remain encapsulated by the silica matrix for various reasons. Several attractive features of silica-based NPs include: water dispersibility, resistance to microbial attack and an optical transparent matrix that allows excitation and emission light to pass through efficiently. The silica NPs are resistant to swelling and remain unchanged in a wide range of solvents that include aqueous based, neutral and acidic solutions. This property makes it especially attractive for use inside the physiological environment. Moreover, the process of doping fluorescent dyes inside the silica particles is extremely simple and effective and the spectral characteristics of the dye molecules remain almost intact. Silica encapsulation provides a protective layer around the dye molecules, preventing the penetration of the reducing oxygen molecule that can photodegrade the dye molecules, both in air and in aqueous medium (dissolved oxygen). As a result, photostability of dye molecules inside NPs increases substantially, especially when compared to bare dyes in solution.

The surface of silica NP can be easily modified to attach biomolecules such as proteins (Qhobosheane *et al.* 2001), peptides (Santra *et al.* 2004b), antibodies (Santra *et al.* 2001b) and oligonucleotides (Del Campo *et al.* 2005) using conventional silane based chemistry. A general synthesis strategy of fluorescent silica NPs is the incorporation of organic or metallorganic dye

molecules inside the silica matrix. The dye doped silica based optical imaging probes are non-isotopic, sensitive and relatively photostable in the physiological environment (Santra *et al.* 2001a, Santra *et al.* 2001b). Additionally, the interaction potential of the silica surface can be easily manipulated to facilitate the interaction with cells (Fang *et al.* 1999, Liu *et al.* 2005, Tan *et al.* 2000). Due to these novel features, fluorescent silica NPs (FSNPs) have found widespread applications in bioanalysis and bioimaging applications.

Two routes for synthesizing dye doped silica nanoparticle have been reported in the literature, namely: (a) Stobers' sol-gel method and (b) reverse microemulsion method.

(a) Stobers' Method. In a typical Stobers' method, alkoxysilane compounds like tetraethyl orthosilicate (TEOS), tetramethylorthosilicate (TMOS), a variety of TEOS or TMOS derivatives etc.) undergo base-catalysed hydrolysis and condensation reaction in ammonia-ethanol-water mixture, forming a stable alcosol. This method has been widely used for synthesizing both pure and hybrid (when more than one silane compound are used, such as dye doped silica particles) silica NPs with particle diameter ranging from a few tens of nanometers to several hundreds of nanometers (sub-micron size). Following the Stobers' protocol (Stober *et al.* 1968) with a slight modification, the synthesis of fairly monodisperse organic dye doped fluorescent silica nanoparticles has been reported (Santra *et al.* 2005c, Santra *et al.* 2001a, Santra *et al.* 2004b). Since organic dyes are normally hydrophobic, doping them inside the hydrophilic silica matrix is not straightforward. Typically, a reactive derivative of organic dye like amine-reactive fluorescein isothiocyanate (FITC) is first reacted with an amine containing silane compound like 3-aminopropyltriethoxysilane (APTS) to form a stable thiourea linkage. Then FITC conjugated APTS and TEOS is allowed to hydrolyze and condense to form FITC-APTS conjugated silica particles. Note that particles so formed will have some amount of bare dye molecules on the

particle surface that is covalently attached. These bare dyes, due to their hydrophobic nature, will somewhat compromise the overall particle aqueous dispersibility and also be prone to photobleaching. Therefore, an additional coating with pure silica is usually applied around the dye-conjugated silica NPs (Santra *et al*. 2001b). Using Stobers' method, bulk amount (kilograms) of silica particles can be easily produced in the laboratory.

(b) Reverse microemulsion (W/O) method. This method is used for the synthesis of pure silica, as well as inorganic and organic dye doped silica NPs. It is a robust technique to produce monodisperse particles in the nanometer size range (tens of nanometers to a few hundreds of nanometers). The W/O microemulsion is an isotropic, single-phase system that consists of surfactant, oil (as the bulk phase) and water (as nanosize droplets). Each surfactant-coated water droplets that are stabilized in the oil phase serve as an individual nanoreactor for the synthesis of silica NPs. The surfactant present at the oil and water interface is responsible for the thermodynamic stability of the W/O microemulsion system. The nucleation and growth process occur inside the confined spherical volume of the nanoreactor. The size of the NPs can be controlled by varying the water to surfactant molar ratio of the microemulsion system.

The fluorescence brightness of dye doped silica NPs can be improved by incorporating high-quantum yield organic dyes having large absorption coefficient values. In other words, brighter probes will improve the image resolution if encapsulated fluorescent dyes do not experience substantial photobleaching during imaging.

1.8.2 Quantum Dot (QD) Nanoparticles

QDs are semi-conductor based nanocrystals typically in the size range of 1–12 nm. They are extremely bright, photostable, and considered a candidate material to be an emerging probe for in vitro and in vivo molecular and cellular imaging (Dubertret *et al*. 2002, Gao *et al.* 2004, Gao *et al.* 2005, Medintz *et al.* 2005, Michalet *et al.* 2005, Rhyner *et al.* 2006, Wu *et al.* 2003). It

has been shown that QDs could improve tumor imaging sensitivity in vivo by at least 10–100 folds. The emission properties of QDs can be continuously tuned from 400 nm to 2000 nm by changing both the particle size and the chemical composition. These materials have a broad absorption band with narrow and symmetric emission bands (full-width at half-maximum at 25–40 nm) which typically span from the visible to the NIR spectral range. The absorption properties are associated with the promotion of electrons from the conduction band to the valence band when the excitation energy exceeds the semiconductor band gap resulting in the formation of an electron-hole pair. Some major optical features of QDs are described below:

(i) Large molar extinction coefficient value. QDs are highly sensitive fluorescent agents (or fluorescent tags) for labeling cells and tissues. Unlike organic fluorescent compounds, QDs have very large molar extinction coefficient value (Leatherdale *et al.*), typically in the order of 0.5–$5 \times 10^6\ M^{-1}cm^{-1}$ which means that QDs is capable of absorbing excitation photons very efficiently (the absorption rate is approximately 10–50 times faster than organic dyes). The higher rate of absorption is directly correlated to the QD brightness and it has been found that QDs are approximately 10–20 times brighter than organic dyes (Bruchez *et al.* 1998, Chan & Nie 1998, Dabbousi *et al.* 1997), allowing highly sensitive fluorescence imaging.

(ii) Excellent photostability. QDs are several thousand times more photostable than organic dyes. This feature allows real-time monitoring of biological processes over a long period of time.

(iii) Much longer lifetime. QDs are highly suitable for time-correlated lifetime imaging spectroscopy. This is possible due to the longer excited state lifetime of QDs (about one order of magnitude longer than that of organic dyes), allowing effective separation of QD fluorescence from the background fluorescence. This will improve the image contrast by reducing the signal-to-noise ratio (Jakobs *et al.* 2000, Pepperkok *et al.* 1999) in time-delayed data acquisition mode.

(iv) Larger Stokes shift value. Unlike in organic dyes, the excitation and the emission spectrum of QDs are well separated which means there is a large Stokes shift value; typically 300–400 nm depending on the wavelength of the excitation light). This allows further improvement of sensitivity in the detection by reducing the high background due to autofluorescence often seen in biological specimens (Gao *et al*. 2004).

(v) Multiple targeting capability. The wavelength of QD emission is size dependent. This is a unique feature of QD materials in comparison to organic fluorescent dyes. The size dependent emission of QDs allows imaging and tracking of multiple targets simultaneously using a single excitation source. This feature is particularly important in tracking a panel of disease specific molecular biomarkers simultaneously, allowing classification and differentiation of various complex human diseases (Gao & Nie 2003).

Two commonly used methods for synthesizing QDs are (a) hot solution phase mediated and (b) reverse microemulsion mediated synthesis.

(a) Hot solution phase mediated QD synthesis. A popular technique of synthesizing QDs, which typically involves synthesis at elevated temperature near the high boiling point of non-polar organic solvents. The Bawendi group (Murray *et al.* 1993) has reported the synthesis of highly crystalline and monodisperse (size distribution 8–11%) CdSe QDs using high-temperature growth solvents/ligands (mixture of trioctyl phosphine/trioctyl phosphine oxide, TOP/TOPO). A combination of tri-n-octylphosphine oxide (TOPO) and hexadecylamine can also be used (Gao *et al.* 2005). There are primarily two reasons for using hydrophobic organic molecules as mixed solvents or as a solvent / ligand mixture: the mixture serves as a robust reaction medium and also coordinates with unsaturated metal atoms on the QD surface to prevent the formation of bulk semiconductors. Following a similar synthesis strategy Qu *et al*. (Qu & Peng 2002) has reported

the formation of CdSe nanocrystals having fluorescence quantum yields as high as 85% at room temperature.

(b) Reverse micelle mediated QD synthesis. The before-mentioned reverse microemulsion technique can also be used for the synthesis of high quality core-shell QDs. Yang *et al.*(Yang *et al.* 2004b) reported the synthesis of manganese (Mn) doped cadmium sulfide (CdS) core and zinc sulfide (ZnS) shell (CdS:Mn/ZnS) QDs using AOT (dioctylsulfosuccinate sodium salt) as a surfactant and heptane as the oil for the reverse microemulsion system. The bright yellow emitting CdS:Mn/ZnS QDs were reported to have an average size of 3.2 nm and highly photostable. A silica coating was applied inside the reverse microeulsion system to increase the photostability and decrease the possibility of cadmium leaching out into the physiological environment (Derfus *et al.* 2004b).

1.8.3 Gold Based Nanoparticles

Recent advances in photonic technology have provided an alternative noninvasive technique to image cells in vivo. Metal-based NPs are especially very attractive because their optical properties are size and shape dependent. Use of gold and silver NPs for staining cells and tissue samples in electron microscopy has been in use for over 30 years. Although nanosize metallic gold and silver do not fluoresce directly, they can effectively scatter light due a phenomenon called ‘surface plasmon resonance’ (Santra *et al.* 2004a). This involves the collective oscillation of the conduction electrons induced by the incident electric field (light). Colloidal particles can then exhibit a range of intense colors in the visible and NIR spectral regions. Various methods (Bajpai *et al.* 2007, Grzelczak *et al.* 2008, Guo & Wang 2007, Huo & Worden 2007, Perez-Juste *et al.* 2005, Santra & Dutta 2007) have been reported in literature for the synthesis of colloidal gold nanospheres. Four major synthesis routes to chemically synthesize gold NPs are as follows (Santra & Dutta 2007, Santra *et al.* 2005b):

(a) Reduction of gold precursors like gold tetrachloride ($HAuCl_4$) using suitable reducing agents such as citrate, sodium borohydride, ascorbic acid and hydrazine.

(b) Microemulsions, copolymer micelles, reversed micelles, surfactants, membranes and other amphiphilic compounds have been used for synthesizing stabilized gold NPs.

(c) Seed-mediated route using preformed metallic seeds as nucleation centers.

(d) Reduction of gold precursors using an appropriate combination of reducing agents and radiation techniques such as ultrasound and heat energy.

Gold NPs, because of their strong surface plasmon resonance (SPR) properties, have attracted considerable attention in bioimaging in recent years. The SPR signal originates from the collective oscillation of conduction electrons upon interaction with absorption photons. The SPR frequency depends on various factors like particle size, shape, dielectric properties, aggregate morphology, surface functionalization and the refractive index of the surrounding medium. Gold NPs have high absorption, and scattering cross section. Due to its excellent biocompatibility (Bright *et al.* 1996, Mann *et al*. 2000, Mrksich 2000), gold NPs have been widely used in immunohistochemistry (gold based staining) and in ultra-sensitive DNA detection assays (Elghanian *et al.* 1997, Rosi & Mirkin 2005). A new class of molecular specific contrast agents for vital reflectance imaging based on gold NPs attached to probe molecules with high affinity for specific cellular biomarkers have been described (Sokolov *et al.* 2003b). The application of gold bioconjugates for vital imaging of precancers was demonstrated using cancer cell suspensions, threedimensional cell cultures, and normal and neoplastic fresh cervical biopsies. They showed that gold conjugates could be delivered topically for imaging throughout the whole epithelium. Geoghegan et. al. (Geoghegan & Ackerman 1976, Geoghegan *et al.* 1978) used colloidal gold as an electron dense marker for the indirect detection of specific cell surface

molecules. Using gold labeled horseradish peroxidase, ovomucoid and rabbit anti-goat IgG, they have successfully detected membrane bound concanavalin A, wheat germ agglutinin and goat anti-human IgM on blood lymphocytes respectively. Zhao et. al. (Zhao *et al.* 2003a, Zhao *et al.* 2003b) have established a simple and effective method for DNA immunization against Japanese encephalitis virus (JEV) infection with plasmids encoding the viral PrM and E proteins and colloidal gold. Inoculation of plasmids mixed with colloidal gold induced the production of specific anti-JEV antibodies and a protective response against JEV challenge in BALB/c mice.

1.9 Surface Functionalization and Bioconjugation

[The following section has been reproduced from Santra & Dutta, 2007, with permission].

For bioimaging applications, the NP based contrast agents have to be appropriately surface modified with suitable targeting molecules. For example, in order to target cancer cells, the particles have to be attached to cancer specific antibodies or folic acid molecules that can be taken up by the tumor cells. This process of surface modification and targeting generally involves a number of steps. Firstly, the particle surface is modified to obtain appropriate functional groups like amines, carboxyls and thiols. Next, NPs are 'bioconjugated' or attached to the bio-recognition molecules like antibodies and folic acid molecules, using suitable coupling reagents. Finally, bioconjugated particles are targeted to cancer cells. A few methods that have been frequently used for attaching specific functional groups on the surface of various NPs are briefly described below (Santra & Dutta 2007).

- Bioconjugation with carboxylated particles. This is a common bioconjugation technique, especially used to immobilize protein molecules on the surface of silica NPs. The surface is modified to attach carboxyl groups (–COOH) by using carboxylated silane reagent. Biomolecules containing free amine functional groups (proteins and antibodies) are then covalently attached to the carboxyl functionalized NP, using carbodiimide-coupling chemistry.

- Bioconjugation with aminated particles.It has been shown that many cancer cells over-express folate receptors. Cancer targeting with folate-conjugated NPs has been recently reported Folates are chemically attached to aminated silica NPs using carbodiimide chemistry.

- Bioconjugation with avidin-biotin binding. Avidin is a protein molecule that contains four specific binding pockets for biotin molecules. There exists a strong binding affinity between avidin and biotin molecules, which is comparable to covalent binding. Avidin coated NPs are typically attached to biotinalated molecules like antibodies and proteins.

- Bioconjugation via disulfide bonding. Sulfohydryl-modified NPs are conjugated to disulfide linked oligonucleotides (like DNAs). In this method, di-sulfide bonding is used to attach the oligonucleotides to the NPs.

- Bioconjugation using cyanogen bromide (CNBr) chemistry. NPs with hydroxyl groups can be activated by the reactive cyanogens bromide. Upon reaction with CNBr, a reactive –OCN derivative of NPs is formed. This derivative then readily reacts with proteins via the amine group and forms a "zero-length" bioconjugate with no spacer in between the particles surface and protein molecule.

1.10 Biodistribution and Toxicity Studies of Engineered Nanoparticles

It is evident that NPs have a lot of potential as contrast agents for applications in biology and medicine. According to GE Medical Systems, the existing market for contrast agents in 2006 was estimated to be about USD 7 billion per year and there has been unprecedented growth in the field in the last two years. Consequently, the critical factor that will evaluate the utility of these materials will be their potential toxicity inside the physiological environment. The manifested toxicity of the nanomaterial could be an outcome of the inherent chemical composition or its other physicochemical properties like particle size, shape, concentration, surface charge, surface functional group and mechanical stability (Hardman 2006, Nel *et al.* 2006, Oberdorster *et al.* 2005b).

NPs as discussed above, range from very simple compositions of pure gold and silver to complex engineered structures of quantum dots, especially where surface modifications have been applied. Some complicated nanostructures can be intentionally produced having special

characteristics for therapeutic applications. This includes 'stealth' properties that enable prolonged circulation in blood, escaping phagocytosis from macrophages, specific targeting to tissues and organs, translocating the blood brain barrier and sustained drug release capabilities.

In contrast to the numerous efforts at exploiting the desirable properties of NPs in the literature, there exist very few systematic investigations into the physicochemical properties of NPs that lead to adverse effects in living systems. The safety evaluations of the NPs cannot rely on the toxicological profiles of their larger counterparts. As yet, there are no paradigms to predict the biological responses of the engineered nanomaterials, let alone the various functional groups and other surface modifications that frequently accompany them. The following sections contain a brief summary of the toxicity outcome from NPs used as contrast agents for this research work. Finally, the effect of various physicochemical parameters of NPs that can affect their biocompatibility and toxicity behavior is discussed in the last section of this chapter.

1.10.1 Amorphous Silica Nanoparticles

Silica is the earth's most abundant mineral, occurring in nature in several crystalline and amorphous forms. The amorphous form of silica, which is used for bioimaging applications, is generally known to be comparatively non-toxic and biocompatible. It is used in the food, paint, coatings and paper industries as a non-traditional biocompatible substance (Barnes *et al*. 2008). However, the crystalline forms of silica, especially α-quartz, are generally associated with major health hazards like silicosis and cancer (Craighead 1988, Craighead 1992, Donaldson & Borm 1998, Driscoll & Guthrie 1997, Schins *et al*. 2002). α-quartz is the most thermodynamically stable crystalline form of silica at room temperature which is converted reversibly upon heating to β-quartz (another crystalline polymorph) (Dutta & Moudgil 2007). The different polymorphic forms are known to exhibit different levels of toxicity (Barnes *et al.* 2008). As the majority of the

population is exposed to α-quartz, most toxicity experiments on silica are conducted using this polymorph (IARC 1997). There are comparatively very few studies (Dutta et al. In Review for Publication, Renovanz 1984) reported on the toxicity aspects of dye doped amorphous silica NPs. All bioimaging applications of silica essentially use the amorphous polymorph which appears to be biocompatible (Dutta et al. In Review for Publication, Rosi & Mirkin 2005) and have strong potential for biological applications (Santra & Dutta 2007, Santra *et al.* 2005b).

1.10.2 Quantum Dots (QD) Nanoparticles

The semiconductor core of the QD nanocrystals is constituted of heavy toxic metallic components. Although these metals contribute towards the unique optical and electronic properties of the QDs, they also make them hazardous for use inside the body. Most of the heavy metals like cadmium, indium, and selenium that constitute QDs are extremely toxic to humans and can lead to renal, hepatic and neurologic deficiencies (Cho *et al.* 2007, Derfus *et al.* 2004a, Hardman 2006, Maysinger *et al.* 2007) if they leach out. Hence for biological applications, it is critical to cap the QDs with a coating material in order to prevent heavy metal leaching. In fact, for decades these novel materials could not be used for biological applications, until protocols for modifying the surface with appropriate coatings were developed in 1998 (Bruchez *et al.* 1998, Chan & Nie 1998) to render the QDs water-soluble, less toxic and attachable to peptides, antibodies, nucleic acids and other low molecular weight biomolecules using covalent bonding. In fact, one of these studies demonstrated for the first time *in vivo* that CdSe/ZnS QDs when coated with mercaptoacetic acid could bond onto blood transferrine (Chan & Nie 1998). These complexes were then taken up selectively by cancer cell (HeLa Cells). The controls particles with no transferrin could not be taken up as there was no receptor-mediated endocytosis.

Over the years, numerous studies have demonstrated the use of QDs coated with different substances for various biological applications (Akerman *et al.* 2002, Dubertret *et al.* 2002, Jiang *et al.* 2004a, Kirchner *et al.* 2005, Klostranec & Chan 2006, Lovric *et al.* 2005a, Lovric *et al.* 2005b, Medintz *et al.* 2005, Michalet *et al.* 2005, Shiohara *et al.* 2004, Smith 2002). However, there is not much information about the disposition and health consequences of QDs in animals and human beings. Most investigations on the QDs available in the literature have been carried out *in vitro* and report contradictory results regarding the toxicity aspects. A large number of these reports demonstrate that no toxicity was observed, while other investigators reveal a variety of cytotoxic symptoms like free radical generation, cell membrane integrity compromise and reduced mitochondrial activity due to incubation with quantum dots. The discrepancies in the literature can be attributed to various factors like lack of toxicology-based studies, differing QD dose and exposure, a wide range of physicochemical properties associated with each QD in the literature and the fact that most of these studies were performed by nanotechnology researchers rather than toxicologists or health professionals. In any case, these studies do provide an insight to the biological responses that could occur with the use of QDs inside the physiological environment.

Existing *in vitro* studies in the literature seems to suggest that certain types of QDs may be cytotoxic. For instance, in an *in vitro* study to evaluate the cytotoxicity of CdSe QDs performed on liver cells it was shown (Derfus *et al.* 2004b) that the viability of hepatocytes incubated with the QDs declined depending on the particle concentration of the solution. The reduction of cell viability was found to be related to particle concentration according to: $0.0625 < 0.25 < 1$ mg/mL and diminished significantly (6%) if the quantum dots were subjected to ultraviolet light for extended time (8 hours). This reduction of cell viability was attributed to the

cadmium ions ($Cd^{2+)}$ that leached out of the quantum dots due to surface oxidation on exposure to ultraviolet light. Encapsulating the QDs in a layer of ZnS, a material that epitaxially matched the CdSe core of the QDs, could reduce this effect. But the Cd^{2+} ion leaching could be actually reduced to zero when the QDs were encapsulated in 98% bovine serum albumen. Similarly, Shiohara *et al.* (Shiohara *et al.* 2004) reported a decrease in the cell viability as observed in three cells lines: kidney epithelial (Vero) cells, cervical cancerous (HeLa) cells and primary human hepatocytes when incubated with mercaptoundecanoic acid (MUA) coated CdSe ZnS QDs with increasing particle concentration. Kirchner *et al.* (Kirchner *et al.* 2005) studied the cytotoxicity of colloidal CdSe and ZnS capped NPs, coated with various surface modifications and exposed to a number of tumor cells and human dermal fibroblasts cells (NRK fibroblasts, MDA-MB-435S breast cancer cells, CHO cells and RBL cells). In case of stable coatings, like applying a silica shell on the quantum dots followed by pegylation, the toxicity manifested was reduced as compared to unstable coatings like mercaptopropionic acid (MPA). Phosphosilicate coatings induced expedited Cd^{2+} leaching inside the shell. Interestingly, polymer-coated gold NPs also displayed a cytotoxic effect compareable to the quantum dots. This seems to indicate that the toxic behavior could be due to the precipitated particles on the cells and not just due to the production of Cd^{2+} ions. Lovric *et al.* (Lovric *et al.* 2005a) reported the cytotoxicity of CdTe QDs coated with two different functional groups in rat pheochromocytoma cells (PC12) at particle concentrations of 10 μg/mL. The two surface coatings applied were mercaptopropionic acid and cysteinamine. It was also reported that uncoated QDs were cytotoxic at 1 μg/mL. Cell death occurred by chromatin condensation and membrane blebbing, both processes indicative of apoptosis in cells. Moreover, use of two different QD sizes showed a more pronounced cytotoxicity for smaller and positively charged QDs as compared to their larger counterparts at

the same particle concentration. The exact mechanism of cell death was not known but was considered to be due to generation of cadmium ions, free radical formation or QD-cell interactions leading to loss of functions. On conducting further detailed analysis of the effect of QD-induced reactive oxygen species on the cell viability, the authors suggested that the toxicity could be partially induced by cadmium.

In another *in vitro* cum *in vivo* toxicity study of QDs, Hoshino *et al.* (Hoshino *et al.* 2004b) intravenously injected 'QDs incorporated into El-4 cells' into nude mice. As a control, they used MUA without any QDs for 12 hours and reported that severe cytotoxicity was observed in murine T-cell lymphoma (EL–4 cells) at 100 μg/mL. Similarly, cells treated with cysteinamine showed weak genotoxicity at the same particle concentration. The QDs could be detected in the kidney, lung, liver and spleen after 7 days with no apparent toxicity or damage to the mice. CdSe/ZnS QDs surface-functionalized with biotin were also shown (Green & Howman 2005) to alter coiled double-stranded DNA by releasing sulphur dioxide (SO_2) that gradually desorbed into solution to generate sulphite radicals. This was due to the surface oxidation of ZnS, which was accelerated in the presence of UV light. The proportion of DNA alterations varied depending on the presence (56%) and absence (29%) of UV light.

Compared to the number of *in vitro* studies, there are only few *in vivo* studies in the literature that report on quantum dot toxicity. In an intravenous mice study, Akermann *et al.* (Akerman *et al.* 2002) reported that the nature of the coating could actually alter the distribution of the QDs in the various organs and tissues. They also demonstrated that QDs having PEG coating could actually reduce the liver and spleen capture by 95% and prolonged the half-life in blood. Various other peptide coatings led to increased distribution in the lungs or in breast tumors in the study.

During in vivo imaging, Dubertret *et al.* (Dubertret *et al.* 2002) microinjected CdSe/ZnS QDs coated with n-poly(ethylene glycol) phosphatidyl ethanolamine (PEG-PE) and phosphadylcholine (PC) into Xenopus frog embryo cells. They concluded that there was no significant toxicity from the 'QD-micelles' during 'embryogenesis' in the study.

1.10.3 Gold Nanoparticles

Metallic NPs having a size range between 10 and 100 nm are known to exhibit the surface plasmon resonance (SPR) effect. This is a process by which the electrons in the metallic structure can resonate to incident radiation. It responds by a combination process of light scattering and absorption of electromagnetic radiation of wavelengths significantly larger than the particle itself. The effect is observed in the visible part of the spectrum for gold, silver and copper NPs.

For gold NPs, the plasmon resonance and consequently the absorption phenomena occurs at 520 nm, corresponding to green light in the spectrum. Although a proportion of the incoming light is scattered, the absorbed quantity of light is sufficient to generate localized heating or 'hyperthermia' in the NPs. This behavior of gold, along with its oxidation resistance properties, can be exploited for therapeutic applications inside the physiological environment (Pissuwan *et al.* 2007a, Pissuwan *et al.* 2006, Pissuwan *et al.* 2007b, Pissuwan *et al.* 2007c). Localized application of heat has been utilized for anti-tumor therapeutic applications for many centuries. Similarly, hyperthermic properties of gold NPs will be used to destroy the diseased tissues or for releasing therapeutic payloads at target sites inside the body (Govorov & Richardson 2007, Govorov *et al.* 2006, Richardson *et al.* 2006, Richardson *et al.* 2007). Any energy source like infra-red lamps, ultrasound or lasers can be used to generate the heat inside the particles. The only challenge is to restrict the NPs and the generated heat inside the target diseased tissues and allow healthy tissues to remain intact.

In recent years, it has been demonstrated (Loo *et al.* 2004, O'Neal *et al.* 2004) that it is more convenient to shift the wavelength of the maximum absorption into the near infra-red region (800 – 1200 nm) as the body tissues are comparatively more transparent in that region . This will allow a higher resolution for deep tissue imaging and thereby enable detection of diseases at the onset. This has been demonstrated using high aspect ratio materials like gold nanorods (Huang *et al.* 2006, Huff *et al.* 2007a, Huff *et al.* 2007b, Maye *et al.* 2000, Niidome *et al.* 2006) which exhibited two plasmon absorption peaks (at 520 and 800 nm respectively) and amorphous silica particles encapsulated inside gold nanoshells (Diagaradjane *et al.* 2008, Hu *et al.* 2003, Loo *et al*. 2005a, Loo *et al*. 2004, Loo *et al.* 2005b) with varying optical properties over a broad range from near-UV to the mid-IR. These nanoshells were shown to possess greater absorption efficiency than conventional near infra-red absorbing dyes by many orders of magnitude. Additionally, the gold nanoshells were less prone to photobleaching. The early accounts of using hyperthermic properties of gold NPs for therapeutic applications were published in 2003 (Hirsch *et al.* 2003) and later (Loo *et al.* 2005a, Loo *et al.* 2004, Loo *et al.* 2005b) where nanoshells along with antibodies were used for actively targeting cancerous cells. A follow up study, reported by the same group synthesized stealth particles by pegylating the gold nanoshells (O'Neal *et al*. 2004) and used it for passively targeting tumors in mice models. It was reported that NIR irradiation of the cancerous tissues led to an approximate temperature rise of 40 to 50º C which was used to preferentially kill the carcinoma.

Colloidal gold NPs have also been used for therapeutic applications (Pitsillides *et al.* 2003). Specific antibodies were conjugated to the NPs and incubated in a co-culture of CD8+ and CD8- lymphocyte cells. On being irradiated with a laser at 532 nm, the NPs led to selective apoptosis in the CD8+ cells. Moreover, certain experimental parameters were manipulated to

control conditions that led to preferential permeabilizing of the cell membrane in the target cells for upto two minutes. This showed that it is possible to use colloidal gold NPs for targeting and accessing intracellular organelles for therapeutic functions.

1.11 Physicochemical Parameters of Nanoparticles affecting their Bioactivity

The unique physicochemical properties of nanosized particulate (NSP) systems can be attributed to their small size (Yin *et al.* 2005), shape, large specific surface area, chemical composition, surface activity and interfacial interactions (Nel *et al.* 2006, Oberdorster *et al.* 2005b). However, these novel characteristics that seem impressive from the material science perspectives could lead to adverse biological responses and develop into a hazard for human health and environment (Hoshino *et al.* 2004a, Karakoti *et al.* 2006, Ryman-Rasmussen *et al.* 2006). In fact, it has been suggested by researchers that NSPs even though sometimes not inherently benign, can affect the biological activities in cells, at the sub-cellular and protein levels (Nel *et al.* 2006). Additionally, certain NSPs are able to travel throughout the body and cross cell membranes to deposit in target organs like the mitochondria to trigger injury and cell death (Xia *et al*. 2007). Therefore, it is crucial that results from existing toxicity studies of NSP systems are assimilated in order to exactly identify the characteristics that potentially pose a health risk and elucidate the underlying toxicity mechanism.

It is indeed a challenge for scientists to design accurate experiments to specifically identify and reproduce these adverse biological interactions. The challenges can be ascribed to several issues (Teeguarden *et al.* 2007): (a) dosimetry or the correct method to express the dose of nanoparticulate systems (mass, dimensions, surface area, surface coating, state of aggregation etc) (b) confidence level regarding the exactly desired form of nanomaterial during dosage (c) difficulties in real-time detection and quantification of the nanomaterials inside the cells and tissues and (d) the need to characterize the NSPs at every stage of toxicological testing. The

following sections include an attempt to establish a correlation between the physicochemical properties of NSPs to their toxicological effects as reported in the literature database.

1.11.1 Effect of Elemental Composition

The different compositions of NSPs lead to variations in the physical and chemical behavior of the material. It is an important parameter that can be correlated to the intrinsic properties (Donaldson *et al.* 2004) of the material to explain the variations in toxicity behavior of different nanomaterials. For instance, in an initial nanotoxicity study (Ferin *et al.* 1990, Oberdorster *et al.* 1990), 20 nm alumina (Al_2O_3) and titania (TiO_2) particles were compared to 500 nm $Al2O_3$ and 250 nm TiO_2 particles. Although both materials in the nanosized dimensions induced significantly greater and more persistent inflammation than their respective larger counterparts, the inflammatory response in rats dosed with Al_2O_3 NPs was far more persistent as compared to rats with TiO_2 NPs. Although the greater specific surface area of Al_2O_3 as compared to TiO_2 played an important role, the material differences also contributed to the toxicity responses. The important role of particle chemistry in NP-induced toxicity was evident from a subsequent inhalation study from the same research group (Oberdorster *et al*. 1995), using 20 nm polytetrafluoroethylene (PTFE) fume particles in rats. They reported that inhalation of 50 $\mu g/m^3$ resulted in an acute pulmonary inflammation with high morbidity rates. The severe inflammatory responses of nano-sized PTFE fume particles contrast the minimal effects observed from 20 nm TiO_2 and Al_2O_3 NPs. Similarly, nanosized carbon black was found to be more severe than TiO_2 NPs (Renwick *et al.* 2004, Renwick *et al*. 2001). Again, both materials induced lung inflammation and damage in rat epithelial cells at greater extents than their larger counterparts. Several other different NPs (polyvinyl chloride, TiO_2, SiO_2, cobalt and nickel) ranging between a mean diameter of 14 nm to 120 nm were studied and only cobalt was found to induce toxicity in

endothelial cells and produce pro-inflammatory cytokine IL-8 (Peters *et al.* 2004). Amongst the other particles, SiO_2 induced minimal IL-8 release while TiO_2 had a substantial one. Although no explanation for the differences in cytotoxicity was presented, it could be due to both material and/or size differences of the various particles. A similar trend of composition dependence was also observed for ultra-fine (particles with mean diameter of less than 1 μm) polymeric biomaterials (Tomazic-Jezic *et al.* 2001). Two different polymers namely polystyrene (PS) and polymethyl methacrylate (PMMA) were delivered into rats by intraperitoneal administration. The PMMA particles were recovered from the spleen while the PS particles, regardless of size, were accumulated primarily in the rat adipose tissue of the peritoneal cavity with very few particles in the spleen.

The response from cells in NP exposure studies has been mostly studied with regard to toxicity behavior. But remarkably enough, it has been shown that certain rare earth NPs like cerium oxide and yttrium oxide can protect nerve cells and retinal degeneration from various oxidative stresses. The neuroprotective behavior was directly material structure-dependent and was observed in NPs with single crystal structure with few twin boundaries or stacking faults and expanded lattice parameters relative to its bulk counterpart. The rare earth NPs act as free radical scavengers and can effectively reduce the amount of available reactive oxygen species which can kill the cells (Das *et al.* 2007, Schubert *et al.* 2006, Tarnuzzer *et al.* 2005).

(a) Effect of Core constituent : Certain nanomaterials are a combination of various components in a core-shell or other complex structures. Depending on the structure and surface chemistry in question, the particle may have reactive groups on the surface that can have an immediate significant effect on the biological responses. It is known that all materials are immediately covered by proteins, as soon as it comes in contact with the physiological environment. So most

of the instantaneous responses generated due to NP-cell interactions are determined by the nature of the deposited protein layer. But after a considerable amount of time, secondary events like material leaching through porous layers or surface layer dissolution may take over and the core constituent can have a more profound effect on the nanotoxicity profile of the material. For this reason, it is imperative that the biological behavior of the surface as well as the core constituent material is also understood while designing a core-shell NP for use in the physiological environment.

It has been reported that the biodistribution behavior of QDs after 28 days from injection into the blood of rats starts to show a shift in the profile to a dual behavior, part of which resembles that of free cadmium (Yang *et al.*). This similarity to free cadmium in the profile is indicative of heavy metal leaching which is extremely dangerous as cadmium is generally associated with various immune diseases. Moreover, possible gadolinium leaching from NP based magnetic contrast agents used for Magnetic Resonance Imaging (MRI) has been reported (Sharma *et al.* 2007). Thus, the release of the core material which is released over a period of time and may have some potent toxicity can become a greater health concern as compared to the first-encountered functional group on the NP surface.

(b) Effect of Surface Composition: The surface composition will affect the uptake of the NP by cells of the phagocytic system inside the physiological environment (Smith *et al.* 2006). This can be modulated to a large extent by intentionally modifying or functionalizing the surface (Schellenberger *et al.* 2004). Use of certain biomolecular linkers anchored on the surface or within vescicles or liposomes (Nardin *et al.* 2000) has been shown to alleviate the biological responses. The affinity of the NP to a particular protein has thus been manipulated so that it can fit and thereby be used to target a certain biomolecular assembly on a membrane or within an

organelle or beneath the cell surface. The specificity of the surface can be used for analytical detection, optical labeling and other applications like drug or gene delivery to cells (Hood *et al*. 2002). In contrast, chemicals adsorbed on the surface may also adversely affect the reactivity of the NPs. Certain fractions from particulate air pollutants were observed to exert toxic effects on cells in vitro (Xia *et al.* 2006).

(c) Effect of Purity: Presence of impurities like metal traces associated with the production of commercial nanotubes as catalysts have been shown to adversely affect biological responses and lead to the generation of free radicals and intracellular oxidative stress(Shvedova *et al.* 2003b). Especially, transition metals such as Fe, Ni and Cu have been shown to induce the formation of reactive oxygen and nitrogen species through a Fenton-like reaction. The biological effect of SWCNTs before catalyst removal and containing 30% iron by mass has been studied in human keratinocyte cells (Shvedova *et al.* 2003a). A decrease in cell viability and glutathione depletion with a dose-dependent relationship was observed, which was considerably reversed by a metal chelator desferrioxamine. This indicates the significant role of the impurities present i.e. iron as a cause of some of the biological responses. Similarly, other investigators have reported on the dual role of essential transition metal ions, like copper and zinc, to act as cofactors as well as catalysts for cytotoxic reactions (Finney & O'Halloran 2003). This implies that the biological responses of the same NSP will differ depending on the percentage purity of the sample in hand and the composition of the "contamination" in question.

1.11.2 Effect of Particle Size, Surface Area and Number

The particle size, surface area and number of the NPs are closely related physical parameters that can influence the health effects of NPs to a large extent. Reducing the size to nanoscale dimensions results in a drastic increase of the surface to volume ratio, which means that there are more molecules of the chemicals are present at the surface. Although it is known

that this would lead to an increase in the intrinsic toxicity (Donaldson *et al.* 2004), the exact extent to which it contributes towards lung deposition, biopersistence is still not clearly understood. A small size of the NPs, with a corresponding large specific surface area, makes them ideal for various applications. The ratio of the surface to total number of atoms or molecules increases exponentially with a decreasing particle size. This leads to increased surface reactivity and enhanced biological activity per unit mass as compared to larger particles. This increase in biological activity can be positive and desirable as for drug delivery and other anti-oxidant applications or negative toxicity behavior as manifested through induced oxidative stresses and cellular dysfunctions or a mix of both.

In vivo studies have been reported using ultrafine particles that elicit more lung injury and pathology as compared to exposure to an equal mass of fine particles of the same material (Driscoll *et al.* 1996, Oberdorster 1993, Oberdorster *et al.* 1992, Oberdorster *et al.* 1994). Due to the large specific surface area available, the particle size/surface area/ number are a more important determinant of potential hazard than the mass of the material, provided the particle chemistry remains unchanged. On dosing rats by intratracheal instillation using 20 nm and 250 nm TiO2 particles with doses of 30 μg and 2 mg, a much greater inflammatory response was generated in the pulmonary system. But when plotted against the surface area of the particles, the neutrophil response fitted the same dose-response curve (Oberdorster 2000). Similar results have been obtained by normalizing the lung weight to inflammatory responses in mice. Other investigators have also reported similar findings using carbon black (Brown *et al.* 2000, Stone *et al.* 2000), barium sulphate (Cullen *et al.* 2000, Tran *et al.* 2000a, Tran *et al.* 2000b) and polystyrene particles.

1.11.3 Effect of Shape

Nanomaterials have been synthesized in various shapes and structures such as spheres, rods, needles, tubes, plates and prisms. Recent evidences have indicated that the shape of the nanomaterials plays a crucial role in influencing the toxicity behavior. NSPs with high aspect ratio shapes like acicular or fiber-like can obstruct phagocyte-mediated clearance mechanisms to induce enhanced toxicity as compared to isotropic structures (Brown *et al.* 2007). Moreover, it is very likely that the shape of the nanomaterial in question also affects the deposition kinetics and surface absorption. Champion *et al.* have used polystyrene particles of various shapes and sizes to study phagocytosis in alveolar macrophage cells (Champion & Mitragotri 2006). They reported that particles shape and not size played a dominant role in the phenomena of phagocytosis. The shapes, defined as the tangent angles at the point of initial contact, dictated whether the macrophages would initiate phagocytosis or would only spread over the particles. Surprisingly, particle size only regulated the completion of phagocytosis, especially in situations where the particle volume exceeded the cell volume. Genome expression array analysis were conducted on human fibroblast cells exposed to multi-walled carbon nano-onions (MWCNO, aspect ratio = 1) and carbon nanotubes (MWCNTs, aspect ratio > 1). Results showed distinct differences in the gene expression profiles: MWCNTs exposure induced genes indicative of immune and imflammatory responses while MWCNOs in genes induced as response to external stimuli (Ding *et al*. 2005). Similarly, Magrez *et al.* (Magrez *et al.* 2006) compared the cellular toxicity of carbon-based nanomaterials: MWCNTs, carbon nanofibers (CNF) and carbon black (CB) NPs as a function of their aspect ratio on lung tumor cells. The number of viable cells decreased in the following order: CBN > CNF > CNT. They attributed the difference in toxicity behavior to the highly reactive sites present on the CBN due to a large number of dangling bonds compared to CNTs or CNFs where they only occur at lattice defects or at the end caps. Very

recently, Poland *et al*. have reported the "asbestos-like pathogenicity" in rats due to exposure to MWCNTs that lead to inflammation and the formation of lesions, also known as granulomas (Poland *et al*. 2008). The CNTs are hazardous fibers (i.e. thinner than 3 μm, longer than 20 μm and biopersistent in the lungs) and if the number of fibers reaches a sufficient level can chronically activate inflammatory cells, become genotoxic and lead to fibrosis and cancer in target cells and tissues.

1.11.4 Effect of Crystal Structure

Shrinkage in size from bulk to nanosized particles may lead to various changes in the material interactions that could indirectly affect toxicity behavior. A decrease in size may lead to an increase in structural defects in the nanomaterial through the formation of discontinuous crystal planes and disrupted electronic configuration. This may lead to the formation of specific surface groups that may become reaction pockets for enhanced biological responses (Nel *et al.* 2006). For example, single-component transition metals or presence of transition metals on the surface can aid in electron capture that can lead to the formation of the superoxide radical. This would lead to the generation of reactive oxygen species (ROS) through a process of dismutation, which is more commonly known as Fenton chemistry, and thus manifest toxicity due to induced oxidative stress.

1.11.5 Effect of Surface Chemistry

As mentioned before, NPs upon exposure to tissues and other biological fluids immediately adsorb macromolecules on their surface. The specificity of the adsorption process depends largely on surface characteristics like surface chemistry and surface energy of the NPs, in question. Moreover, the degree of hydrophilicity and hydrophobicity of the surface regulates biological activities like cell-surface adhesion, protein denaturation at the interface and selective adsorption of materials at the interface. A variation in hydrophobicity leads to different

translocation routes in many biological compartments and differences in interfacial activities between nanomaterials and cells (Cauvel *et al.* 1997, Fubini 1997, Karakoti *et al.* 2006).

1.11.6 Opsonization and Phagocytosis

The clearance process of any foreign organism or particles that enters the blood generally occurs in three steps: opsonization, phagocyte-opsonin protein binding and final ingestion of the foreign materials by the phagocytes (Owens & Peppas 2006). The process by which the foreign material gets covered by the opsonin proteins is known as opsonization. This process is followed by 'phagocytosis' which involves engulfing and finally clearing the foreign materials from the blood stream (Dobrovolskaia *et al*. 2008). These two clearance mechanisms inside the body make it possible to restrict undesirable elements larger than the renal threshold limit to reside in blood. Opsonization (Dobrovolskaia *et al.* 2008, Owens & Peppas 2006) generally occurs in the blood circulation and it can take anytime between a few seconds to several days for the process to complete. The precise mechanism by which this process (Moghimi & Hunter 2001, Moghimi & Szebeni 2003) is activated is very complex and not completely understood but components like immunoglobulins, C1, C2 and C3 are known to be the common opsonins. Other blood serum proteins like laminin and fibronectin have been shown to play an important role in the clearance process using inherited and deficient animal models (Owens & Peppas 2006).

The opsonon proteins, which are generally present throughout the blood, can come into contact with any introduced foreign nanoparticle system by random Brownian motion. However, once the proteins get close enough to the particle surface, they start interacting using several attractive forces like van der Waals, electrostatic, ionic, hydrophilic and hydrophobic, leading to opsonin binding on the particle surface. It is known that without the presence of the surface bound opsonin proteins, it will not be possible for the phagocytic cells to recognize, bind and clear the foreign material.

The inactive opsonin protein present in the blood serum after encapsulating the foreign matter generally undergoes conformational changes to an activated protein structure that can be recognized by the phagocytes. There are several methods of phagocyte attachment onto the opsonin proteins. The phagocytic cells surfaces contain special receptors that function to interact with the modified conformation of the opsonins and acts to alert the phagocytes about the presence of foreign materials in the environment. Other non-specific attachment processes, especially between phagocytes and blood-serum proteins that have opsonized on hydrophobic materials have also been demonstrated (Moghimi & Hunter 2001, Moghimi & Szebeni 2003, Owens & Peppas 2006). The last and final step of ingestion involves endocytosis of the foreign material by the phagocyte. Secret enzymes and other oxidative-reactive chemical factors (superoxides, peroxides and nitric oxide) are secreted to break down the phagocytosed material.

As the initial opsonization of particles is the critical step towards phagocyte recognition and clearance from the blood-stream, most research towards drug delivery makes use of stealth NPs (Moghimi & Hunter 2001, Moghimi & Szebeni 2003) that can either avoid or delay this process. Although, today there are no known techniques to block opsonization completely and effectively, research in the last few decades has successfully slowed the process, effectively increasing the blood circulation half-life by using stealth NPs for therapeutic applications.

1.11.7 Pegylation of Nanoparticles

Several researchers have demonstrated a correlation between the particle surface charges to the induction of opsonin proteins. In general, it has been reported that the tendency of opsonization on hydrophobic surfaces is more and much quicker as compared to the hydrophilic surfaces. This is due to the enhanced adsorbability of blood serum proteins on the hydrophobic surfaces. Similarly, neutrally charged surfaces are known to have a lower rate of opsonization than their charged counterparts (Owens & Peppas 2006, Roser *et al.* 1998). Thus, a widely used

method to prevent opsonization is to use surface adsorbed or shielding groups that block any electrostatic and hydrophobic interactions that can aid the proteins to bind on the particle surfaces. Generally, these groups (Owens & Peppas 2006) are long hydrophilic polymer chains or non-ionic surfactants like polyethylene glycol (PEG), polyacrylamide and poly(vinyl) alcohol. Other copolymers that contain PEG like poloxamers, polysorbates, poloxamines have also been used. The best stealth properties have been observed in PEG and PEG containing co-polymers (Moghimi & Hunter 2001, Moghimi & Szebeni 2003). 'Pegylation' refers to the molecular attachment of polyethylene glycols of various molecular weights (Moghimi 2006) to particles or active drug molecules to impart stealth functionality. Typically, these polymers are long, flexible and highly hydrophilic and can effectively shield hydrophobic or charged particles from the blood protein (Carstensen *et al.* 1992, Muller *et al.* 1992, Norman *et al.* 1992) . More importantly, they are neutral in charge and can reduce the electrostatic interactions (Owens & Peppas 2006).

CHAPTER 2
SPECIFIC OBJECTIVES AND RESEARCH APPROACH

2.1 Gap Analysis

The gap analysis outlined in this section is based on the critical literature review presented in the previous chapter. Two major gaps were identified in the literature for this research effort: 1) absence of a NP system with multifunctional capability of bioimaging and therapy, and 2) absence of any clear correlation between the effects of physicochemical properties of nanoparticles (NPs) and their influence on the cellular uptake (*in vitro)* and clearance behavior (*in vivo)* and systematic particokinetic studies on NPs to comprehend their biodistribution behavior. Physicochemical characterization of NPs especially in biofluids and biological environment continues to be a challenge for developing reliable structure-property performance correlation.

The first gap relates to the fact that there currently exists limited research work on the development of multifunctional NPs for bioimaging and therapy. It is known that quantum dots (QDs) possess the best fluorescent properties as compared to all other contrast agents. Gold NPs have been shown to have excellent absorbance properties that can be used for bioimaging applications. Additionally, gold has the potential for therapeutic applications due to its hyperthermic properties. Combining these two material properties, provide an avenue to synthesize NPs with two different modes of contrast in the physiological environment as well as impart therapeutic property. There are numerous studies showing the bioimaging potential of QDs, but many of them also highlight the toxic aspect of these particles. However, not many attempts have been made to mitigate the toxic nature of QDs and study its blood clearance behavior in the physiological environment.

The second major gap identified for this research effort was the absence of adequate studies into the effect of physicochemical parameters of nanosized particulates on uptake and clearance. Two of the major physicochemical properties of NPs that can influence their biological activity are material composition and surface chemistry. The nature of the NP surface plays an important role in determining the toxicity of the material (Karakoti *et al*. 2006). The presence of different functional groups on the surface can potentially regulate the extent of cell-surface interactions, protein adsorption and selective interaction of other components from the physiological environment, thereby governing their biological activity *in vitro* and *in vivo*.

2.2 Hypothesis

Physicochemical parameters of NPs like material composition, particle size and surface functionalization can influence the cellular uptake and biodistribution, and thereby determine its toxicity behavior. It is also known that QDs are extremely bright and photostable and have tremendous potential as bioimaging probes. However, due to the presence of heavy metals that can leach from the QDs, they are considered toxic. Attempts are being made to use amorphous silica, a potential biocompatible material, to encompass the QDs and mitigate its toxicity. Further, deposition of gold speckles on the outer silica shell can confer hyperthermic properties thereby imparting therapeutic functionality to the resultant NPs. Gold also imparts additional contrast capability due to its excellent absorbance properties. Additionally, modification of the NP surface can be utilized for selective uptake, which can be exploited for potential targeted-therapeutic applications.

2.3 Specific Objective

The overall objective of this research work is to develop engineered nanoparticulate systems for bioimaging applications and investigate the influence of their physicochemical

parameters on the cellular uptake (*in vitro)* and blood clearance (*in vivo*). Two specific objective of this research work were:

- Develop (synthesis and characterization) NP systems for bioimaging applications and impart therapeutic functionality to the particles.
- Study the effect of various physicochemical parameters of the NPs like material composition, particle size, surface charge and functionality on the cellular uptake (*in vitro)* and blood clearance (*in vivo)*.

2.4 Research Approach

As a first step towards developing engineered NPs, fluorescent silica nanoparticles (FSNPs) were developed as bioimaging contrast agents by doping the amorphous silica matrix with organic fluorescent dyes. The cellular uptake was visually and qualitatively observed using confocal microscopy and quantitatively confirmed using protein assay techniques. Cell viability tests using conventional bioassay (LDH) were conducted to assess the biocompatibility of amorphous silica.

CdS:Mn/ZnS QD NPs were then synthesized and coated with a biocompatible amorphous silica layer to form the silica coated quantum dot NPs (QDS). Leaching studies were performed on QDS NPs at different pH and temperatures to determine the amount of cadmium that could leach out. Gold speckled silica coated quantum dots (QDSG) were developed by depositing gold speckles on QDS. The QDSG NPs were used for imaging studies with daphnia and A549 cells. Heating studies were also conducted with the QDSG NPs to confirm the hyperthermic properties of the gold speckles.

During this research effort, attempts to surface functionalize the QDSG NPs did not succeed. Therefore, colloidal gold NPs with positive, negative and near neutral surface charge were synthesized as auxiliary particles to study the effect of surface charge on the biological responses of NPs. *In vivo* studies were carried out to understand the behavior of

the engineered NPs in rat blood. For this study five different particles were used: a) bare colloidal gold particles (negative surface charge), b) gold particles conjugated with PEG (near neutral surface charge), c) Cysteine-amine conjugated gold particles (positive surface charge), d) silica coated quantum dots and e) gold speckled silica coated quantum dots.

The NPs were intravenously injected into rats through the surgically attached cannulae tube on their jugular vein. Thereafter, blood was drawn out from each animal at predetermined time-points. The blood samples with NPs collected from the rats were digested and analyzed for gold and cadmium using inductively coupled plasma - mass spectrometric (ICP MS) technique. A curve of NP concentration in blood versus time of draw was generated. Using this data and a one-compartmental model developed using equations from first-order reaction kinetics, the half-lives ($t_{½}$) of the various NPs in rat blood were determined. Protein adsorption studies were conducted to explain the blood clearance behavior of the different NPs.

2.5 Dissertation Outline

The first chapter of this dissertation provides an introduction followed by a critical literature review to put the current research effort in perspective. In Chapter 2, (current chapter) the gap analysis from the literature review was presented, followed by the hypothesis and specific objectives of the present study. The research approach towards achieving these objectives was also outlined in Chapter 2. Chapter 3 presents the synthesis and characterization of all the NPs studied in the current research work. Chapter 4 discusses the work related to in vitro studies conducted using the fluorescent dye doped silica NPs and quantum dot-cored NPs. Chapter 5 describes the particokinetic studies of gold and quantum dot-cored NPs in rat blood. The conclusions and the significance of this research work along with recommendations for future work are presented in Chapter 6.

CHAPTER 3
SYNTHESIS AND CHARACTERIZATION OF ENGINEERED NANOPARTICLES

The synthesis and characterization of the various engineered nanoparticles (NPs) of interest for this research work is described in this chapter. As outlined in the Research Approach, the various particles developed for this research effort are (i) fluorescent silica nanoparticles (FSNPs), (ii) colloidal gold spheres (G-), (iii) silica coated quantum dot-core NPs (QDS) and (iv) gold speckled silica coated quantum dot-core NPs (QDSG). In the first section, synthesis and bioconjugation protocols for these four NPs are presented. The second part of the chapter deals with characterization of the NPs. This involved particle size and shape, surface charge, and spectroscopic (absorbance and fluorescence) studies. The rationale was to choose the physicochemical properties of NPs that have been shown to influence their biological responses (Hardman 2006, Hoshino *et al.* 2004a, Nel *et al.* 2006, Oberdorster *et al.* 2005a, Oberdorster *et al.* 2005b, Ryman-Rasmussen *et al.* 2006). The last section discusses the challenges faced during the research effort of optimizing the QDSG synthesis protocol.

3.1 Synthesis and Bioconjugation Techniques

Most applications in nanobiotechnology demand a homogenous morphology and monodispersed particles, which generally leads to a more consistent set of physical, chemical and biological properties. A wide range of techniques have been developed in recent years, a few can partially, while others effectively control the size and shape of the synthesized NPs (Sau *et al.* 2001). Sol gel processing, which is one of the most commonly used techniques can produce NPs of sizes 1–20 nm with consistent composition and structure but with a variable degree of monodispersity (Dutta *et al.* In Review for Publication). In fact, the size variations between the particles can even vary to 20%; however, for best ‘nano-size’ related properties it is desirable that the variations are reduced to less than 5%.

Recently, the use of a reverse or inverted micelle based system for NP synthesis has been developed for better control on the size and stability of particles (Santra *et al.* 2001a, Santra *et al.* 2004b, Santra *et al*. 2001b). Reverse micelles, also called water-in-oil (W/O) microemulsion (ME) system, are an isotopic, thermodynamically stable environment made of a homogenous mixture of oil, water and surfactant molecules. The surfactant capped water droplets remain uniformly dispersed in the bulk oil phase and the water droplets serve as a tiny reactor for the synthesis of nanomaterials. Some of the advantages of the reverse microemulsion technique are that it does not require extreme reaction conditions such as high temperature or high pressure and has a better control over the morphology and dispersity of the final product. But a prime drawback is the notably small volume of output from this synthesis technique which makes it difficult to scale up the synthesis process. The size of the NP is controlled by varying the water to surfactant molar ratio (W_d). Continuous collision between the water nano-reactors due to Brownian motion leads to exchange between the short-lived dimers that lead to the formation of droplets (Santra *et al.* 2001a).

In the present study, we have used the sol gel technique to synthesize amorphous silica NPs (150 nm and above) and 15 nm colloidal gold NPs. The reverse micelle ME based technique was used for synthesizing amorphous silica NPs (below 150 nm), silica coated quantum dots (QDSS) and gold speckled silica coated quantum dot cored NPs (QDGS). The synthesis protocols of all the above-mentioned NPs are described below.

For bioimaging, it is highly desirable that the NPs are appropriately surface modified with targeting molecules. For example, for cancer imaging applications, it is necessary that cancer specific antibodies and folates are attached to the surface of the NPs to achieve tumor targeting properties. Usually the targeting molecules are not attached directly to the surface

of the NPs. An intermediate coupling molecule is used which is a surface-functional group on the NP and the other end of which is attached to the targeting molecules such as folate and anti-bodies. Firstly, the NP surface is functionalized with groups such as amines, carboxyls and thiols that can facilitate bioconjugation. Next, the bio-recognition molecules such as antibodies and folates are attached to the surface-functionalized NPs with the use of suitable chemistries like carbodiimide chemistry. These steps are usually carried out in aqueous based solutions. Finally, the bio-conjugated NPs have to be dispersed in suitable biological solvents (depending on the specific bio-imaging application) for practical applications.

3.1.1 Fluorescent Silica Nanoparticles (FSNPs)

As mentioned above, silica-based amorphous NPs for this research work were synthesized using two methods: (a) Stobers' method (sol gel technique) for 190 nm NPs (Stober *et al.* 1968) and (b) reverse ME technique for 100 nm NPs. The Stobers' method is generally used to produce large scale suspensions of sub-micron sized silica NPs while reverse microemulsion system yields monodisperse particles in the nano-sized regime. The particle diameter can be controlled by manipulating the process parameters like temperature, reagent concentration and water to surfactant ratio for reverse microemulsion technique only.

Unlike QDs and gold NPs, amorphous silica particles do not possess any inherent properties that can be exploited for imaging applications. In order to overcome this limitation, amorphous silica NPs are frequently doped with organic and inorganic fluorescent dyes that can be traced using fluorescent microscopy (Santra *et al.* 2005c, Santra *et al.* 2001a, Santra *et al.* 2004a, Santra *et al.* 2004b, Santra *et al.* 2001b). Moreover, fluorescent silica NPs have some important features (Qhobosheane *et al.* 2001, Santra *et al.* 2001a, Santra *et al.* 2001b) that make them attractive for bioimaging applications. First, excellent sensitivity can be achieved by incorporating thousands of dye molecules into a single NP system for

example dye doped silica NPs. Second, dye photostability is improved due to the protective encapsulation of fluorescent dyes by the host silica matrix. Third, the spectral characteristics of fluorophores remain intact in the host silica matrix, making them suitable for both *in vitro* and *in vivo* applications. Finally, fluorescent amorphous silica NPs may be more biocompatible, relative to other types of photostable labels such as QDs.

The synthesis protocols described in the following section provide details for the synthesis of amorphous silica NPs with different types of dyes incorporated into the silica matrix. The two dyes used for this research work are (a) fluorescein-isothiocyanate (FITC) which is an organic dye and (b) tris(2,2'-bipyridyl)dichlororuthenium(II) (Rubpy) which is a metallorganic dye. FITC was chosen on the basis that organic dyes are inherently biocompatible. However, in order to overcome the limited photostability (Santra *et al.* 2006) of FITC the metallorganic dye, Rubpy, was used as an alternative fluorescent dye.

3.1.1.1 Synthesis strategies: FSNPs

(a) Stobers' method. In the typical Stobers' method, alkoxysilane compounds (e.g. tetraethyl orthosilicate (TEOS), tetramethylorthosilicate (TMOS) and a variety of TEOS or TMOS derivatives) undergo base-catalysed hydrolysis and condensation reactions in ammonia-ethanol-water mixture, forming a stable alcosol. Following the Stobers' protocol (Stober *et al.* 1968) with a slight modification, fairly monodisperse organic dye doped fluorescent silica NPs have been synthesized for this research work. Since organic dyes are normally hydrophobic, doping them inside the hydrophilic silica matrix is not straightforward. Typically, a reactive derivative of FITC, amine-reactive fluorescein isothiocyanate, is first reacted with an amine containing silane compound, 3-aminopropyltriethoxy silane (APTS), forming a stable thiourea linkage. Then the FITC-APTS and TEOS are allowed to hydrolyze and condense to form FITC conjugated silica NPs.

Although the positively charged amine functional groups on the surface of the silica NPs facilitate bioconjugation in the next step, it also shifts the (negative) zeta potential towards zero. A zeta potential close to zero could lead to enhanced agglomeration. In order to reduce this possibility, 60 µl of a negatively charged silane agent, 3-(trihydroxysilyl) propyl methylphosphonate (THPMP) (Gelest, Inc., Morrisville, PA) was added at the end, to increase the zeta potential of the silica surface.

Using sol-gel techniques or Stobers' method, bulk amount of silica NPs can be produced in a typical laboratory setup. Initially, a stable 0.1M FITC-APTS conjugate is prepared by adding 69 mg APTS and 5.25 mg FITC and mixed together in 1 mL of absolute ethanol in dry nitrogen and stirred magnetically for 24 hours. This FITC-APTS solution is protected from light during reaction using an aluminum foil on and around the beaker and later stored carefully in order to prevent photobleaching. The FITC molecules were covalently conjugated to the silica particles in order to minimize dye leaching from the NPs.

To prepare the 190 nm fluorescent silica NPs using Stober's Method, 800 µL ammonium hydroxide (NH_4OH) was combined with 10 mL absolute ethanol in a 20 mL round-bottom flask with magnetic stirring. After 5 minutes, 400 µL TEOS and 200 µL of the 0.1M FITC-APTS conjugate were added, followed by 60 µL of THPMP after 30 min. Magnetic stirring was continued for 24 hours. All experiments were conducted at room temperature. After 24 hours, 10 mL of absolute ethanol was added to the solution and sonicated (Branson 1510, Kell-Strom, Wethersfield, CT) for 5 minutes. These amine modified NPs were washed thoroughly four times with ethanol and two times with DI water by ultra-centrifugation (Eppendorf Centrifuge 5804 R, Eppendorf North America, Westbury, NY) at 5000 rpm for 30 minutes per wash. Vortexing (Vortex Genie 2, A. Daigger and

Company, Vernon Hills, IL) and ultrasonication techniques were applied between two successive washes. The washed FSNPs were stored away from light till further use.

In the case of Rubpy-doped particles, first a stock solution of 0.1 M Rubpy was prepared by adding 74.8 mg in 1 mL of de-ionized water. To synthesize the amorphous silica NPs doped with Rubpy, everything else remained the same as above except 100 µL of this stock solution and 100 µL of APTS was added to the mixture (instead of 200 µL of 0.1M FITC-APTS) followed by 60 µL of THPMP after 30 min and stirred for 24 hours. The procedure for washing the particles remained the same as described above.

(b) Reverse microemulsion method. The reverse or water-in-oil (W/O) microemulsion technique was used to synthesize 100 nm amorphous silica NPs, inorganic and organic dye doped as well as NPs with no dyes. A schematic representation of the synthesis of dye doped silica NP using reverse-microemulsion technique is shown in Figure 3-1. The W/O microemulsion system was created by adding 0.44 g of de-ionized water to 7.7 mL cyclohexane (Sigma-Aldrich, St Louis, MO) along with a 1.77g of the surfactant Triton X-100 (Sigma-Aldrich (St Louis, MO) and 1.6 mL of the co-surfactant n-hexanol (Sigma-Aldrich (St Louis, MO). This solution was magnetically stirred for 15 minutes resulting in the formation of nano-sized water droplets. After fifteen minutes, 50 µL of the 0.1M FITC-APTS conjugate was first added; followed by the addition of 100 µL TEOS five minutes later. The hydrolysis of the silane reagents was then initiated by the addition of 100 µL NH4OH. After 30 min, 15 µL THPMP was added dropwise and stirring was continued for twenty-four hours. The 100 nm dye doped amorphous silica NPs were formed inside the water droplet in the W/O microemulsion. These particles were then washed with a procedure similar to the one described above for NPs made by Stober's method.

The synthesis of Rubpy-doped FSNPs was carried out using the method described above, except 40 µL of 0.1M Rubpy stock solution and 25 µL of APTS was added to the mixture (instead of 50 µL of 0.1M FITC-APTS) followed by 15 µL THPMP after 30 minutes and stirred for 24 hours. The procedure for washing the NPs also remained the same as described before. The synthesis of FSNPs of both sizes using both techniques was repeated four times to verify the reproducibility of the synthesis technique and consistency of the physicochemical parameters of the product during characterization.

3.1.1.2 Surface functionalization and bioconjugation: FSNPs

In order to facilitate the process of targeting cancer cells in the present study, the amorphous silica NPs were conjugated to folic acid molecules. For survival and proliferation, most animal cells require the vitamin folate. Folic acid is an essential component for nucleotide synthesis. As animal cells cannot synthesize folic acid by themselves, they express folate receptors on their surface for capturing exogenous folates (Antony 1992, Santra *et al.* 2005c). Neoplastic cells such as breast adenocarcinoma (Antony 1992, Ross *et al.* 1994, Santra *et al.* 2005c), lung adenocarcinoma (Franklin *et al.* 1994), oral carcinoma (Ross *et al.* 1994) and pituitary adenoma (Evans *et al.* 2003) overexpress folate receptors because they proliferate rapidly. Folic acid receptors are therefore considered as one of the significant tumor biomarkers for these neoplasms. Clinically challenging brain tumors such as malignant gliomas may also overexpress folate receptors, however adequate experimental evidence in this favor is currently unavailable.

Folate enables a “Trojan horse” strategy, fooling tumor cells into taking up a folate molecule linked to an imaging or therapeutic agent (Antony 1992, Leamon & Low 1991) This is called folate-mediated up-take (endocytosis). Covalently coupling folate to various

molecules yields a conjugate that can be endocytosed into tumor cells. Examples (Santra *et al.* 2005c) include radiopharmaceutical agents, chemotherapeutic agents, antisense oligonucleotides and ribozymes, proteins and protein toxins, immunotherapeutic agents, drug molecule loaded liposomes and plasmids, all of which have been successfully delivered to cancer cells via folate mediated transport mechanisms. Phase I and II clinical studies for the first folate-containing imaging agent were initiated in 1999, and clinical trials of folate-conjugated therapeutic agents may soon follow. Folate-mediated macromolecule delivery, such as liposome-DNA complexes (<200 nm) and monoclonal antibodies have been demonstrated *in vivo*, suggesting that larger molecules can be targeted to tumors. Similarly, successful targeting of folate immobilized NPs carrying contrast agents and drugs to tumor cells have been recently reported.

Due to the presence of APTS and THPMP on the surface, the amorphous silica NPs have an amine-modified surface that is used to attach the folic acid molecules. The structure of folic acid contains two independent fluorescent moieties, p-aminobenzoic acid (PABA) and methylpteridin (MTE) as shown in Figure 3-2. Folic acid was covalently attached to the positively charged amine functional groups on the surface of the silica NPs using conventional carbodiamide coupling chemistry as shown in Figure 3-3. As per published protocols (Santra *et al*. 2005c), two solutions were prepared separately. Solution I was prepared by adding the following and magnetically stirring for one hour:

1. 10mM folic acid (7.0 mg folate in 1.0 mL dimethyl sulphoxide (DMSO) in a glass container,
2. 4.1 mg of N-Hydroxy Succinamide (NHS) in 1.5 mL de-ionized water and
3. 34.2 mg of 1-ethyl-3-(3-dimethylaminopropyl) carbodiimide hydrochloride (EDC) in 1.5 mL de-ionized water.

Solution II contained 20 mg amine modified FSNPs in 1.0 mL DMSO to which 2 μL triethylamine was added in a glass container. Both solutions were combined in a glass beaker and sonicated for five minutes, then stirred magnetically for one hour to obtain folate-conjugated (folated) FSNPs. The NPs remained well dispersed in DI water for several hours without any noticeable settling. These particles were washed by centrifuging five times with DI water and stored and protected from light until further use. Following synthesis the NPs were first characterized and then used for *in vitro* experiments to show their potential as fluorescent probes for bioimaging applications. Results from characterization experiments conducted on these particles have been described later (Section 3.2.1).

3.1.2 Colloidal Gold Nanoparticles (NPs)

Gold NPs of 15 nm particle diameter were prepared using sol gel technique. This is a widely used method for the synthesis of gold NPs, or what are more popularly known as gold colloids, and was chosen primarily for its simplicity and ease for relatively large-scale synthesis of gold NPs.. A detailed description of the synthesis protocol used is given below.

3.1.2.1 Synthesis strategy: Gold NPs

10 mL of 2 mM Gold Tetrachloride ($HAuCl_4$) solution (Sigma-Aldrich, St Louis, MO) was added to 10 mL of nanopure de-ionized (DI) water (NANOpure, Barnstead International, Dubuque, Iowa) in a 100 mL beaker. This solution was boiled on a hot plate while stirring using magnetic stir bar. When the solution started to boil, 2 mL of 1% sodium citrate solution (Sigma-Aldrich, St Louis, MO) was added. Over the next few minutes the color of the boiling solution progressively changed from light yellow to transparent to light blue or pale purple to deep purple to deep red. The color changes were indicative of the nucleation and growth of colloidal gold particles (Huo & Worden 2007). Boiling was continued for ten additional minutes and the solution is then brought down to room

temperature. This solution was left on a magnetic stirrer for 24 hours. This was followed by addition of de-ionized water to bring the total volume of the solution to 20 mL. Ultra-centrifugation of this solution was carried out at 6000 rpm for 15 minutes. The supernatant was carefully removed with a micro-pipette and the centrifugation process was repeated. The resulting product, a dark colored solution containing 15 nm gold spheres is stored till further use.

3.1.2.2 Surface functionalization and bioconjugation: Gold NPs

Zeta potential measurements showed that the 15 nm bare gold spheres (G-) exhibit a negative charge on the NP surface. As mentioned in the Research Approach, one of the objectives of this research effort is to study the effect of surface functionalization of the gold NPs on the blood clearance behavior in rats. For this purpose, the negatively charged gold colloids were surface-modified with appropriate functional groups to obtain positively and neutrally charged gold particles. The bare gold colloids were used as the negatively charged particles in the studies. Near neutral charges on the gold NPs was obtained by pegylation and a positively charged surface was obtained by using cysteine-amine chemistry to conjugate amine functional groups on bare gold NPs.

Pegylation is a process of attaching polyethylene glycol (PEG) on the surface of a particle. In order to synthesize PEG-conjugated gold NPs (GP), thiol-terminated methoxypoly (ethylene glycol) (mPEG-SH) of 5000 molecular weight was used (Sigma-Aldrich, St Louis, MO). The solution containing the bare 15 nm colloidal gold NPs was increased in concentration to 200 mg/L by centrifugation. 15 mL of this solution was added to 75 µL of 1 mM mPEG-SH-5000 in a 20 mL beaker. The solution was magnetically stirred for 12 hours after which it was washed twice using de-ionized water by centrifugation at

6000 rpm for 15 minutes, the supernatant was removed and the pegylated gold particles collected and stored in bottles inside the refrigerator.

To synthesize positively charged gold NPs (G+), first, a stock solution of 0.00001N cysteine-amine in aqueous solution was prepared. 1 mL of this stock solution was added to 8 mL of the bare colloidal NP solution at a concentration of 1000 mg/mL. It was magnetically stirred for 12 hrs followed by washing with de-ionized water by centrifugation at 6000 rpm for 15 minutes. The supernatant was carefully removed and the positively charged amine-modified gold NPs collected and stored till further use. The protocols for the synthesis of all three gold NPs (G-, G+ and GP) were repeated four times to confirm the reproducibility of the technique and the consistency of the physicochemical parameters of the NPs.

3.1.3 Silica Coated Quantum Dot Nanoparticles (QDS NPs)

A variety of techniques have been reported in the literature to synthesize QDs of different elemental compositions and sizes. Some of these techniques have been described in chapter one. In this research work, a modified version of Yang *et al.*'s (Yang & Holloway 2004, Yang *et al.* 2004a, Yang *et al.* 2004b) synthesis protocol, using the reverse-microemulsion technique, was employed for the synthesis of silica coated quantum dots (QDS). The modified synthesis protocol is described briefly below.

3.1.3.1 Synthesis strategy: QDS NPs

Reverse micelle mediated CdS:Mn/ZnS QD synthesis. The reverse-microemulsion (ME) technique described at the beginning of the chapter can also be used to synthesize QDs, as reported by Yang *et al.* (Yang *et al.* 2004b). This is a robust method that has been used at room temperature and normal atmospheric pressure for the synthesis of manganese (Mn) doped cadmium sulfide (CdS) core and zinc sulfide (ZnS) shell (CdS:Mn/ZnS) quantum dots. The ME system employed in the present study, consisted of AOT (dioctylsulfosuccinate

sodium salt) as a surfactant and heptane as the oil. The bright orange emitting CdS:Mn/ZnS quantum dots had an average quantum dot size of 10 nm, and were determined to be highly photostable. The protocol was modified to apply a post coating of amorphous silica layer to prevent the possibility of any cadmium leaching (Derfus *et al.* 2004b) into the physiological environment. A schematic for the QDS synthesis process is shown in Figure 3.4.

Briefly, cadmium acetate or $Cd(CH_3COO)_2.2H_2O$, manganese acetate or $Mn(CH_3COO)_2$, zinc acetate or $Zn(CH_3COO)_2$, dioctyl sulfosuccinate, sodium salt (AOT), heptane, tetraethyl orthosilicate (TEOS) and NH_4OH (30% by wt.) (Sigma Aldrich, St Louis, MO) were used to prepare three aqueous solutions in 20 mL vials. Solution I contained 0.24 g of cadmium acetate and 0.0031 g of manganese acetate in 9 mL of de-ionized water. Solution II contained 0.2812 g of sodium sulphide in 5.4 mL of de-ionized water. Solution III contained 0.2642 g zinc acetate in 5.4 mL of de-ionized water. All three solutions were magnetically stirred for fifteen minutes to dissolve all solutes.

Three ME systems were then prepared in three different conical flasks. Flask A contained 4.46 g of AOT in 100 mL of heptane. One-fifth of the solution I was added to Flask A and left to magnetically stir for 30 minutes. Flask B contained 13.38 g of AOT in 300 mL of heptane. All the contents of solution II were added to Flask B and left to stir for 30 minutes. After 30 minutes, the contents of Flask A and Flask B were mixed together and stirred for three hours. The color of the solution changes to yellow and the flask was enclosed in an aluminum foil to shield it from light. Flask C contained 13.38 g of AOT in 300 mL of heptane. The contents of solution III were added to Flask C and left to stir for 3 hours. The contents of Flask C were introduced into the beaker containing the mixture of Flask A and

Flask B, using a variable flow mini-pump at 1.5 mL per minute. After this addition, the resulting solution was left to stir for 30 minutes to obtain the CdS: Mn / ZnS core-shell QDs.

In order to apply an amorphous silica coating on the QDs, 2.5 mL of TEOS was added to the solution and allowed to stir for fifteen minutes. 1.5 mL of NH_4OH was added to a ME system made of 3.685 g of AOT in 82.5 mL of heptane. This ME system was added to the QD-TEOS solution and left to stir for 24 hours. NH_4OH initiated the hydrolysis of TEOS and condensation reaction to form a silica coating over the QDs. Since the reactions take place in a ME system, a relatively long reaction time of 24 hours was required for achieving the desired coating.

In order to aid the bioconjugation process, the outer silica surface needs to be functionalized with amine functional groups. Consequently, 1.25 mL of TEOS and 1 mL APTS was added to the silica coated QD solution after twenty-four hours. This was followed by the addition of another ME system of NH_4OH, which was composed of 1.5 mL of NH4OH added to 3.685 g of AOT in 82.5 mL of heptane. This mixture was left to stir for 24 hours. The amine-modified silica coated quantum dots (QDS) were precipitated by the addition of a 25 mL methanol per 25 mL of the QDS solution. The particles were then washed by centrifugation at 6000 rpm for 30 minutes. This was followed by two additional washes in methanol and 2 washes in de-ionized water with vortexing and sonication in between each wash. The particles were then stored away from light till further use.

The QDS NPs were used as control particles in this research work. In addition to characterizing the QDS NPs, further preliminary leaching studies were carried out in cell media under normal (25°C and pH 7.4), acidic (25°C and pH 3) conditions, and at elevated temperature (57°C and pH 7.4) to emulate different environments inside the cells like the

acidic pH 5 of lysosome (Kobayashi *et al.* 2008, Yamamoto 2004) and elevated temperature (Levine & Robbins 1970). Analytical detection techniques were used to check the possibility of any cadmium leaching from the quantum dots inside the biological media. An Inductively Coupled Plasma Mass Spectrometer was used for cadmium detection and quantifying in the supernatant of A549 cells. The results of this leaching study have been included later in this chapter.

3.1.4 Gold Speckled Silica Coated Quantum Dot Nanoparticles (QDSG NPs)

In order to conjugate gold speckles on the QDS NPs, two separate ME systems are prepared. ME I was prepared by adding 4.8 mL of 5% HAuCl4 solution (in de-ionized water) to 13.38 g of AOT in 300 mL of heptane. ME II was prepared by adding 2.4 mL of 0.05M hydrazine to a solution of 13.38 g of AOT in 300 mL of heptane.

The QDS NPs were first prepared using the exact same protocol described above except that they were allowed to remain in the ME system at the end. This means, that the NPs were not precipitated using methanol and the washing steps described in the previous section were not carried out. In order to conjugate the gold speckles on the QDS NPs, 200 mL of this QD ME solution is added to 200 mL of ME I and stirred for 3 hours. After this, 200 mL of ME II was added and the set up is left on a magnetic stir plate for 48 hours. This leads to the formation of gold speckles on the amine-modified silica coated QDS NPs. The particles were then precipitated using methanol, washed three times with methanol and two times with de-ionized water, as described for the QDS NPs, and stored away from light till further use. A schematic for the QDSG synthesis process is summarized in the flowchart shown in Figure 3.5. A schematic representing the QDSG NPs structure is shown in Figure 3.6.

3.2 Characterization of Nanoparticles (NPs)

The NPs synthesized for this research effort and described in the previous section were characterized for particle size and shape, surface area and charge, absorbance and fluorescence spectroscopy. The following section describes the characterization results of each set of NPs.

3.2.1 Fluorescent Silica Nanoparticles (FSNPs)

The FSNPs were characterized for particle size, shape, surface charge, absorbance and fluorescence spectroscopic properties.

3.2.1.1 Particle size measurements

Particle size measurements for FSNPs in the dry state were conducted using transmission electron microscopic (TEM) imaging using a Hitachi H-7000 microscope (Japan). For TEM sample preparation, a drop of the FSNPs dispersed in denatured ethanol solution was directly placed onto a carbon-coated copper grid (200 mesh). The average particle size was measured using Image Tool software (Wilcox *et al.* 1995). The average size was obtained based on the diameter measurement of 100 particles. Particle size of FSNPs synthesized using Stober's method was measured to be 190±30 nm whereas FSNPs synthesized using reverse ME method were 100±10 nm in size, (Figure 3.7a and b respectively).

Particle size in de-ionized water was also measured using Coulter light scattering technique (Coulter LS 13 320), as this would reflect the state of particle dispersion in biological solutions such as cell media. The samples were dispersed in de-ionized water by five minutes each of sonication and vortexing. Based on Coulter data, ME mediated FSNPs were found to be monodispersed and the particle size was calculated to be 104 nm, Figure 3.8b, in DI water. Coulter data also showed that NPs produced using Stober's method were

monodisperse with average particle size of 221 nm, Figure 3.8a, in DI water. Both TEM and Coulter data were in good agreement, suggesting that particles remained well dispersed in DI water. Coulter data also confirmed the effectiveness of the surface modification protocol using THPMP as a dispersant to improve NP dispersibility in water.

For the *in vitro* studies (Chapter 4), the FSNPs were pre-conditioned with cell media (RPMI 1640) before dosing the cells. It was therefore important to measure particle size in the cell media. The samples were dispersed in cell media by five minutes each of sonication and vortexing. Coulter measurements showed that particles tend to agglomerate in cell media (Figure 3.9). The larger 190 nm NPs (Figure 3.9a) exhibited more aggregation as compared to the smaller 100 nm NPs (Figure 3.9b). The apparent size of the smaller particles in the cell media was found to be in the range of 40 nm to 20 microns and the larger particles exhibited an apparent size range of 2 to 200 microns. It was found that the NPs can be usually dispersed by increasing the time of sonication and vortexing prior to particle size measurements. However, excessive application of these processes could lead to disintegration of the proteins constituting the cell media. This would amount to changing the basic physical, chemical and/or biological characteristics of the media. Thus, for this research work the NP dispersion was attempted by limiting sonication and vortexing each to 5 minutes prior to particle size measurements using Coulter light scattering technique.

3.2.1.2 Surface charge measurements

The surface charge of a particle in a suspension determines the dispersibility of the particles and the stability of the suspension. Zeta potential is a measure of the surface charge of the particles in a particular suspension. Thus the magnitude of zeta potential of the suspension is an indication of its potential stability. If the particles have an effective positive or negative surface charge, they tend to repel each other and thus preclude the possibility of

agglomeration. Generally, particles with zeta potential values greater than +20 mV or lesser than -20mV are expected to form stable suspensions.

Non-amine-modified (bare) silica NPs and amine-modified silica NPs with and without THPMP were suspended in aqueous solutions at 200µg/mL and characterized for surface charge in Brookhaven Zeta PALS. The bare silica NPs had a zeta potential value of -35.73 ± 6.3 mV and, as expected, and remained well dispersed in water. The amine-modified silica NPs without THPMP were found to have a zeta potential of 0.39 ± 0.11 mV and this caused the particles to agglomerate in water. In order to prevent agglomeration, THPMP was added to these particles, as discussed before. This caused the zeta potential of the particles to increase to a value of -31.27 mV and prevent particle agglomeration.

3.2.1.3 Absorbance and fluorescence spectroscopy

The ultraviolet-visible (UV-Vis) absorption and steady-state fluorescence spectra for pure folic acid, aminated FSNPs and folated FSNPs were recorded in de-ionized water. The absorption spectra were recorded on a spectrophotometer (Shimadzu UV-Vis model 2410 PC) in de-ionized water. Steady-state fluorescence excitation and fluorescence emission spectra were recorded on a spectrofluorometer (Fluorolog Tau-3, Jobin Yvon Spex Instruments, S.A. Inc. equipped with a 450 W xenon lamp as an excitation source) to confirm the presence of both folic acid and FITC in aminated FSNPs. All measurements were performed at room temperature and all experimental solutions were prepared in de-ionized water.

Folic acid contains two independent fluorescent moieties, p-aminobenzoic acid (PABA) and methylpteridin (MTE) (Figure 3.2). PABA absorbs at 265 nm and emits at 336 nm, and its emission is highly pH dependent (Tanojo *et al.* 1997). MTE has two absorption bands at 275 nm and 352 nm and it emits at 447 nm (Espinosa-Mansilla *et al.* 1998). In the

following sections, spectroscopic characterization of folate, amine-FSNPs and folate-FSNPs will be discussed.

The absorption spectra of folate, amine-FSNPs and folate-FSNPs are shown in Figure 3.10. Folate showed a combined absorption from PABA and MTE moieties. The absorption band maxima appeared at 280 nm and 355 nm for folate (Figure 3.10a). Folate immobilized FSNPs (Figure 3.10c) showed the absorption maximum at 280 nm with two shoulders at longer wavelengths (355 nm and 490 nm). The absorption band at 280 nm and the appearance of shoulder at 355 nm confirmed the presence of folate on folate-FSNPs. As expected, amine-FSNPs did not show any folate characteristic peaks or shoulder in this region but a shoulder at around 490 nm (Figure 3.10b). The appearance of 490 nm shoulder is due to the absorption of FITC molecules that are doped in FSNPs.

The fluorescence excitation and emission spectra of folate are shown in Figure 3.11. Upon excitation at 280 nm, folate showed dual emission at 355 nm and 447 nm, which corresponds to the emission from PABA and MTE, respectively (Figure 3.11b). When excited at 355 nm, folate showed the only emission from the MTE moiety at 447 nm, which is similar to what was reported in the literature (Santra *et al.* 2005c) (Figure 3.11a). Fluorescence excitation spectra of folate, when recorded at 447 nm emission, showed two excitation peaks at 280 nm and 355 nm due to the MTE moiety (Figure 3.11d). Similarly, folate excitation spectra recorded at 355 nm emission showed an excitation peak at ~289 nm (Figure 3.11c), which is due to the PABA moiety. Folate emission band at 447 nm was found stronger than the 355 nm emission band (Espinosa-Mansilla *et al.* 1998, Santra *et al.* 2005c). We, therefore expect to see the 447 nm emission band in folate-FSNP.

Multiple fluorescence bands appeared from folate-FSNPs due to the presence of both FITC and folate. When excited at 492 nm, folate-FSNPs showed emission band maximum at 512 nm, which is the characteristic emission of FITC molecule (Figure 3.12a). The excitation spectra recorded at 512 nm emission showed a sharp peak at 492 nm and a broad band at 360 nm (Figure 3.12c). The appearance of 360 nm emission is due to the MTE moiety of folate. When excited at 355 nm, folate-FSNPs showed dual emission at 450 nm and 509 nm (Figure 3.12b). This is due to the fact that the excitation at 355 nm caused excitation of both folate and fluorescein molecules. The 450 nm and 509 nm emission bands, which are close to 447 nm and 512 nm emission bands, were therefore assigned to folate and FITC emission, respectively. The observation of folate emission from folate-FSNPs at 450 nm confirmed the successful folate immobilization onto the FSNPs. The excitation spectra recorded at 447 nm emission showed band maxima at 375 nm (Figure 3.12d). The 375 nm excitation band is assigned to the folate. The spectral shift of characteristic folate excitation and emission band maxima in folate-FSNPs is due to the folate immobilization, confirming the fact that the microenvironment of immobilized folate is different from free folate molecules present in the solution.

3.2.2 Colloidal Gold Nanoparticles (NPs)

The results of particle characterization carried out for all three gold particles: (a) bare gold (G-), (b) aminated gold (G+) and (c) pegylated gold (GP) are discussed in this section. As before, the particles are characterized for size, shape, surface charge (zeta potential), absorbance and fluorescence spectroscopy.

3.2.2.1 Particle size measurements

Gold NPs were synthesized for a target particle size of 15 nm. The samples were dispersed in de-ionized water using five minutes each of sonication and vortexing. The

particle size measurements were carried out using a Differential Sedimentation CPS Disc Centrifuge^{TM}. The particle size measurements for the gold NPs in de-ionized water showed a narrow size distribution range of 15±5 nm. It indicated that the particles were well dispersed without any significant agglomeration. The samples were dispersed in cell media by five minutes each of sonication and vortexing. The particle size measurements in cell-media showed a wide range of size distribution of 15 nm to 350 μm. In the context of the size distribution in de-ionized water, it can be concluded that the particles tend to agglomerate in cell media. This could possibly be due to change in the surface charge of the NPs as a result of adsorbed proteins from the biological media onto the particle surface.

The shape of the gold NPs was visualized using Transmission Electron Microscopy (JEOL TEM JEM-200CX). The TEM image in Figure 3.13 indicated that although not very monodisperse, the particles are spherical in shape.

3.2.2.2 Surface charge measurements

The zeta potential values of the three particles were measured using a Brookhaven Zeta PALS. The values obtained were -34.5 ± 7.8 mV for G-, +24 ± 5.8 mV for G+ and -5 ± 1.9 mV for GP particles. These values clearly confirmed the fact that the surface functionalization of the bare gold NPs achieved the desired results.

3.2.2.3 Absorbance and fluorescence spectroscopy

The ultraviolet-visible (UV-Vis) absorption and steady-state fluorescence spectra for gold NPs dispersed in de-ionized water were recorded at room temperature on a fluorescent plate reader using the Softmax Pro V5 software. The results of absorbance spectroscopy of the particles are shown in Figures 3.14. It has been reported that 15 nm gold NPs absorb light at 520 nm (Maye *et al.* 2000) and there is a peak in the region in the absorbance spectra in Figure 3.14 which confirms that the particles are indeed 15 nm in size. Gold NPs do not

possess any inherent fluorescent property. Therefore, as expected the fluorescent spectra of gold NPs (not shown) only showed a peak at 470 nm, which was identified as the first harmonic peak of the Raman spectra of water (Frost *et al.* 2006).

3.2.3 Silica Coated Quantum Dot Core Nanoparticles (QDS and QDSG NPs)

The silica coated quantum dot (QDS) and gold speckled silica coated quantum dot (QDSG) NPs were characterized for size, shape, surface area, surface charge (zeta potential), absorbance and fluorescence spectroscopy.

3.2.3.1 Particle size measurements

The QDSG and QDS NPs were synthesized for a target particle size of 15 nm. In order to determine their actual particle size, the particle size measurements were carried out using the Differential Sedimentation CPS Disc Centrifuge^{TM}. The QDSG and QDS samples were dispersed in de-ionized water by sonication and vortexing for five minutes each before the particle size measurements were conducted. It was evident that there was no variation in the particle size due to the conjugation of gold specks on the QDS particles. TEM image of QDSG NPs in the dry state is shown in Figure 3.15. The sample for TEM images was prepared in the same way as described earlier for FSNPs.

3.2.3.2 Surface area measurements

The BET (Brunauer, Emmett and Teller) method was used to measure the specific surface area of QDS and QDSG NPs using the Quantachrome Autosorb IC-MS. In order to measure the specific surface area, 1 mg of each of the NPs as dispersed in ethanol were placed inside a vacuum chamber and dried. The values obtained for QDS and QDSG were 151.2 and 229.7 m^2/gm respectively.

3.2.3.3 Surface charge measurements

The zeta potential values for the QDS and QDSG NPs were measured using a Brookhaven Zeta PALS. The values of zeta potential measurements were 6.3 ± 2.9 mV for QDS and 4.1 ± 1.7 mV for QDSG particles respectively. Therefore, it was not possible to draw any conclusive evidence regarding the effect of additing the gold speckles on the positively charged aminated silica coating on the QDS particles. As bare gold has a negative surface charge, the addition of the specks may have caused a slight drop in the zeta potential value in the QDSG NPs.

3.2.3.4 Absorbance and fluorescence spectroscopy

The ultraviolet-visible (UV-Vis) absorption and fluorescence spectra for QDSG and QDS NPs in de-ionized water were recorded at room temperature on a fluorescent plate reader using the Softmax Pro V5 software. The absorbance and the fluorescence spectra of QDSG and QDS are shown in Figure 3.16 to 3.18.

The absorption spectra of bare gold NPs (Figure 3.14) show a peak at 530 nm, near the characteristic wavelength of 520 nm of gold NPs. From the literature (Huff *et al.* 2007a, Huff *et al.* 2007b, Tong *et al.* 2007), it is known that gold nanorods have a characteristic peak maxima at 790 nm. The absorbance spectra for QDSG (Figure 3.16) show a shoulder at 530 nm and another absorption maximum at 790 nm. The first shoulder at 530 nm and the absorption peak at 790 nm belong to the gold specks with possible nanosphere and nanorod shapes on the surface of the particle.

The fluorescence excitation and emission spectra of QDSG and QDS are shown in Figure 3.17 and Figure 3.18 respectively. Both NPs display the quantum core spectral characteristics, when excited at 355 nm, emission spectra of both NPs showed a peak

maxima at 590 nm from the QDs, with a small shoulder at 430 nm which is due to the excitation wavelength and the first harmonic peak in the Raman spectra of water.

The absorbance spectra taken between 300 nm and 800 nm confirmed the absence and presence of gold specks on the QDS and QDSG NPs respectively. On the other hand, the fluorescence spectra (emission spectra taken at the excitation wavelength of QDS at 355 nm and excitation spectra taken at the emission wavelength of QDS at 590 nm) confirmed the fluorescent properties of the quantum dot core for both the particles. The absorbance and fluorescence measurements on the particles also confirmed that neither the gold specks nor the quantum dots had quenched one another and the particle synthesis had the desirable optical properties.

3.2.4 Leaching Studies of Silica Coated Quantum Dot Nanoparticles (QDS NPs)

As cadmium and most of the heavy metal constituents of QDs are extremely toxic and undesirable to the physiological environment, any possibility of metal leaching is one of the biggest challenges for the use of QDs for bioimaging applications. As mentioned before, preliminary leaching studies of QDS NPs were carried out to determine whether or not cadmium is leaching out through the silica coating of the NPs.

Phosphate buffer saline (PBS) solution is a biological medium frequently used to inject test samples in animal studies. The leaching studies were carried out by dispersing the particles in PBS solution at two different pH values, 3 and 7.4, and two different temperatures, 25°C and 57°C. The low pH value of 3 and a high temperature of 57°C were chosen to simulate the highly acidic and elevated temperatures inside an abnormal cellular environment.

Stock solutions of the QDS NPs were prepared in PBS solution at concentrations of 100 and 1000 μg/mL. Four six-well plates were used for the experiment. Plate A contained

two wells each with 2 mL of 100 μg/mL QDS solution, another two wells each with 2 mL of 1000 μg/mL QDS solution and the remaining two wells contained 2 mL of pure PBS solution (as controls). The PBS solution maintains a pH value of 7.4 and Plate A was maintained at room temperature (25°C). Plate B has exactly the same contents as Plate A except it was maintained at 57°C. Plate C initially had identical contents as Plate A. The acidity of all the wells was decreased to pH value of 3 by the addition of a few drops of hydrochloric acid. The content of Plate D was identical to that of Plate C but was maintained at 57°C. All four plates were placed in an incubator for 72 hours.

The samples were taken out after 72 hours and centrifuged at 4000 rpm for 30 minutes. The supernatant from each well was then collected and acid-digested by adding concentrated nitric acid. These samples were then diluted with de-ionized water and made up to 5 mL. These samples were then analyzed in ICP MS to detect cadmium.

The ICP MS analysis results for the samples from Plate A, B and C yielded cadmium levels of less than 1 part per billion (ppb) and the sample from Plate D showed a cadmium level of 10 ppb. The normal level of cadmium in human body is 0.5 ppb (Godt *et al.* 2006). The detected amount of cadmium in the samples was assumed to be within the biological error with minimum cadmium leaching from the QDS NPs in PBS solution incubated for 72 hours.

3.3 Challenges in QDSG NP Synthesis

This following section presents the challenges that were encountered during the development of the synthesis protocol for the novel QDSG NPs. Most challenges were overcome except for one, which has been listed as a part of the future work in Chapter 6.

3.3.1 Optimization of Quantity of Gold and Thickness of Silica Coating

The synthesis protocol for QDSG and QDS NPs described (Sections 3.1.3 and 3.1.4) was a novel route developed as part of this research work. During synthesis of QDSG NPs, the amount of silica and gold had to be optimized so as to obtain the right fluorescence and absorbance characteristics for the NPs. As will be shown in this section, excess of gold speckles on the surface of silica in QDSG NPs could lead to quenching of the fluorescence properties of the particle. But reducing the gold speckles too much would make the hyperthermic aspect of the particles less effective. Therefore, an optimized amount of gold speckles need to be conjugated to the silica surface of the QDS NPs so that the resultant QDSG NPs possess both fluorescence and hyperthermic properties.

Two different methods were conceived to obtain optimized fluorescence and hyperthermic properties. The first method was to vary the amount of gold on the silica coating. The second method was to increase the spacing between the QD-core and gold speckles. The rationale behind the choice of the second method is that the quenching of the fluorescence properties by gold can be reduced by increasing the spacing between the QD-core and gold speckles (Santra *et al.* 2006).

In the first method, the amount of gold was varied by adding different concentrations of $HAuCl_4$ solution, while keeping all other parameters constant. The different concentrations of $HAuCl_4$ solutions that were used for the study were 0.1, 0.2, 0.3, … , 1.0, 2.0, 3.0, … , 6.0, 10.0%. The NPs thus obtained were characterized for absorbance, (Figure 3.19), and fluorescence (Figure 3.20) spectroscopy. From the absorbance spectra in Figure 3.19, it can be concluded that an increasing concentration of $HAuCl_4$ leads to an increased deposition of gold speckles on the silica coating to form the resulting QDSG NPs. The intensity of absorbance was low for HAuCl4 concentration values of 1% and below and

increases considerably for values 3, 5 and 10%. The fluorescence spectra in Figure 3.20 show the quenching characteristics of increased amount of gold speckles on the QDSG NPs. The fluorescence intensity of the QD-core is highest for 0.1% of $HAuCl_4$ and was lowest for 10%. By comparing the two curves the 3–5% range was chosen as the optimized concentration of $HAuCl_4$ solution.

In the second method, the thickness of the silica shell on the QD-core can be varied by varying the amount of TEOS added. Two different amounts of TEOS were used for this study: 1.25 mL and 2.5 mL. All other synthesis parameters were kept constant. From the fluorescence spectra it was found that the fluorescence intensity was higher for the particles synthesized with 2.5 mL TEOS than with 1.25 mL. The absorbance spectra for these same particles showed no significant difference. These observations support the conjecture that increasing the spacing between QD-core and gold speckles leads to improved fluorescence properties. However, increasing the thickness of silica coating makes the particles larger in size. Therefore, the 2.5 mL TEOS addition was accepted for the synthesis of the particles.

The absorbance spectra in Figure 3.16 and the fluorescence spectra in Figure 3.17 for QDSG (that were discussed in Section 3.2.3) are for particles that were synthesized with an optimum $HAuCl_4$ concentration of 5% and TEOS volume of 2.5 mL.

3.3.2 Gold Speckle Conjugation in Microemulsion

The protocol for gold speckles' conjugation on the outer silica coating was described in Section 3.1.4. Briefly, the two reagents for gold speckle formation namely HAuCl4 and hydrazine were prepared in two different microemulsion systems and introduced to the quantum dots, which were suspended in another microemulsion system. This process produced the QDSG NPs with the best fluorescence and absorbance properties. However, the final process was settled upon after trying out three other processing routes. In the first trial,

no microemulsion systems were employed. Both the reagents were added directly to the washed quantum dot NPs that were dispersed in de-ionized water. In the second trial, the two reagents were added to quantum dot that were suspended in the microemulsion system (in which they were synthesized). In the third trial, $HAuCl_4$ was in a microemulsion system while hydrazine was added directly to quantum dots in microemulsion system. It was observed from the fluorescence and the absorbance spectra (not shown) that with each trial both the properties improved considerably. The improvement is probably due to the better control of the reactions occurring in a microemulsion system instead of direct addition (Zhang *et al.* 2007).

3.3.3 Addition of Hydrazine

Earlier in this chapter, it was mentioned that the addition of hydrazine (using a ME system) was carried out after three hours after the addition of $HAuCl_4$. In some of the early trials, hydrazine was added immediately after the addition of $HAuCl_4$. From the fluorescence and absorbance spectra (not shown) of the particles synthesized with these two different times of hydrazine addition, it was found that the delayed addition resulted in superior absorbance properties. The fluorescence properties remained unchanged for the NPs at both times of hydrazine additions. A possible explanation for this observation could be that the delay in addition allowed more time for the $HAuCl_4$ to enter the nanoreactor (water droplets). This led to an improved deposition of gold speckles on the silica outer layer, thus, resulting in enhanced absorbance properties.

3.3.4 Attempt at Direct Conjugation of Gold Spheres onto QDS NPs

An attempt was made to directly conjugate already formed 2 nm gold spheres on to the silica outer layer of the QDS NPs using thiol chemistry in de-ionized water instead of carrying out the gold speckle conjugation in a microemulsion system. The rationale behind

this attempt was that in this method the gold conjugation can be carried out at a much larger scale than when compared to the use of microemulsion system. Unfortunately, this route did not produce the desired gold conjugation. The TEM images showed inconsistent gold speckles on the QDSG NPs. It also resulted in the presence of a large amount of unreacted gold nanospheres in the solution. Therefore, this method of gold conjugation was discarded.

3.3.5 Optimization of the Amount of APTS Added

The addition of APTS at the time of coating the QD-surface with silica leads to creation of positively charged amine functional groups on the outer surface of the silica coating. These amine groups are used subsequently to aid in the conjugation of gold speckles. However, if there is unreacted APTS in the solution there is a possibility of formation of a gold-APTS complex. This resulted in the formation of gold nanospheres in addition to QDSG NPs. This formation of gold nanosphere was confirmed via analysis of TEM images. In order to avoid this undesirable result, the amount of APTS addition was optimized to values stated earlier in the optimized established protocol.

3.3.6 Unsuccessful Attempt to Surface Functionalize the QDSG NPs

One of the initial objectives was to study the effect of surface functionalization of QDSG NPs for biodistribution studies. The as synthesized QDSG NPs had a slight positive surface charge (4.1 ± 1.7 mV). Conjugation with thiol polyethylene glycol molecules was successfully carried out to produce QDSG NPs with a nearly zero surface charge. However, attempts to produce particles with large positive surface charge by conjugating cysteinamine molecules or large negative surface charge by conjugating thiol propionic acid were unsuccessful. In both cases, the particles started agglomerating immediately after the addition of the reagents and soon formed a clear solution with black precipitates.

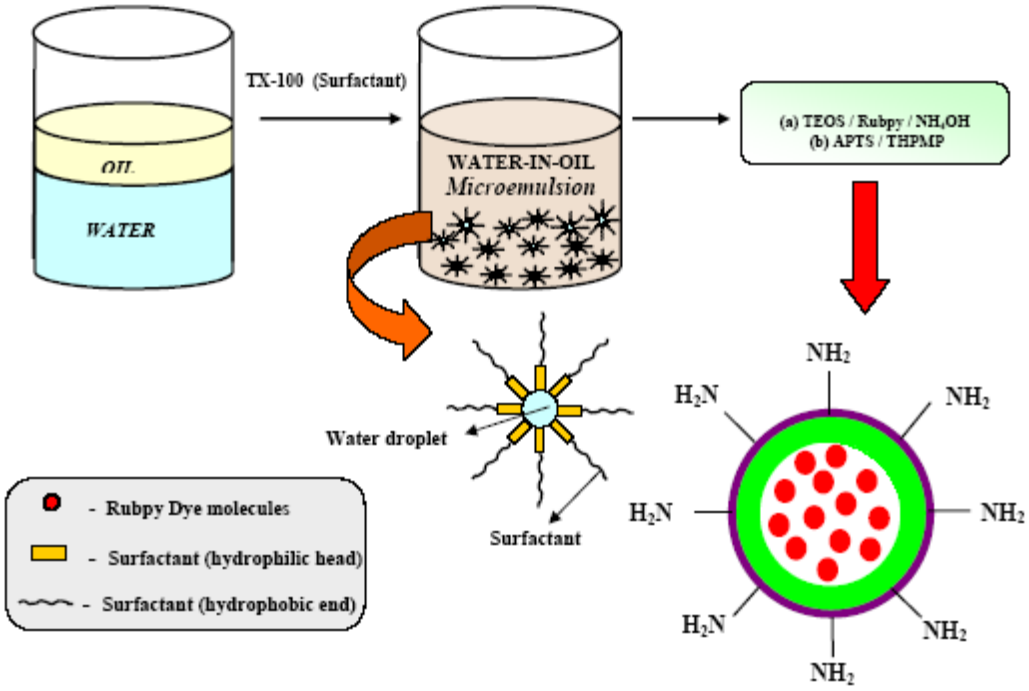

Figure 3-1. Synthesis of fluorescent silica nanoparticles using reverse-microemulsion technique

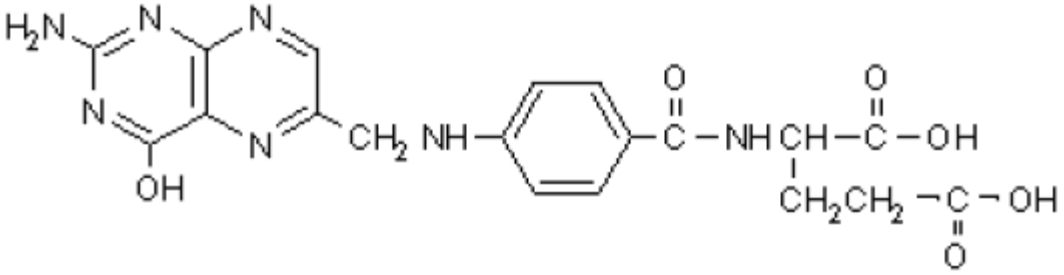

Figure 3-2. Structure of folic acid [Figure reproduced co-authored publication with permission from Journal of Nanoscience and Nanotechnology]

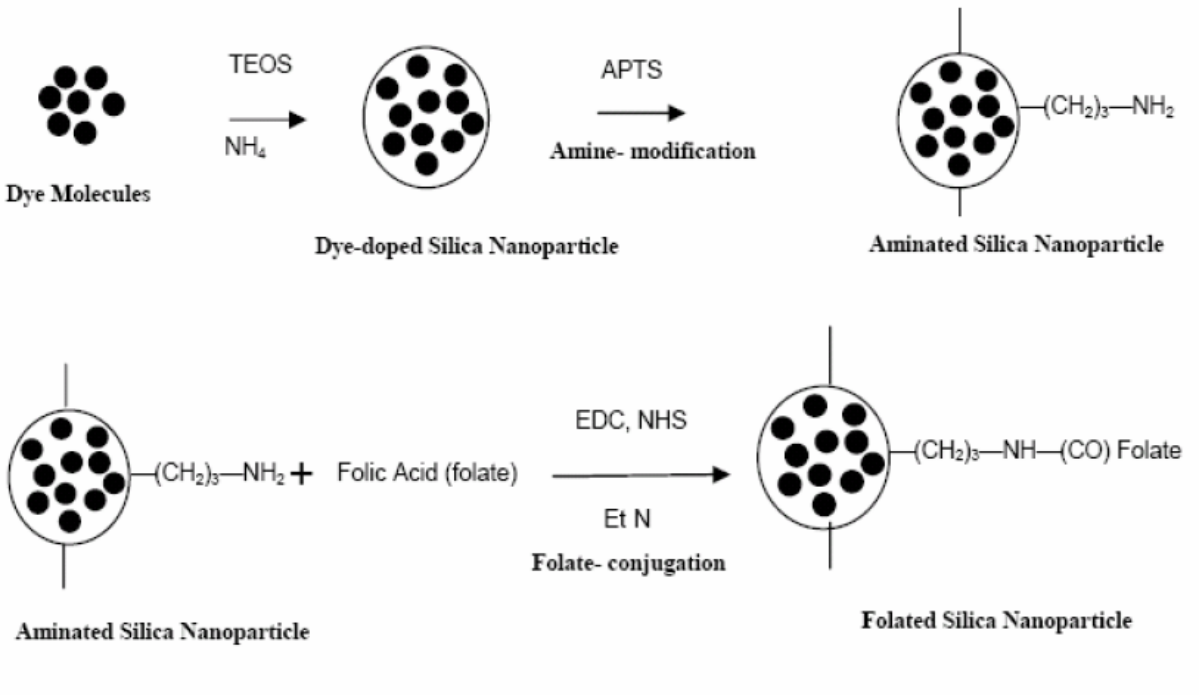

Figure 3-3. Folic acid conjugation on the fluorescent silica nanoparticles.

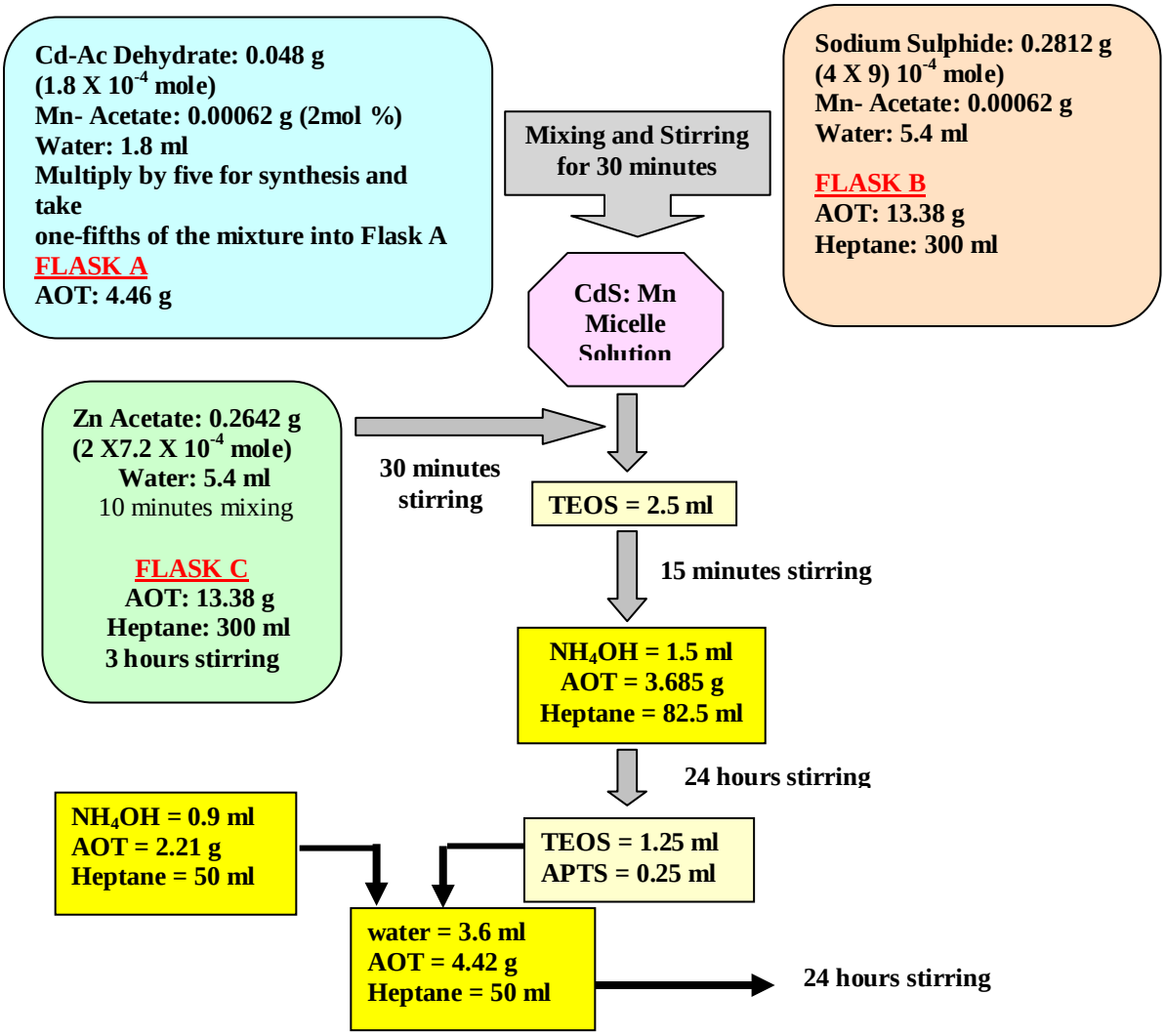

Figure 3-4. Synthesis protocol for QDS nanoparticles

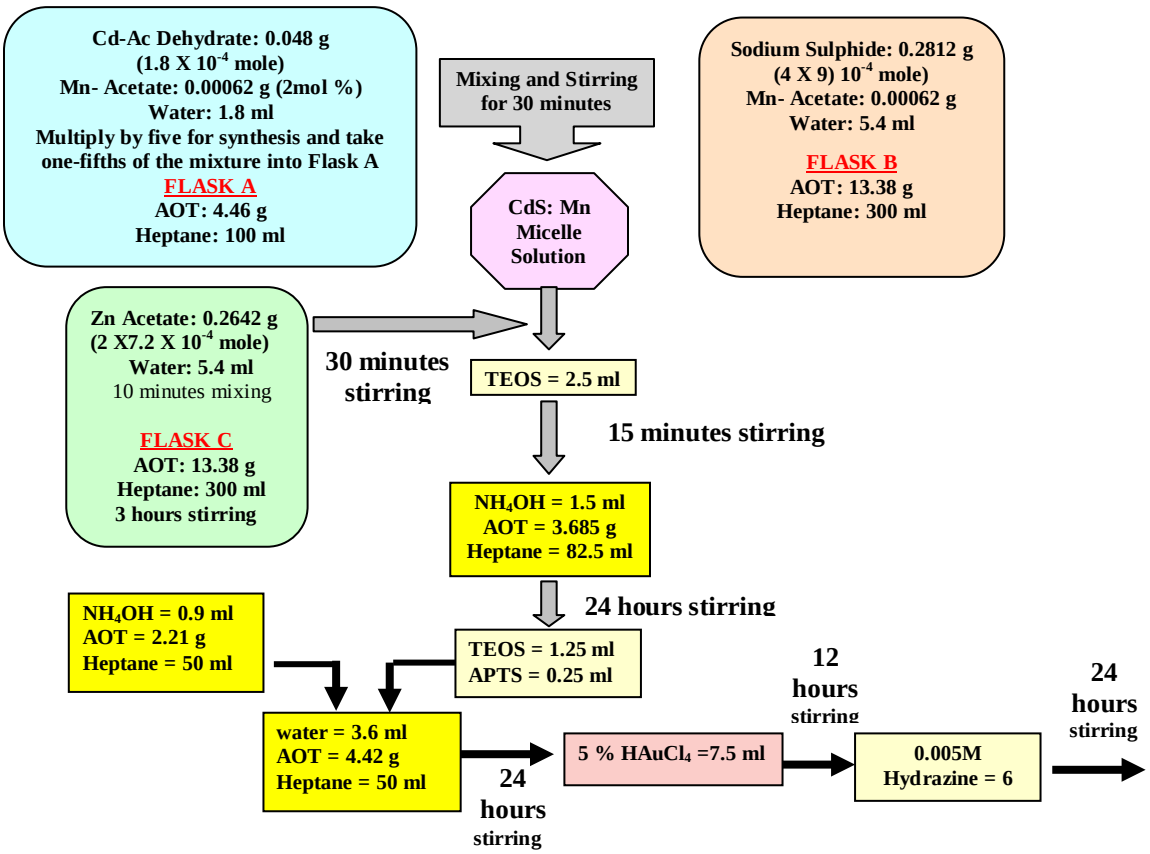

Figure 3-5. Synthesis protocol for QDSG nanoparticles.

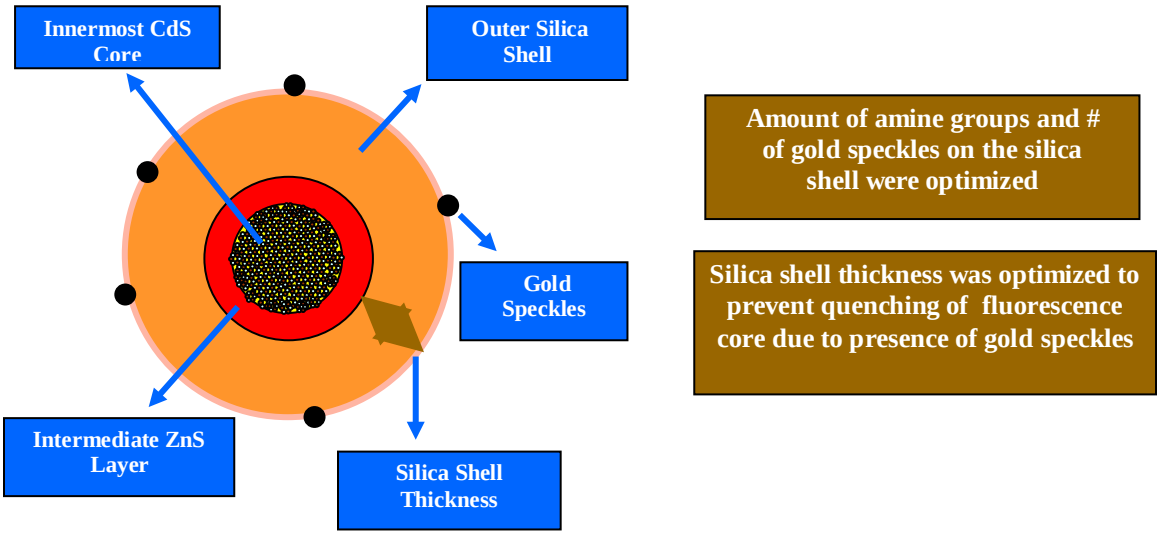

Figure 3-6. Structure of QDSG nanoparticles

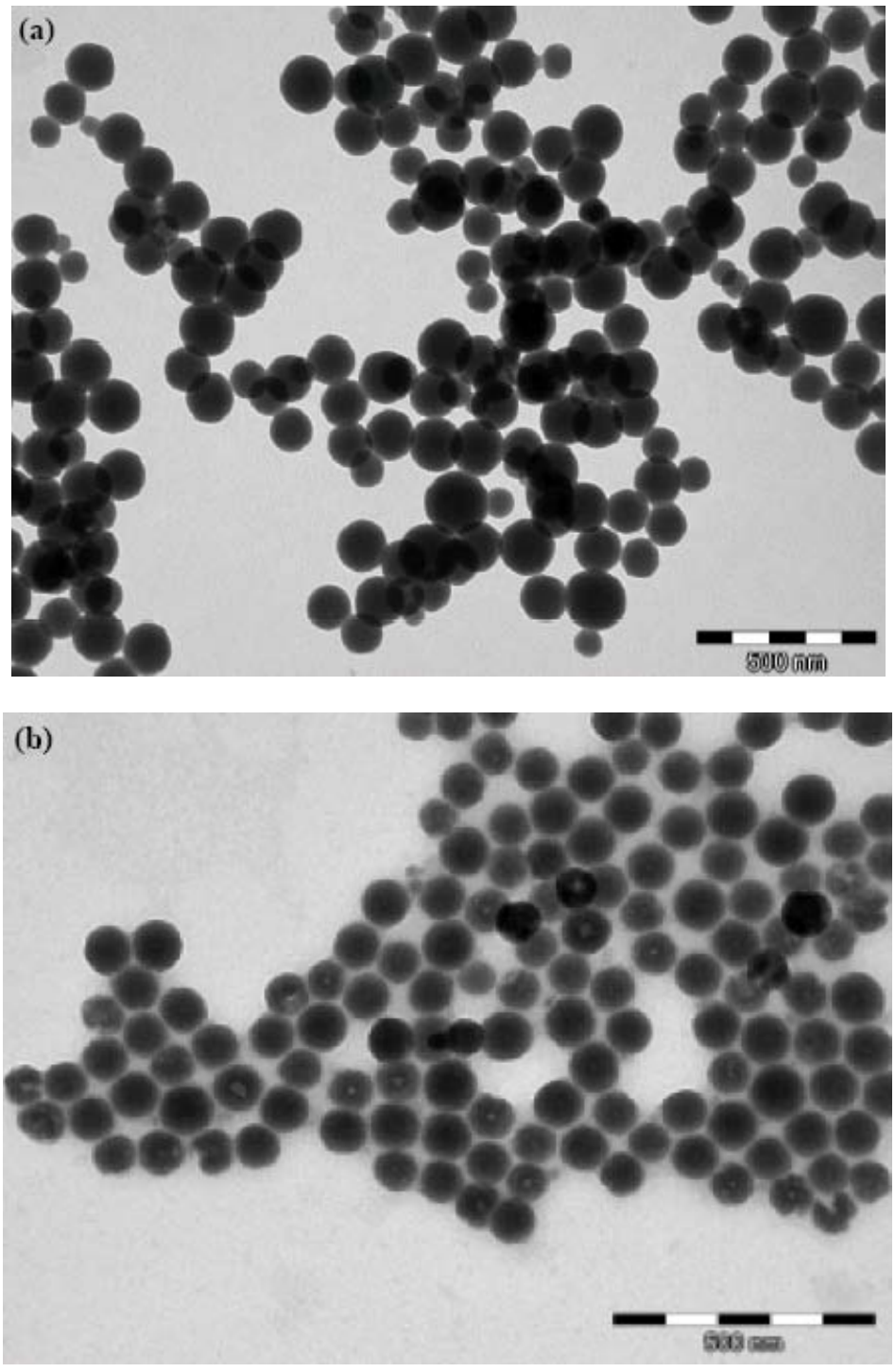

Figure 3-7. Transmission electron microscopic images of FSNPs of particle sizes (a) 190 nm and (b) 100 nm. In both images the scale bar represents 500 nm.

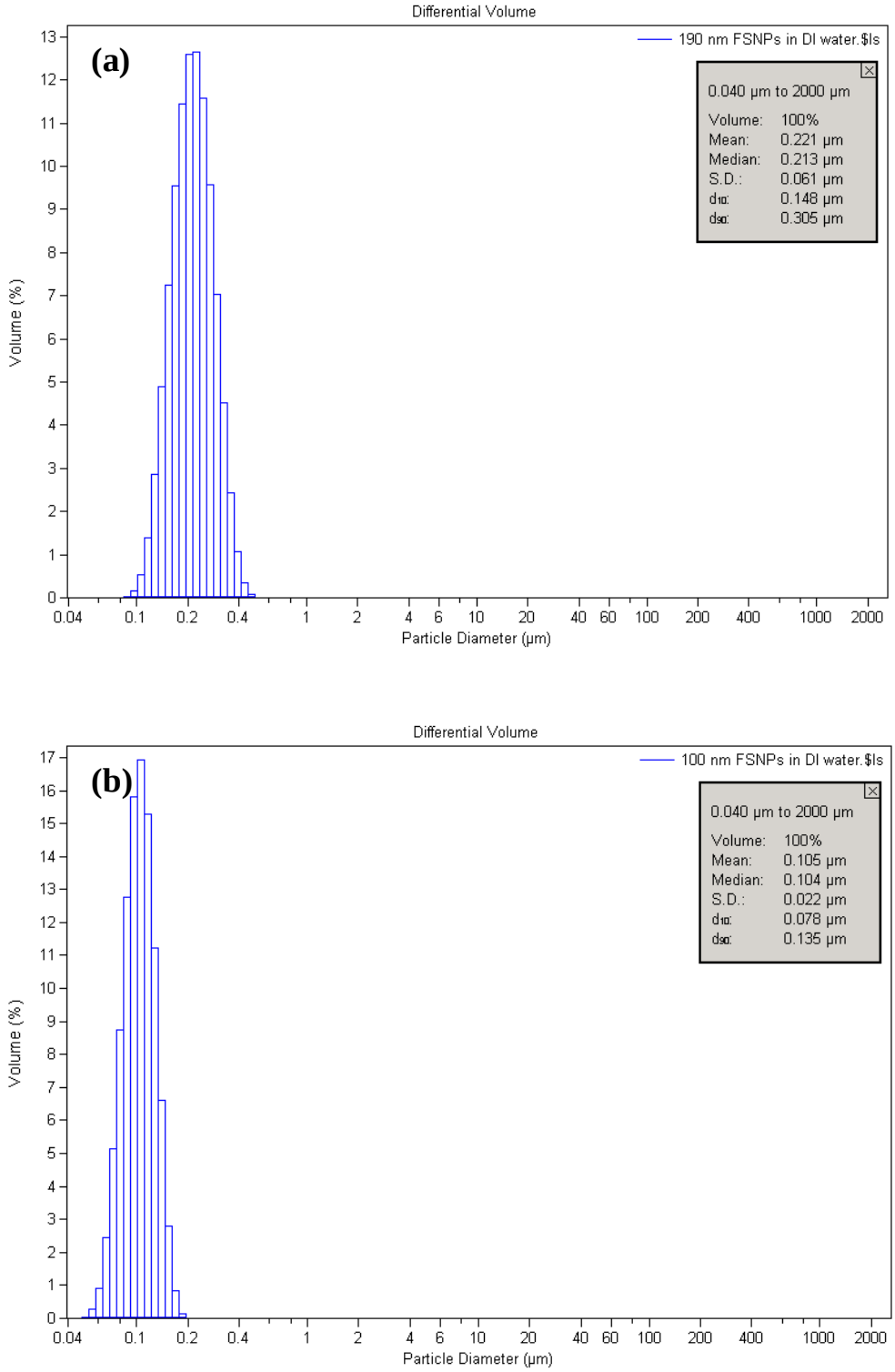

Figure 3-8. Coulter light scattering particle size measurements of FSNPs in DI water (a) 190 nm and (b) 100 nm.

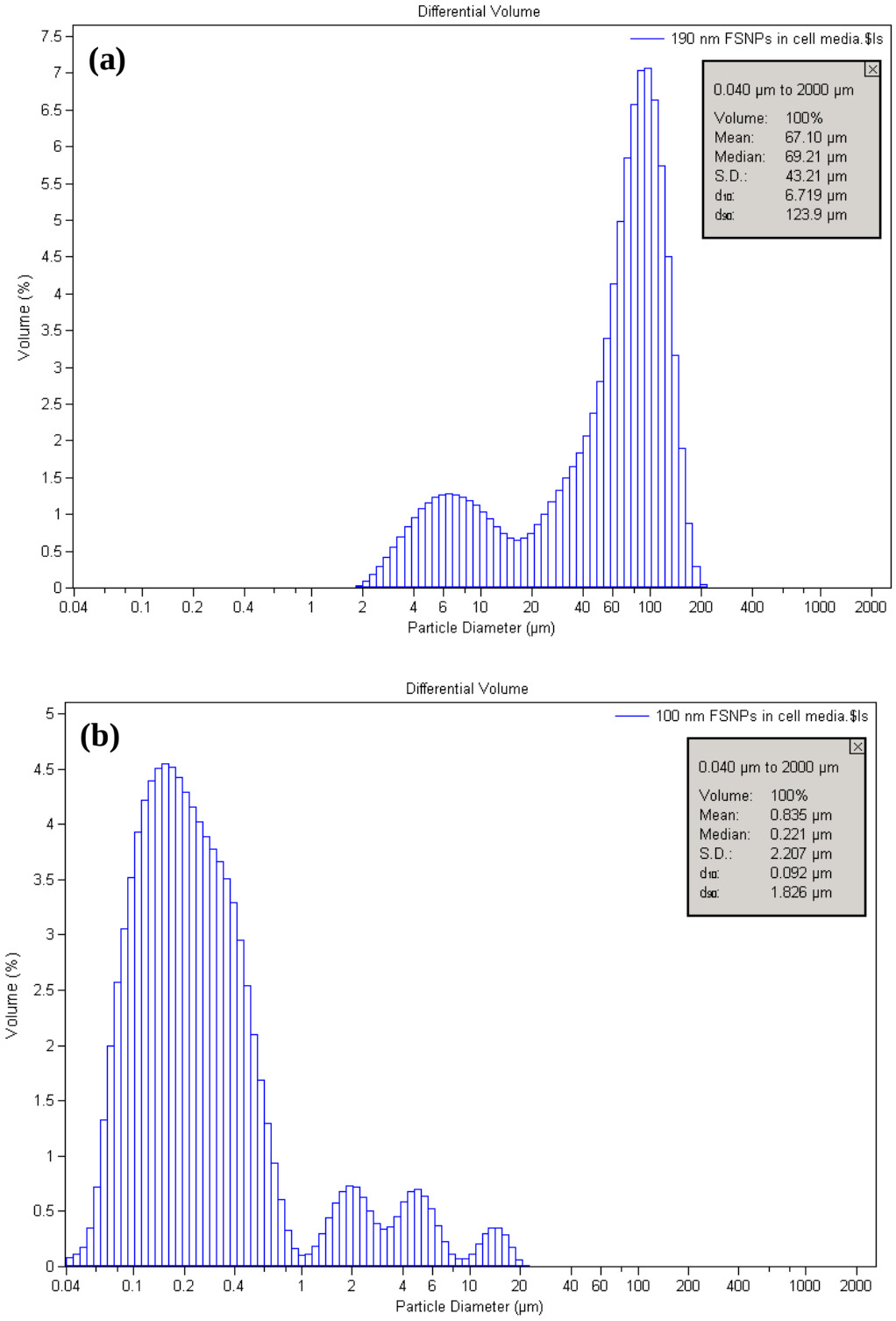

Figure 3-9. Coulter light scattering particle size measurements of FSNPs in cell media (a) 190 nm and (b) 100 nm.

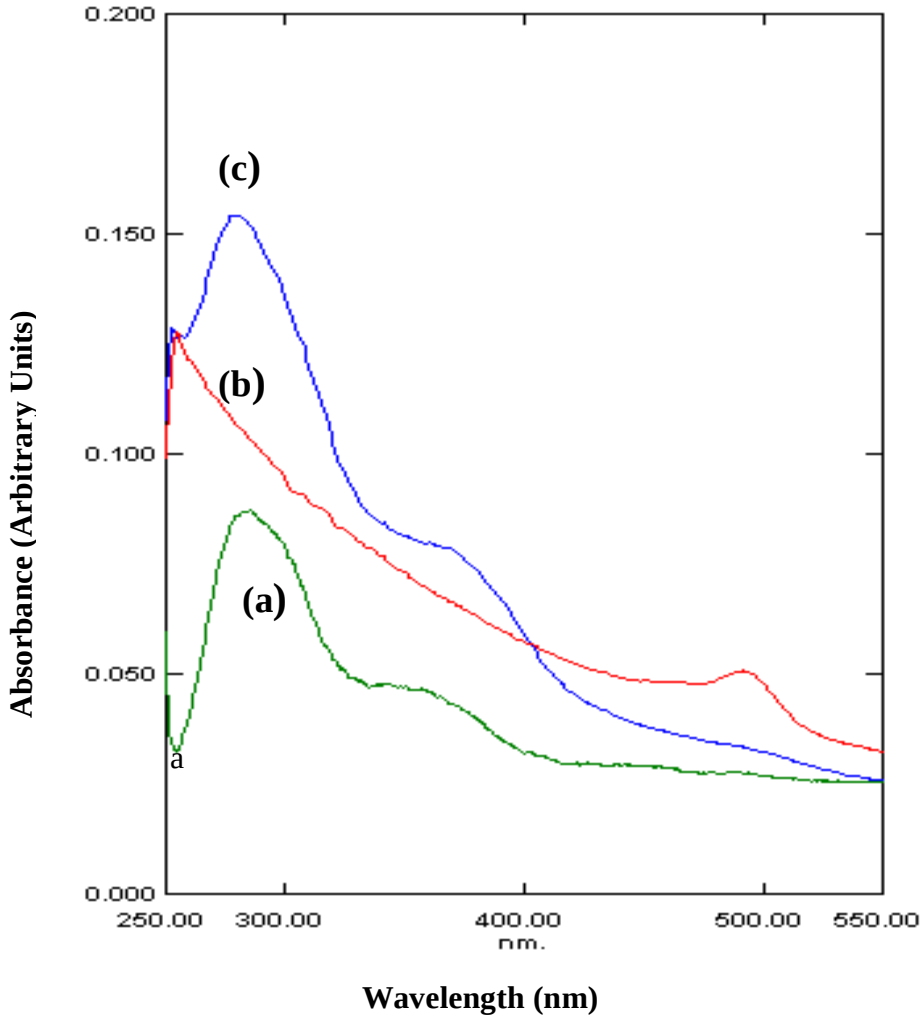

Figure 3-10. Absorption spectra of (a) pure folate (b) 190 nm FITC-doped aminated FSNPs and (c) FITC-doped 190 nm folated FSNPs. [Figure reproduced with permission from Journal of Nanoscience and Nanotechnology]

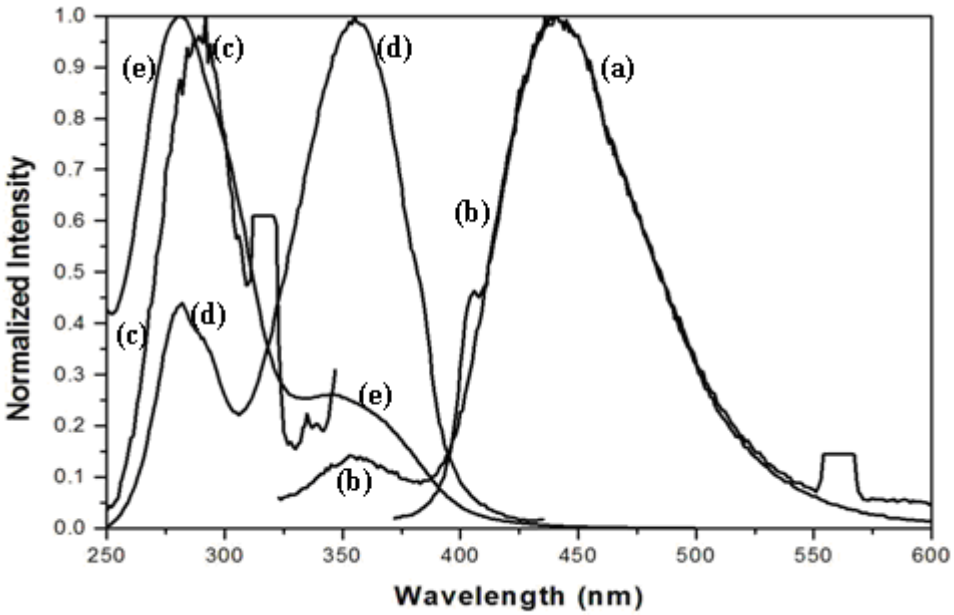

Figure 3-11. Normalized fluorescence emission and excitation spectra of pure folate in DI water. Emission spectra (a) and (b) at 355 nm and 280 nm excitation wavelengths, respectively and excitation spectra (c) and (d) at 355 nm and 447 nm emission wavelengths, respectively. (e) Absorption spectrum of folate. [Figure reproduced with permission from Journal of Nanoscience and Nanotechnology]

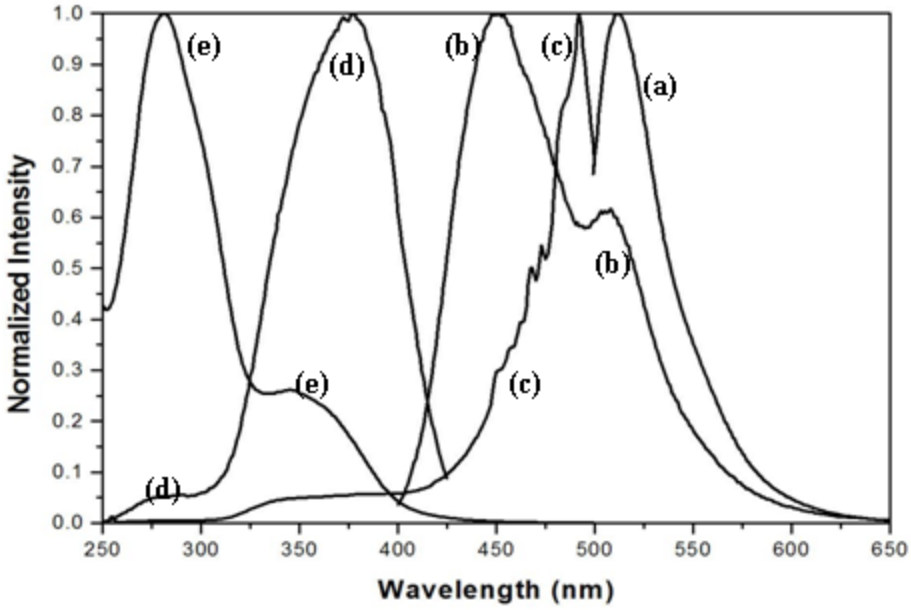

Figure 3-12. Normalized fluorescence emission and fluorescence excitation spectra of folate-FSNPs in water. Emission spectra (a) and (b) at 492 nm and 355 nm excitation wavelengths, respectively and excitation spectra (c) and (d) at 512 nm and 447 nm emission wavelengths, respectively. . Absorption spectrum (e) of folate [Figure reproduced with permission from Journal of Nanoscience and Nanotechnology]

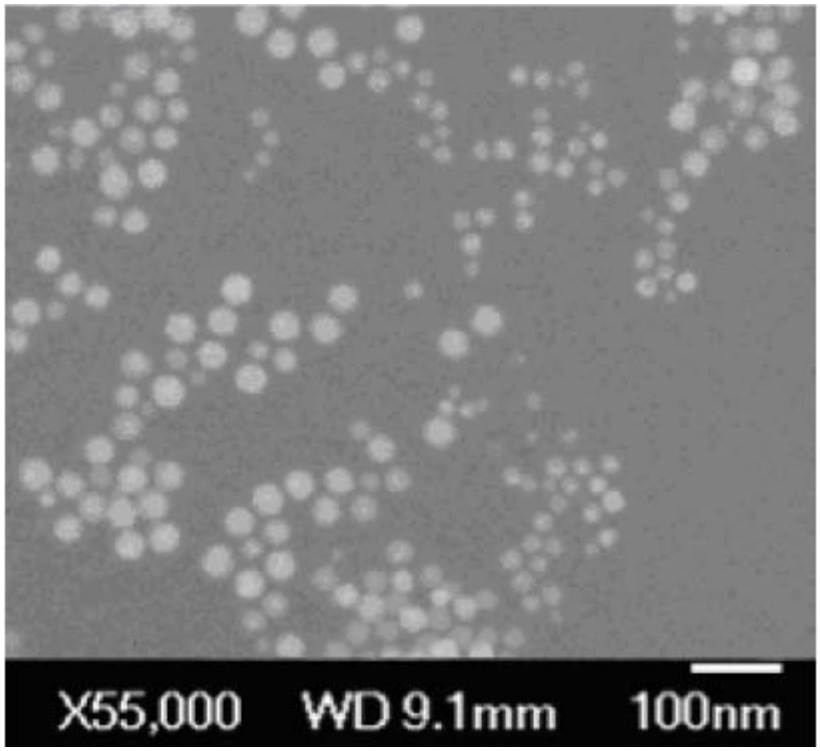

Figure 3-13. Transmission electron microscopic image of gold nanoparticles.

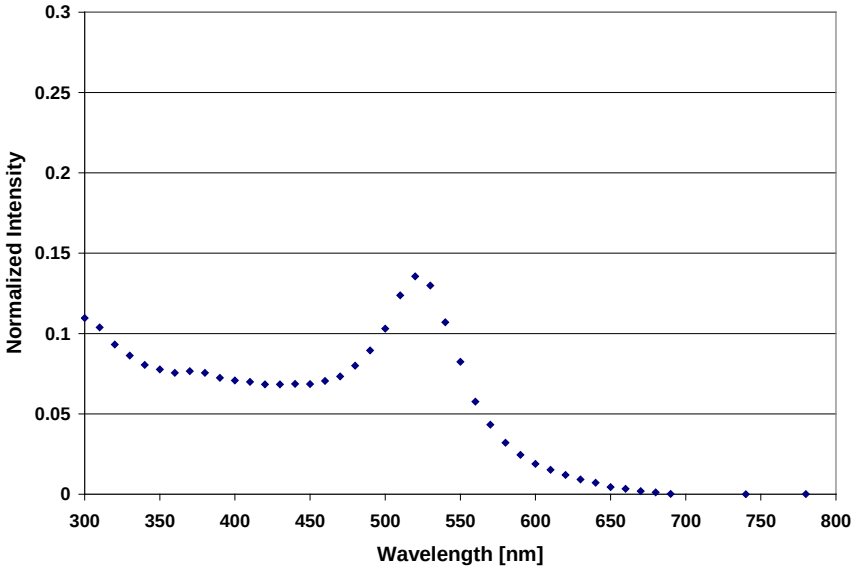

Figure 3-14. Absorbance spectra of gold nanoparticles in de-ionized water.

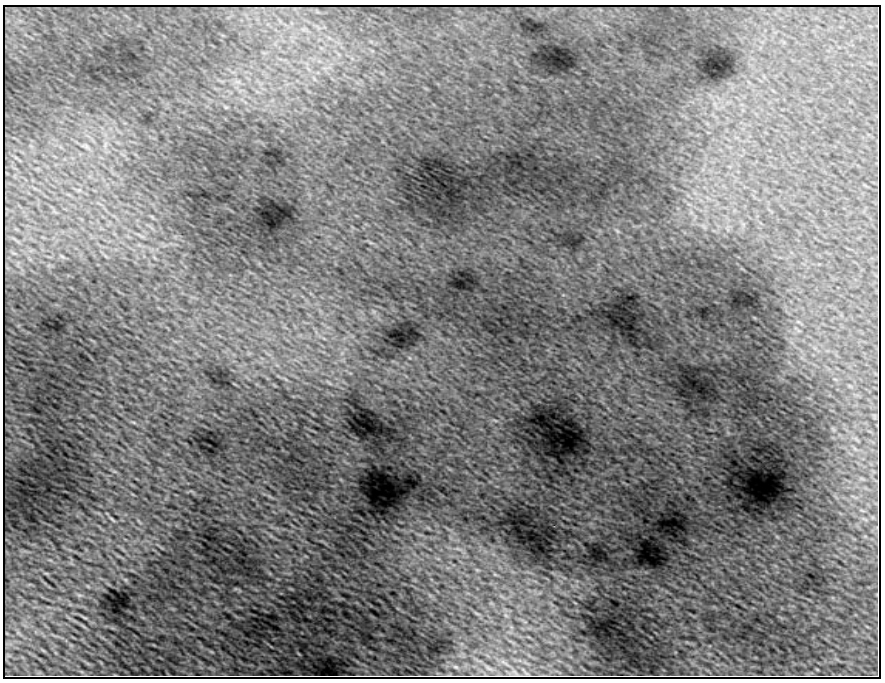

Figure 3-15. Transmission electron microscopic image of QDSG nanoparticles.

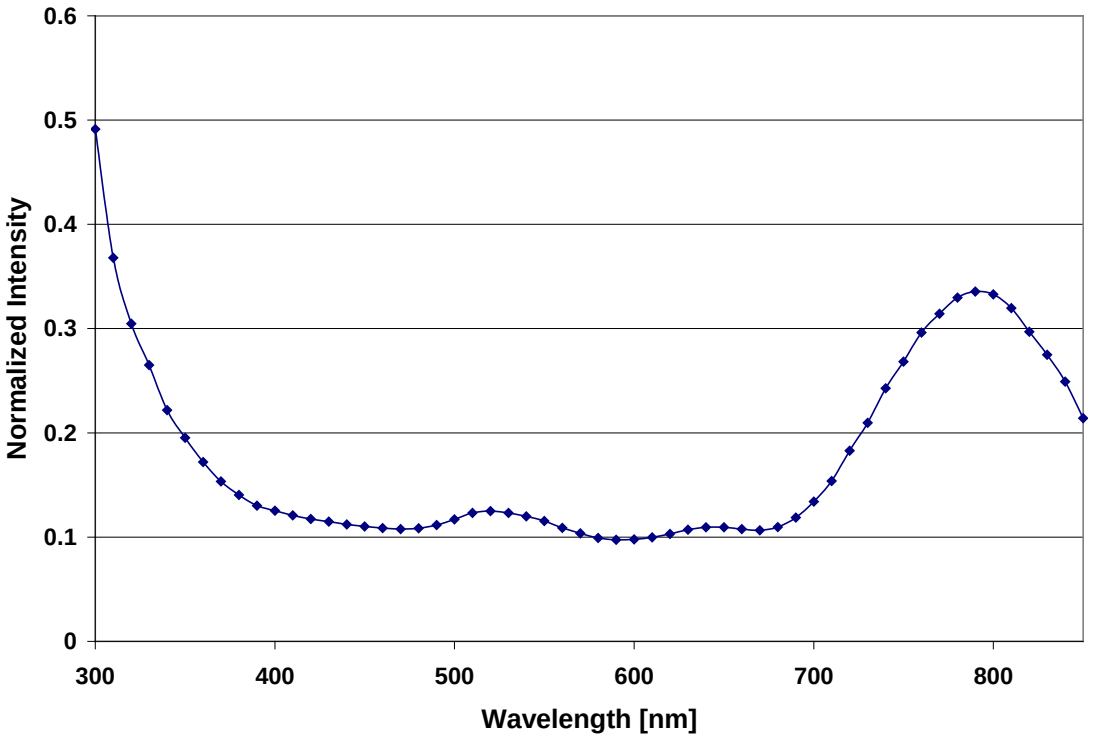

Figure 3-16. Absorbance spectra of QDSG nanoparticles in de-ionized water.

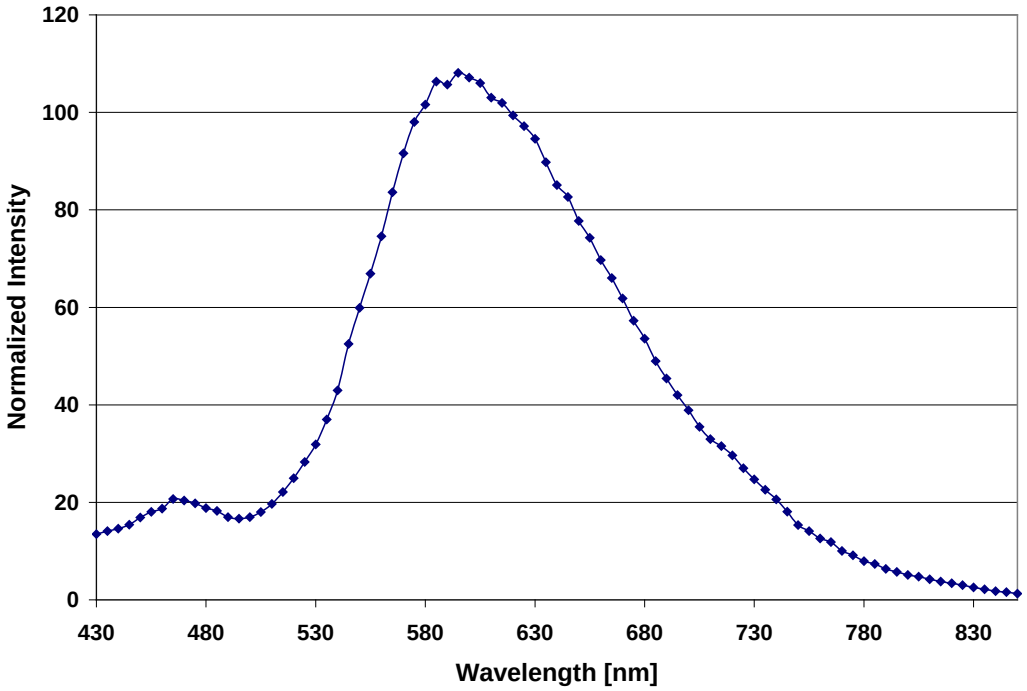

Figure 3-17. Fluorescence spectra of QDSG nanoparticles in de-ionized water.

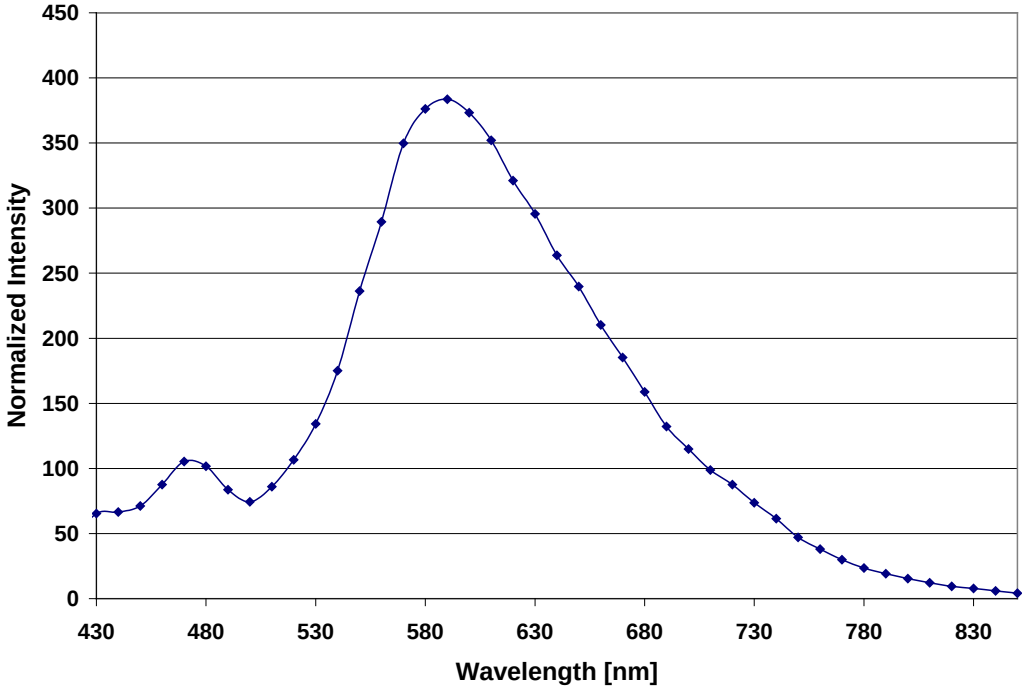

Figure 3-18. Fluorescence spectra of QDS nanoparticles in de-ionized water.

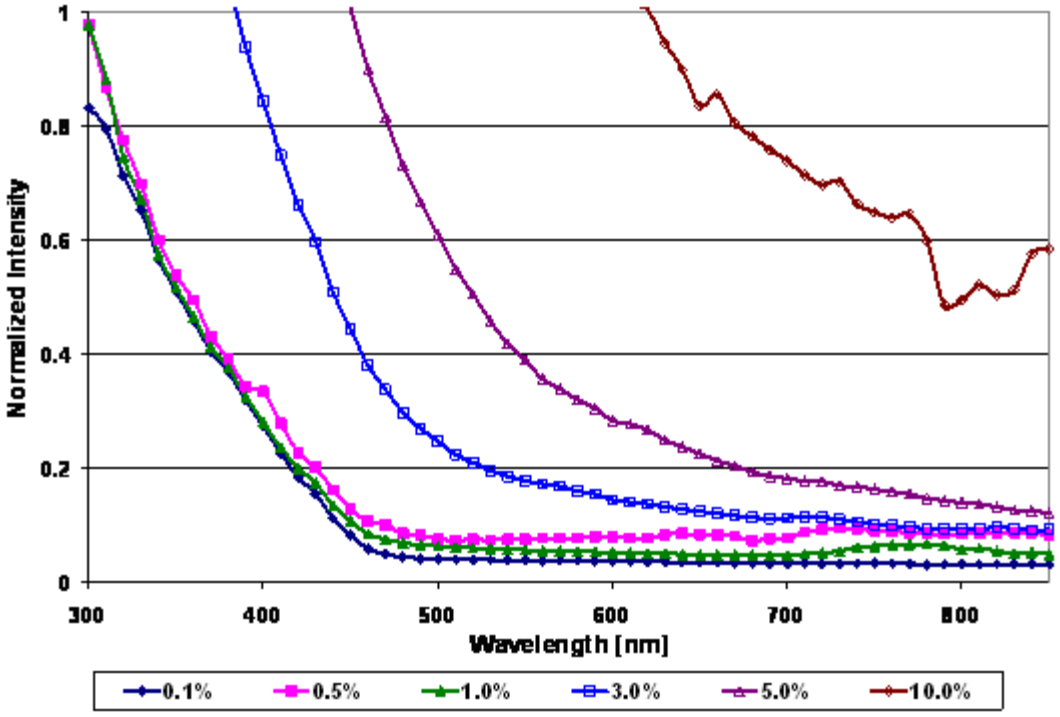

Figure 3-19. Variation of absorbance spectra with increasing gold concentration.

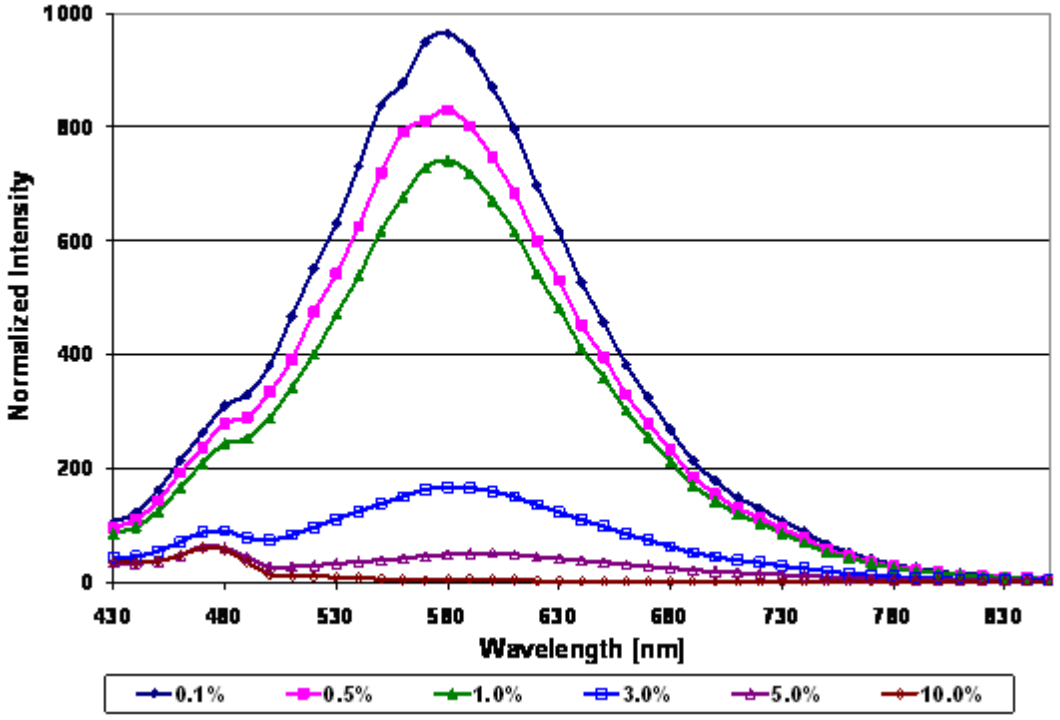

Figure 3-20. Variation of fluorescence spectra with increasing gold concentration.

CHAPTER 4
ENGINEERED NANOPARTICLES IN BIOLOGICAL SYSTEMS

The nanoparticles (NPs) that have been discussed in the previous chapter were developed as a part of this research effort for use in biological systems as contrast agents with multi-functional therapeutic properties. This chapter presents the use of these NPs in biological systems to demonstrate their bioimaging and therapeutic potential, and identify the different physicochemical parameters of the NPs that influence their uptake behavior and biocompatibility in cells.

The first part of the chapter presents the cellular uptake and viability studies carried out with fluorescent silica NPs (FSNPs). Previous investigators have established that the biological responses of NPs are largely governed by their physicochemical properties like particle size (Carstensen *et al*. 1992, Hamoir *et al.* 2003, Warheit *et al.* 2005), shape (Brown *et al.* 2007, Chithrani & Chan 2007, Chithrani *et al*. 2006), concentration (Dutta *et al.* In Review for Publication), surface chemistry (Hoshino *et al.* 2004a, Karakoti *et al.* 2006) and state of agglomeration (Borm *et al.* 2006, Teeguarden *et al.* 2007). *In vitro* experiments using FSNPs were carried out to understand the effect of particle size, concentration, incubation time and surface functionalization on particle uptake in cells. Cell viability tests were conducted using conventional biological assays to confirm the biocompatibility of the FSNPs.

The second section deals with bioimaging studies using the engineered quantum dot (QD) cored NPs. Preliminary cellular uptake studies were conducted using gold speckled silica coated quantum dot cored nanoparticles (QDSG NPs) in cells and daphnia. The hyperthermic property of gold speckles on QDSG was confirmed using polymeric stearates and A549 cells.

4.1 *In Vitro* Experiments with Fluorescent Silica Nanoparticles (FSNPs)

Amorphous silica NPs with two different surface modifications – amine-modified (aminated) and folate-conjugated (folated) – were synthesized as described before. In order to develop a bioimaging agent, it is important to establish the various parameters that can influence particle uptake and also by quantifying the amount of uptake by the cells. Subsequently, it is important to study any potential toxic effects of the NPs inside the cells.

Bioimaging and biocompatibility studies of the surface modified FSNPs were carried out using microscopic and spectroscopic techniques. Laser scanning confocal microscopy (LSCM) along with transmission electron microscopic images (TEM) allowed the visual observation of NPs uptaken by cells. Fluorescence techniques and conventional protein assays were used for quantifying NPs that had been taken up or were associated with the cells. Finally, toxicity assessment using lactate dehydrogenase (LDH) homogenous membrane integrity assay was conducted to determine whether the cell membrane integrity had been compromised during NP exposure. The effect of particle size, particle concentration and incubation time were studied. In order to test this possibility that folic acid conjugated NPs can be used to selectively target tumor cells, confocal microscopic imaging, uptake quantification studies and toxicity assessments were conducted using amorphous silica NPs with (folated) and without folic acid (aminated).

4.1.1 Cell Culture and Nanoparticle Incubation

Human lung carcinoma A549 cells (a model cancer cell line) and normal human dermal fibroblast cells (both from American Type Culture Collection, Rockville, MD) were grown in RPMI 1640 cell media supplemented with 10% fetal bovine serum, 2 mM L-Glutamine, and an antibiotic-antimycotic mixture (Cellgro, Mediatech, Inc.). For confocal imaging, trypsinized cells (200 µL of a 2.0×10^4 cells/mL suspension that had been treated

with 0.25% w/v Trypsin/ 0.53 mM EDTA solution for detachment, Cellgro, Mediatech, Inc.) were plated in four 16-well glass slides (Lab-Tek, Nalge Nunc Intenational, IL). Cells were placed in the cell culture chamber for at least 24 hours to allow them to adhere to the slide surface and begin logarithmic growth. At this point, cells were generally 50% confluent and ready for nanoparticle exposure. Both 100 nm and 190 nm size aminated and folated amorphous silica NPs were first conditioned for 15 minutes in cell media at particle concentrations of 50, 100, 200 and 400 μg/mL. The particle concentrations for dosing the cells were selected from preliminary *in vitro* studies that showed NP uptake at these concentrations after five hours. In preparation for NP treatment, expent cell media was removed from each 16-well slide with cells and replaced by media containing NPs. Exposure was carried out for 5, 15, 24 and 48 hours in a humidified cell culture chamber containing 5 % CO_2 at 37^{o}C. After incubation, cells were rapidly washed 6–7 times with cold phosphate buffer saline (PBS) solution for pH 7.4. Care was taken to ensure that all unbound NPs have been washed out during washing process. Cell morphology remained unaltered before and after PBS washing, indicating no noticeable effect of PBS during washing.

4.1.2 Bioimaging Using Confocal Microscopy

Laser scanning confocal microscopy (LSCM) has been employed to obtain optical images with high-resolution. In LSCM, a laser beam passes through a light source aperture which is then focused into a small focal volume within a fluorescent specimen by an objective lens. A mixture of emitted fluorescent light and reflected laser light is obtained from the focal volume. This light mixture is recollected by the objective lens. The laser light is separated from the light mixture by a beam splitter, which allows the laser light to pass through while reflecting the fluorescent light into the detection apparatus. A photodetection

device detects the fluorescent light and records it on a computer. The laser scans over the plane of interest creating an image of the whole area. The brightness of the resulting image depends on the relative intensity of emitted fluorescent light. Images can be collected at different focal planes by raising or lowering the microscope stage. The computer can generate a three-dimensional picture of a specimen by assembling a stack of these two-dimensional images from successive focal planes. The use of confocal microscopy enables noninvasive, optical sectioning of intact, thick, living specimens and it requires a minimum of sample preparation. As LSCM depends on fluorescence of the specimens, a sample is usually treated with fluorescent dyes to make the objects visible.

Olympus FluoView 500 (Olympus America, Center Valley, PA) laser scanning confocal microscope was used for imaging cells for this research work. The data was analyzed using FluoView software (MicroSuite FIVE, Version 5, Olympus America, Center Valley, PA) that was integrated with the microscope. In addition to the fluorescent photodetection device, this microscope has another detector for collecting the reflected laser light. In the fluorescent images described below, images generated by both these detectors are shown adjacent to one another. The excitation and emission wavelengths for fluorescent dye (FITC) were 490 nm and 515 nm, respectively. The effect of both 100 nm and 190 nm size aminated and folated NPs on the cellular uptake process was investigated at particle concentrations of 50, 100, 200 and 400 μg/mL. The studies were conducted for incubation times of 5, 15, 24 and 48 hours. The qualitative effects of increasing the incubation time from 5 and 24 hours on the particle uptake process for both aminated and folated amorphous silica NPs are shown in Figure 4.1. The microscopic images showed that signals from the images of cells dosed with folated NPs (Figures 4.1c and 4.1d) exceeded that of their

aminated counterparts (Figures 4.1a and 4.1b) even after 24 hours. From this data, it was evident that on keeping the particle concentrations and incubation time constant and comparing between the folated and aminated FSNPs, a much higher quantity of the former are internalized by the A549 cells as compared to the latter. The differences in the particle uptake between the folated and aminated NPs was expected as folic acid molecules are preferentially uptaken by cancer cells that overexpress folate receptors (Wang & Low 1998).

The confocal images did not provide conclusive data to differentiate the particle uptake at different incubation times. The figures for 5 hours and 24 hours do not show a discernable difference. It appears that the particles are internalized by the cells within five hours and there is no substantial increase in uptake with time for folated FSNPs and slight increases for aminated FSNPs. The effect of increasing particle concentration (50 and 200 μg/mL) on the uptake process for both aminated and folated FSNPs is shown in Figure 4.2. It can be observed that the uptake of aminated FSNPs (Figures 4.2a and 4.2b) increased with increasing particle concentration. However, similar conclusion could not be drawn for the folated FSNPs (Figures 4.2c and 4.2d) as they were being aggressively uptaken by the cells, irrespective of particle concentration. It appears that cells that overexpress folate receptors can uptake as many folated NPs as possible to the extent of saturating the receptors (Santra *et al.* 2005c). The effect of particle size on the cell uptake is shown in Figure 4.3. Larger FSNPs seemed to result in relatively more fluorescence signal intensity for both aminated (Figures 4.3a and 4.3b) and folated (Figures 4.3c and 4.3d) NPs. This could be either due to increased particle uptake by the cells or an increased number of fluorescent dye molecules inside the larger particles which can emit a higher intensity of fluorescence. There was no conclusive evidence to relate the effect of particle size to the cellular uptake from these results.

4.1.3 Quantification of NP Uptake

The confocal microscopic study provided a visual method to observe the cellular uptake of the FSNPs. As shown in the previous section, the effect of some parameters such as size and particle concentration was not clearly understood with visual observations. Thus, a method to carry out a semi-quantitative analysis of the NP uptake was developed.

Since the NPs are fluorescent, an assay was developed that uses NP fluorescence intensity as a marker to quantify the number of NPs uptaken by the cells. For this purpose, calibration curves of fluorescence intensity versus particle concentration, (Figure 4.4), and absorbance intensity versus cell protein concentration, (Figure 4.5), were generated. As per the established protocols (Dutta *et al.* In Review for Publication), amount of cell-associated particles was estimated by calculating the fluorescent intensity and the corresponding amount of protein in the cell lysate from each well in a ninety-six well microtiter plate.

For total protein assays, A549 cells were plated at a density of 7000 cells per well in four 96 well Fluoro Nunc^{TM} tissue culture plates (Fisher Scientific, Pittsburg, PA) and cultured for 24 hours (37^{o}C, 5% CO_2) to obtain an adherent monolayer of cells. Cell media from tissue culture plates was removed just before addition of NPs solutions. Stock solutions of folated and aminated FSNPs were freshly prepared in cell media (pH 7.2) at a concentration of 800 μg per mL for each solution. Serial dilutions from NPs' stock solutions were performed and added to cells in 96 well plates so that the final concentrations were 400, 200, 100, 50, and 0 μg/mL (200 μL/well). Each assay point was conducted in quadruplicates. The incubation time for this study was fixed at five hours as it was established that a higher incubation time seemed to have a minor effect on the particle uptake. Cells were washed five times with ice-cold sterile PBS (pH 7.4) to remove unbound NPs and lysed in 75 μL lysis

solution (1% w/v SDS, 1% v/v NP40, 150 mM NaCl, 50 mM Tris, pH 7.5, and 0.125 U/μL benzonase, Novagen, San Diego, CA). Twenty-five μL of cell lysate from each well was used to determine the total cell protein content using a Micro BCA protein assay kit (Pierce Chemical Company, Rockford, IL).

The remainder of the cell lysate was used for the quantification of cell-associated FSNPs at various concentrations and incubation times. A fluorescent plate reader (Safire, Tecan Group Ltd., Mannedorf, Switzerland) was calibrated with standard solutions containing varying concentrations of the FSNPs between 0.0122 μg/mL to 6.25 μg/mL in cell lysate solution (generated by homogenizing 10,000 untreated A549 cells in 200 μL of the above mentioned lysis solution). The excitation and emission wavelengths of FITC, 490 nm and 515 nm respectively, were used for the study. According to established protocols (Dutta *et al.* In Review for Publication), the quantified protein was expressed as milligram of cellular protein and the corresponding NP uptake was expressed as micrograms of FSNPs per milligram of cellular protein (mg of particles/mg of protein).

The results of the uptake quantification study are plotted in Figure 4.6. It can be observed that for all particles the uptake steadily increases with particle concentration. Comparing the uptake of the folated and the aminated NPs it can be seen that, in general, the uptake for folated particles is higher than the aminated particles at all particle concentration except for the 400 μg/mL value where the two values are almost identical. It is known that particles can enter the cells through diffusion process (Limbach *et al*. 2005, Zhu *et al*. 2006). Further, cells that overexpress folate receptors are known to aggressively uptake folic acid molecules through receptor mediated endocytosis process (Santra *et al*. 2005c). Based on the fact that cancer cells do overexpress folate receptors, it is perhaps not surprising that we

observed receptor-mediated endocytosis of folated NPs by A549 cells. However, it is unlikely that aminated FSNPs would be internalized in a similar fashion as folated FSNPs. In the case of folated NPs, both the phenomena of passive process of diffusion and the active process of receptor mediated uptake complement each other to increase the particle uptake as compared to the aminated NPs in which only the passive diffusion process governs the uptake. However, at the high concentration of 400 μg/mL, the diffusion process itself is sufficient to saturate the particle uptake by the cells, which is indicated by the approximately same mass of particles uptaken for the two sizes (100 nm and 190 nm) of folated NPs and the larger (190 nm) aminated NPs. It is therefore clear that particle concentration has a direct correlation with NP uptake by cells. However, increase in particle size due to agglomeration could not be ruled out as this would also result in higher fluorescent signal intensity.

It can be clearly seen that the particle uptake is anomalously low in the case of 100 nm aminated NPs as compared to the others. There is an explanation to rationalize this observation. It was observed from the particle size measurements using Coulter Light Scattering results (Figures 3.7a and 3.7b), that the particles agglomerated resulting in larger sizes in cell media as compared to the same measurements in de-ionized water

Tests were conducted to measure the effective particle size of 100 and 190 nm FSNPs in cell media. As previously shown in Figure 3.8b, particle size measurements of 100 nm FSNPs indicated an apparent size range of 40 nm to 20 microns whereas 190 nm FSNPs in cell media, (Figure 3.8a) indicated an apparent size range of 2 to 200 microns. Particles in this size range are suspected to appear to cells as a foreign material leading to non-specific phagocytosis (a cellular process to engulf bacteria, virus and other non-viable cells) (Dutta *et al.* In Review for Publication). The 190 nm particles are in a higher size range compared to

the 100 nm particles and, therefore, could be more actively uptaken by the cells through the non-specific phagocytosis process. This is a possible explanation to the comparatively low uptake values of the 100 nm aminated particles. However, for folated NPs of 100 nm particle size, the receptor mediated endocytosis dominates the process of uptake and thus is much higher when compared to its aminated counterpart.

4.1.4 Cell Viability Studies

The confocal imaging and NP uptake quantification studies provide insight into cellular uptake of the folated and aminated NPs. After observing particle internalization, the next step was to carry out cell viability studies to assess the cytotoxicity of the FSNPs and thereby determine their biocompatibility. Potential cytotoxicity of A549 cells when treated with either aminated or folated FSNPs was evaluated using the CytoTox – ONE Homogenous Membrane Integrity Assay Kit from Promega (Madison, WI). If the cell membrane integrity is compromised as a result of cytotoxic agents, the intracellular lactate dehydrogenase (LDH) will leak out of the cell membrane and will be found in the extra-cellular media. The assay detects and quantifies the amount of LDH that was released into the cell media. This is a cell lysis (cell death) quantification method based on the measurement of LDH activity released from the cytosol of damaged cells into the supernatant. Cytotoxicity is expressed according to the following expression:

$$\text{Cytotoxicity}\,(\%) = \frac{\left(\text{LDH}_{\text{treated cells}} - \text{LDH}_{\text{untreated cells}}\right)}{\left(\text{Max LDH}_{\text{treated cells}} - \text{Max LDH}_{\text{untreated cells}}\right)} \qquad (4\text{-}1)$$

In the enzymatic assay, a resazurin compound is bioreduced to a soluble resorufin in the presence of LDH. Resazurin is a non-fluorescent compound and becomes fluorescent when it is reduced to resorufin (excitation and emission wavelengths of 560 and 590 nm, respectively). The amount of released LDH during nanoparticle exposure was measured at

various particle concentration and incubation times. The details of the procedure are given below as we have modified the original assay protocol to adapt NPs as testing materials.

Cells were seeded into 96 well microtiter plates at approximately 4-5 x 10^3 cells/200 µL. The plates were incubated overnight at 37 ^oC in a humidified cell culture chamber at 5 % CO_2, to allow cells to adhere to the bottom of the wells. Stock solutions of either aminated or folated FSNPs at 800 µg/mL particle concentration (as described in previous section) were used for cell dosing. NPs were added to wells so that final concentrations tested were 400, 200, 100, 50, and 0 µg/mL, in quadruplicates (200 µL/well). The plates were then incubated at 37^oC for different periods of incubation (5, 15, 24 and 48 hours), akin to the NP uptake experiments. A set of wells without cells was included in the assay for background controls.

After incubation, 100 µL of the media from each well (well A1 in Figure 4.7) of the original 96 well assay plate (referred to as plate I) was transferred to a fresh 96 well plate (referred to as plate II). Rest of well contents was termed as pellets. Cells in each pellet were then lysed using 10 µL of diluted (1:5) lysis solution (Promega, Madison, WI). This modification of the Promega kit procedure allowed us to determine the total releasable LDH from each well and account for possible pipetting errors during cell plating. Both plates I and II were centrifuged at 3500 rpm at 25^oC for 4 minutes. The purpose of centrifugation was to separate NPs from cell media containing LDH. After centrifugation, 50 µL of supernatant from each well of Plate I and Plate II was transferred into two fresh 96 well plates (referred to as Plates III and IV, respectively). Following assay protocol, 50 µL of the CytoTox ONE^{TM} reagent was then added to each well of Plates III and IV, and then incubated for 30 minutes. The stop solution was added after incubation and plates were read using a fluorescence plate reader (Model Safire, Tecan, NC).

LDH assay data were compiled and presented in Figure 4.8 at three different incubation times, 5 hours (Figure 4.8a), 24 hours (Figure 4.8b) and 48 hours (Figure 4.8c). In these experiments, cells with no NPs and quartz were treated as the negative and positive controls respectively. The LDH value of cells with no NPs was established as the baseline at 0% and that of quartz was found to be 24%. It was observed that both aminated and folated NP were relatively non-cytotoxic to A549 cells as compared to quartz particles. The maximum percentage of cytotoxicity value was calculated to be 8% when aminated FSNPs were pre-conditioned with cell media containing serum proteins and incubated with cells for 48 hours at a particle concentration of 200 μg/mL.

Considering all experimental parameters such as particle size, concentration and incubation time, data from the present LDH study showed that both pre-conditioned aminated and folated FSNPs appeared to be non-cytotoxic to A549 cells. The percentage of toxicity was about 8% for the highest nanoparticle concentration and longest incubation times tested. One can argue that pre-conditioned particles appeared to be non-cytotoxic because they are already coated with the serum proteins that are present in the cell media. Therefore, pre-conditioned FSNPs for all practical purposes should be considered as protein coated particles rather than aminated or folated particles.

In order to resolve the effect of pre-conditioning the NPs on their cytotoxicity, further experiments were performed where A549 cells were incubated with either aminated or folated NPs without pre-conditioning with cell media. These experiments were performed similar to those with preconditioned NPs by including parameters such as incubation time, particle size and particle concentration. The results from the LDH experiments in which A549 cells were incubated with non pre-conditioned 100 nm and 190 nm aminated and

folated FSNPs for 2 hours are shown in Figure 4.9. An increase in the cytotoxicity values for all NPs as compared to their pre-conditioned counterparts was observed. The average percentage of cytotoxicity for non pre-conditioned aminated and folated FSNPs was observed to be 20%. This suggested the possibility of surface passivation of FSNPs by serum proteins when pre-conditioned in cell media. However, it was also clear that pre-conditioning did not completely passivate particle surface because of the fact that folated FSNPs were more aggressively uptaken than the aminated FSNPs.

Whether or not FSNPs were pre-conditioned, there was no significant difference between the aminated and folated FSNPs in terms of percentage cytotoxicity. It can be concluded that within the limits of biological variation (±10%) pre-conditioned FSNPs, in general, whether aminated or folated, were non-cytotoxic to A549 cells. However, FSNPs that were not pre-conditioned manifested toxicity behavior that became comparable to quartz.

4.2 Gold Speckled Silica Coated Quantum Dot cored Nanoparticles (QDSG NPs)

Bioimaging studies were carried out with QDSG NPs using A549 cells and daphnia. Further, heating studies were carried out both in polymeric stearates and A549 cells to confirm the hyperthermic properties of the gold speckles. These three studies are described in the subsequent subsections.

4.2.1 Bioimaging Studies in A549 Cells Using QDSG NPs

The cell culture and incubation procedure for A549 cells is similar to the description in Section 4.1.1. A volume of 1 mL of A549 cells at a concentration of 2.0×10^4 cells/mL were plated in six-well plates. QDSG & QDS NPs (particle sizes of 15 nm) were pre-conditioned in cell media for 30 minutes to prepare a stock solution of 1000 µg/mL. This stock was used to prepare QDSG solutions of concentrations 100, 200 and 250 µg/mL. These solutions were then added to the six-well plates containing A549 cells in duplicate wells and

incubated for 24 hours. After incubation, the supernatant was removed and the cells were washed with cold PBS to remove all non-associated particles, thereby only keeping back NPs that have been either internalized or are attached to the cell surface. Using the same process as described in Section 4.1.2, confocal microscopy studies were conducted on QDSG NPs. The excitation and emission wavelengths used for imaging these NPs were 355 nm and 590 nm, respectively.

The results of LSCM studies on amine-modified QDSG (Figure 4.10) show that the NPs were uptaken by the A549 cells in 24 hours. The QDSG NPs were not aggressively internalized and behaved similar to the aminated FSNPs (described in Section 4.1.2). Most likely, the QDSG NPs are taken up by the A549cells by an active process of diffusion, similar to the aminated FSNPs. As before, the amount of NP uptake in cells would depend on the range of particle size encountered by the cells after any particles agglomeration that might occur in cell media.

4.2.2 Bioimaging Studies in Daphnia Using QDSG NPs

In order to demonstrate the bioimaging functionality of QDSG NPs in living systems, a very simple animal model of daphnia was used for this study. The use of daphnia for NP uptake studies has been shown by previous investigators (Lovern *et al.* 2008). A brief description of the experiment on daphnia for bioimaging using QDSG NPs is given below.

A glass beaker of one liter volume was filled with fresh water and QDSG NPs were added to make a stock solution of 8 mM cadmium concentration. A large number of daphnia was introduced into this aqueous stock solution and left undisturbed for 24 hours. The daphnia was then taken out of the water, washed several times with cold PBS and depurated to remove all non-associated particles from the organism and leave behind only the internalized NPs inside. The daphnia was then imaged with a fluorescent microscope using

the excitation and emission wavelengths of the QD-core in the QDSG for bioimaging. The microscopic images of daphnia with orange colored (region of interest has been marked with arrows) QDSG NPs in the gastrointestinal tract are shown in figures 4.11a and 4.11b. The control daphnia with no NPs are shown in Figure 4.11c and 4.11d which have no fluorescence signal in the images. Similarly, the control daphnias with amorphous silica NPs, without any dyes, showed no fluorescence. This experiment demonstrated the bioimaging capability of the QDSG NPs in simple models of living organisms.

4.2.3 Hyperthermic Characteristics of QDSG NPs

The gold speckles on the silica coated quantum dots were expected to impart hyperthermic properties to QDSG NPs. Previous investigators have reported on hyperthermic properties of gold nanostructures (Govorov & Richardson 2007, Govorov *et al.* 2006, Huff *et al.* 2007b, Richardson *et al.* 2006). In order to confirm this hypothesis, heating studies were conducted using the QDSG NPs. First, the particles were tested with polymeric stearate, which began to melt easily with heat generated from the NPs. Next, these NPs were incubated with A549 cells and tested for hyperthermic properties. In both cases, the excitation of gold was carried out using a laser source at 785 nm wavelength. This arrangement was used for real time observation of the effect of laser on the NPs in polymeric stearates and cells.

Stock solutions of QDSG and QDS NPs at a concentration of 1 mg/mL was prepared in ethanol, which dries up rapidly when exposed to atmosphere. 500 mg of commercially available polymeric stearate (Sigma-Aldrich, St Louis, MO) was measured and added to each well in a six-well plate. 1 mL of the stock solution of QDS was added to 2 wells and 1 mL of QDSG stock solution to two other wells. The other two wells contained only the polymeric stearate and were used as controls for the experiment. The plates were exposed to atmosphere

(in a hood) for one hour to allow complete evaporation of ethanol from the wells. Following this, the six-well plates were exposed to the laser source that produced laser beams at 785 nm wavelength in the Bio Raman Spectroscope. It was observed that the polymeric stearate in the wells with QDSG NPs began to heat up and melt after approximately five minutes. After further heating for five minutes, smoke started to emanate from the wells and the polymeric stearate turned black locally in the area where the beam was focused. At this point, the experiment was stopped. This same procedure when applied to the control wells and wells containing QDS NPs showed no visible heating even after 30 minute of exposure to the laser beam. These observations clearly confirm the hypothesis that the gold speckles impart hyperthermic properties to QDSG NPs.

The hyperthermic experiments were conducted in A549 cells, which were plated in six-well plates in a similar manner as described before (Section 4.2.1). A stock solution of QDSG and QDS NPs were prepared in cell media at a concentration of 1 mg/mL. 1 mL of the QDS stock solution was added to two wells each containing cells ($2.0x10^4$ cells/mL) in 1 mL of cell media. This brought the effective concentration of the solution in the wells to 500 μg/mL. The same procedure was repeated in two other wells using QDSG stock solution. The last two wells were left with cells and no particles, to be used as controls. The cells were incubated with the NPs for 24 hours. After incubation, the supernatant was removed from all six wells and washed three times with cold PBS in order to remove the NPs that are not associated with the cells. The six-well plate was introduced into the BioRaman Spectroscope and each well is exposed to the laser beam at 785 nm. Cells incubated with QDSG NPs began to change their shape and eventually disintegrate. During the process of disintegration, initially it appeared that the cells swelled up like a bubble and then the “bubble” burst leaving

behind a black hole in the area were the beam was focused with cellular debris strewn around it. This disintegration process was not observed in the control wells and the wells with QDS NPs. This confirmed that the hyperthermic property of the gold speckles on the QDSG NPs was active *in vitro*. The effect of exposing the A549 cells, dosed with QDSG and QDS NPs, to the laser source can be seen in Figure 4.12. Figures 4.12 (a) and (b) shows the A549 cells dosed with QDSG NPs before and after exposure to laser. A small black hole and other changes due to heating (marked with black circles in the figure) could be observed in the cells after laser exposure. Similar changes could not be seen in the cells dosed with QDS NPs, as seen in Figures 4.12 (c) and (d), before and after exposure to laser and in control cells with no NPs as seen in Figures 4.12 (e) and (f), before and after exposure to laser .

The bioimaging and therapeutic functionalities of the engineered NPs developed for this research work has been successfully demonstrated in this chapter. The effect of various physicochemical parameters of the NPs on the cellular uptake was studied qualitatively and semi-quantitatively using confocal microscopy and protein assays. Biocompatibility assessments on NPs were carried out to study the effects of pre-conditioning using cell media. As mentioned in Chapter one, in order to establish any NP-based contrast agent, it is important to understand the biodistribution behavior of the particles inside living systems. Consequently, the use of the NPs developed for this research work, in rat model for blood clearance studies shall be discussed in the following chapter.

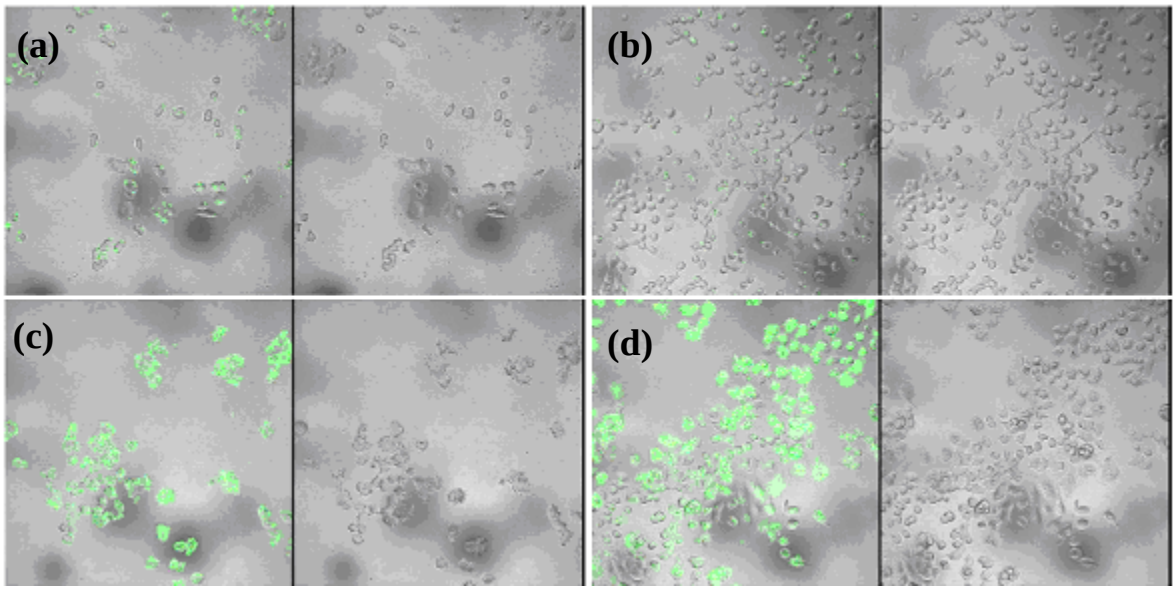

Figure 4-1. Fluorescence and transmission image of A549 cells incubated with 100 nm aminated FSNPs for time of incubation (a) 5 hours and (b) 24 hours and 100 nm folated FSNPs for time of incubation (c) 5 hours and (d) 24 hours at particle concentration 100 μg/mL. Presence of folic acid has led to the uptake of a substantial amount of particles by the cells.

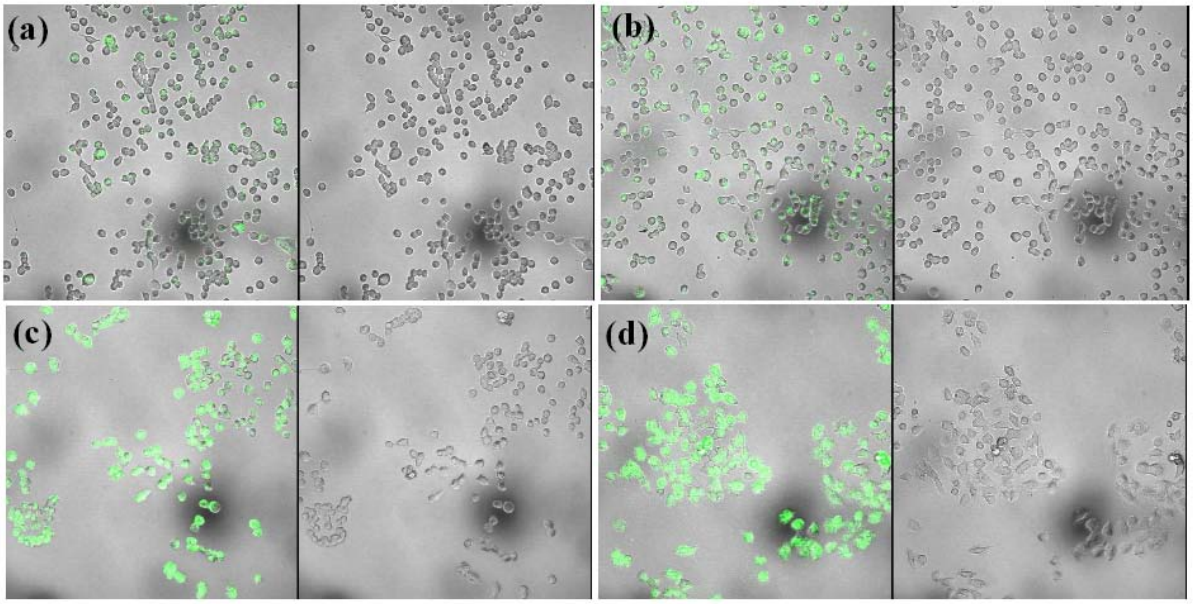

Figure 4-2. Fluorescence and transmission image of A549 cells incubated for 15 hours with 100 nm aminated FSNPs at particle concentration (a) 50 μg/mL and (b) 200 μg/mL and 100 nm folated FSNPs at particle concentration (c) 50 μg/mL and (d) 200 μg/mL. There is a reduced amount of aminated nanoparticles uptake by the cells.

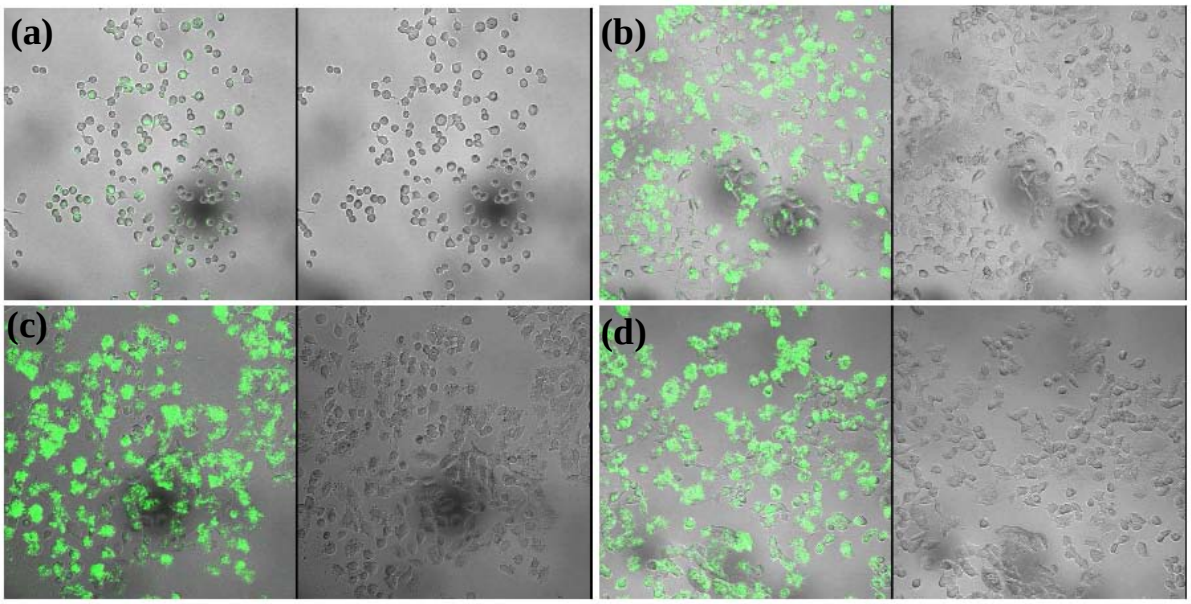

Figure 4-3. Fluorescence and transmission image of A549 cells incubated for 15 hours at particle concentration 200 μg/mL with (a) 100 nm and (b) 190 nm aminated FSNPs and (c) 100 nm and (d) 190 nm folated FSNPs. Although there is an increase in the fluorescence intensity for the larger nanoparticles it does not necessarily imply that this is due to an increase in the nanoparticle uptake, as the larger nanoparticles can enclose a greater amount of dye molecules.

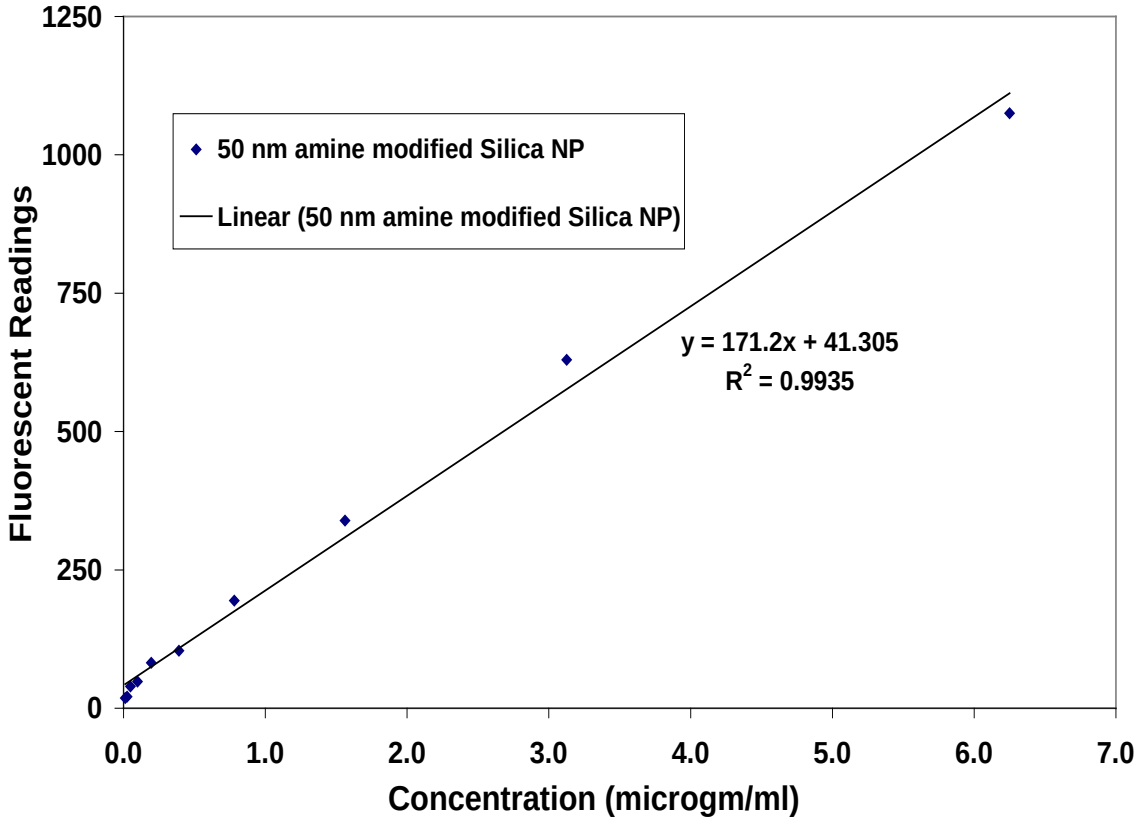

Figure 4-4. Typical particle concentration vs. fluorescence readings curve used as for calibration to compare and determine unknown particle concentrations. The curve has been plotted for 100 nm aminated amorphous silica nanoparticles.

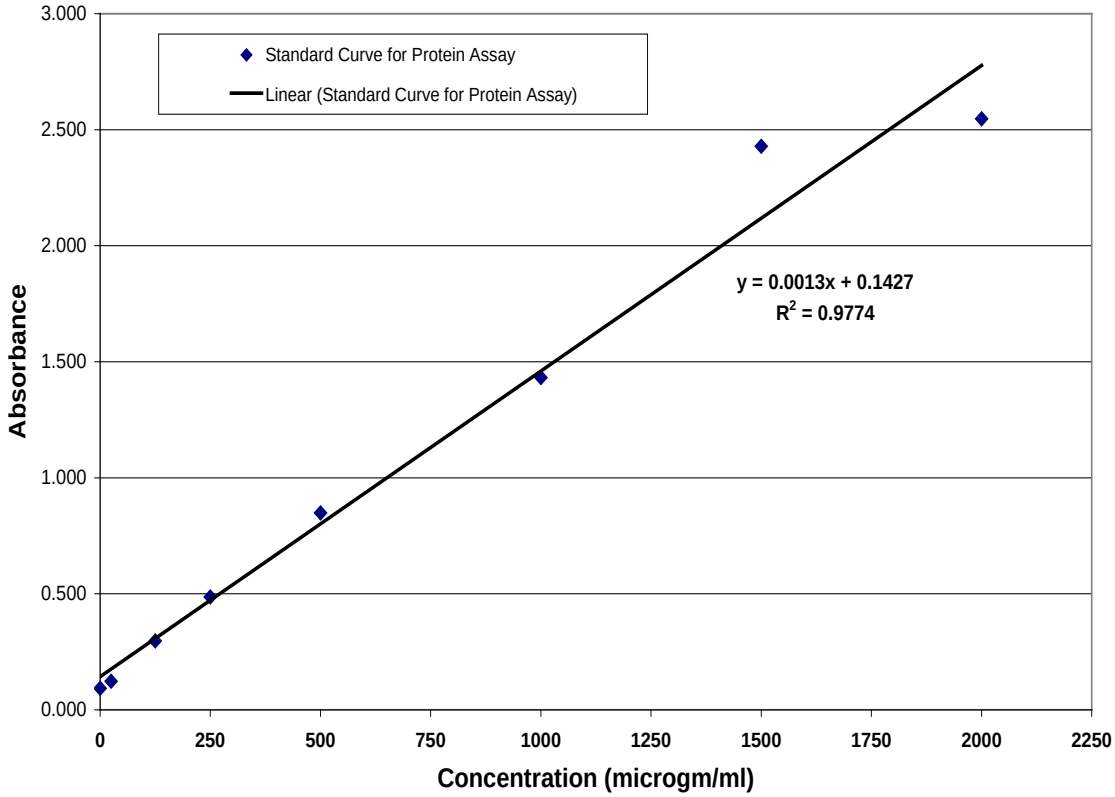

Figure 4-5. Typical protein concentration vs. absorbance readings curve used as for calibration to compare and determine unknown protein concentrations. The curve has been plotted for 100 nm aminated amorphous silica nanoparticles.

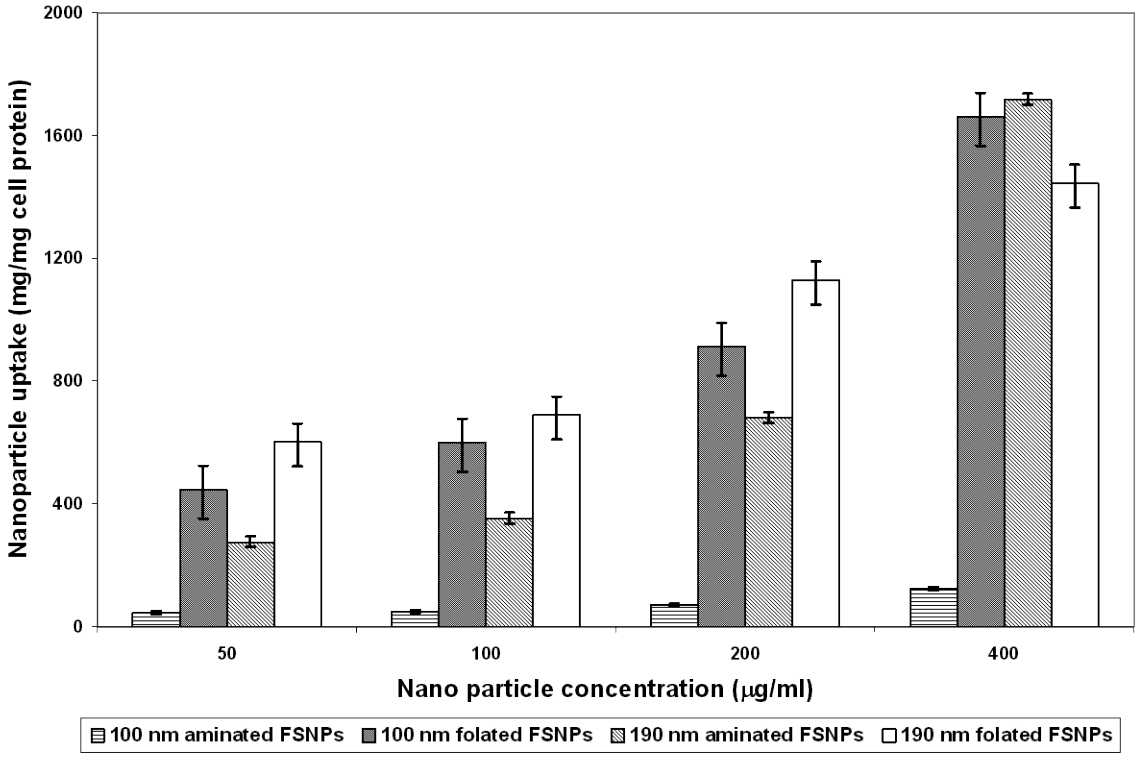

Figure 4-6. Quantification of cellular nanoparticle uptake.

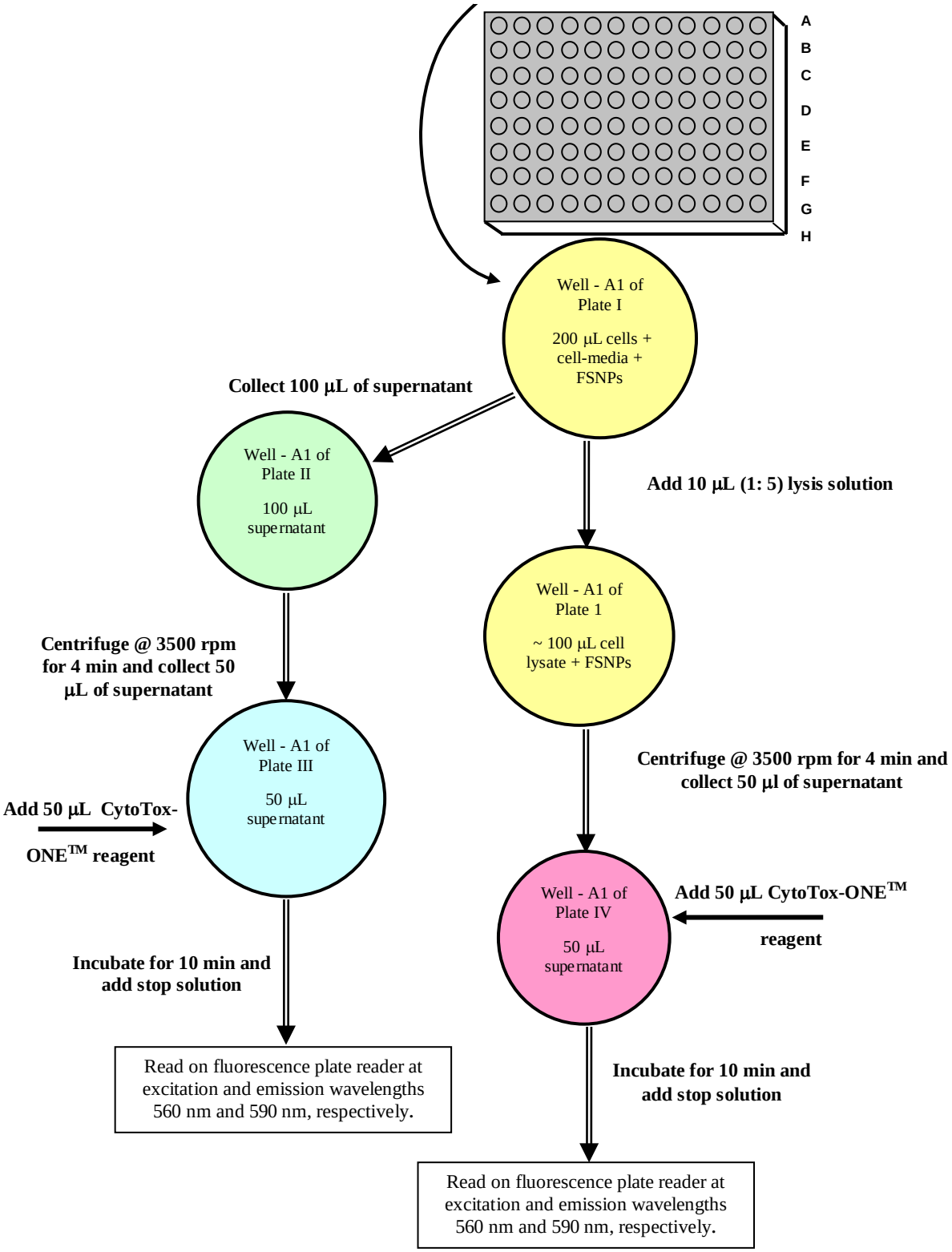

Figure 4-7. Procedure for the cell viability test based on LDH membrane integrity assay.

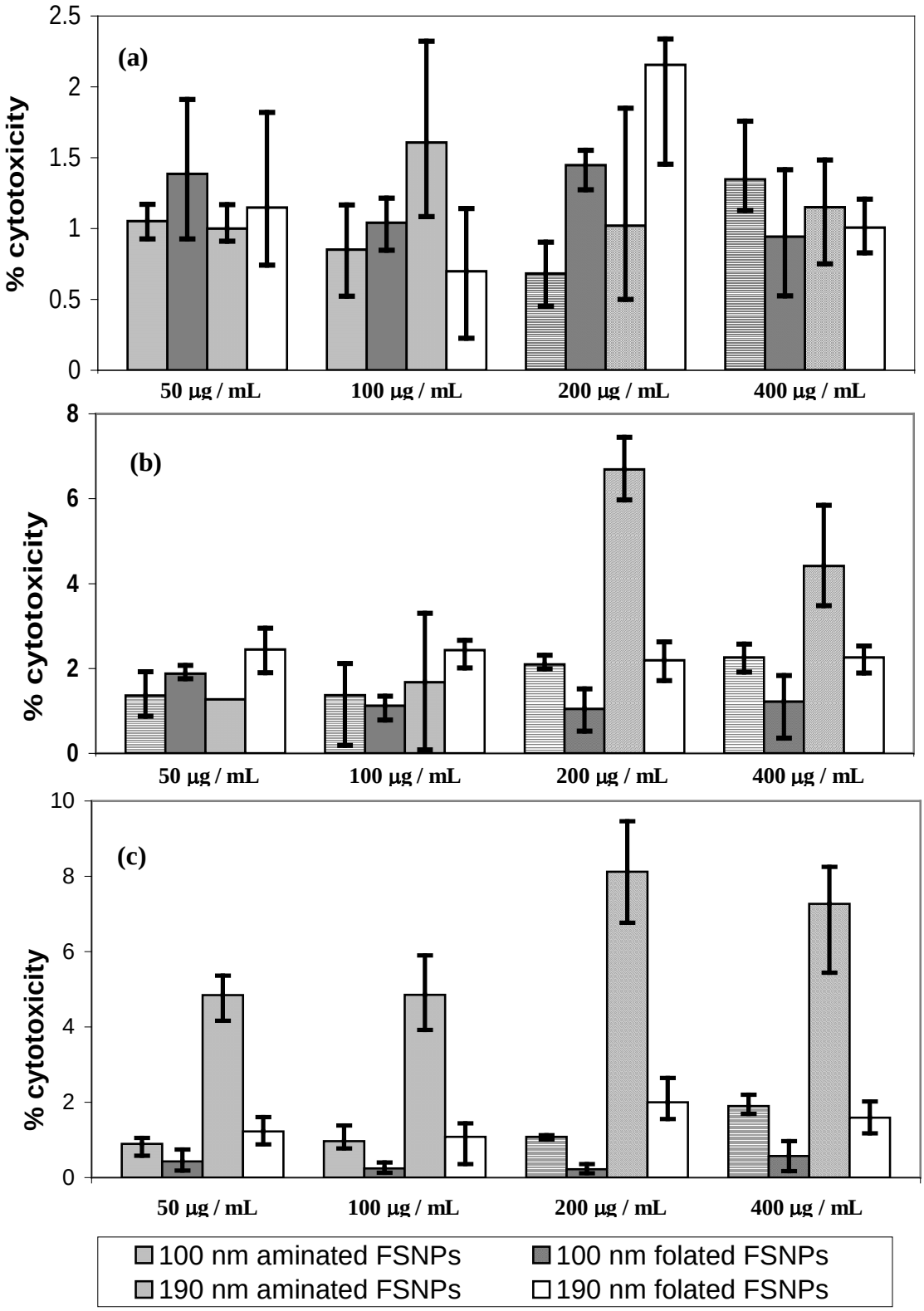

Figure 4-8. Percentage cytotoxicity of 100 nm and 190 nm aminated and folated FSNPs preconditioned in media and incubated for (a) 5 (b) 24 and (c) 48 hours.

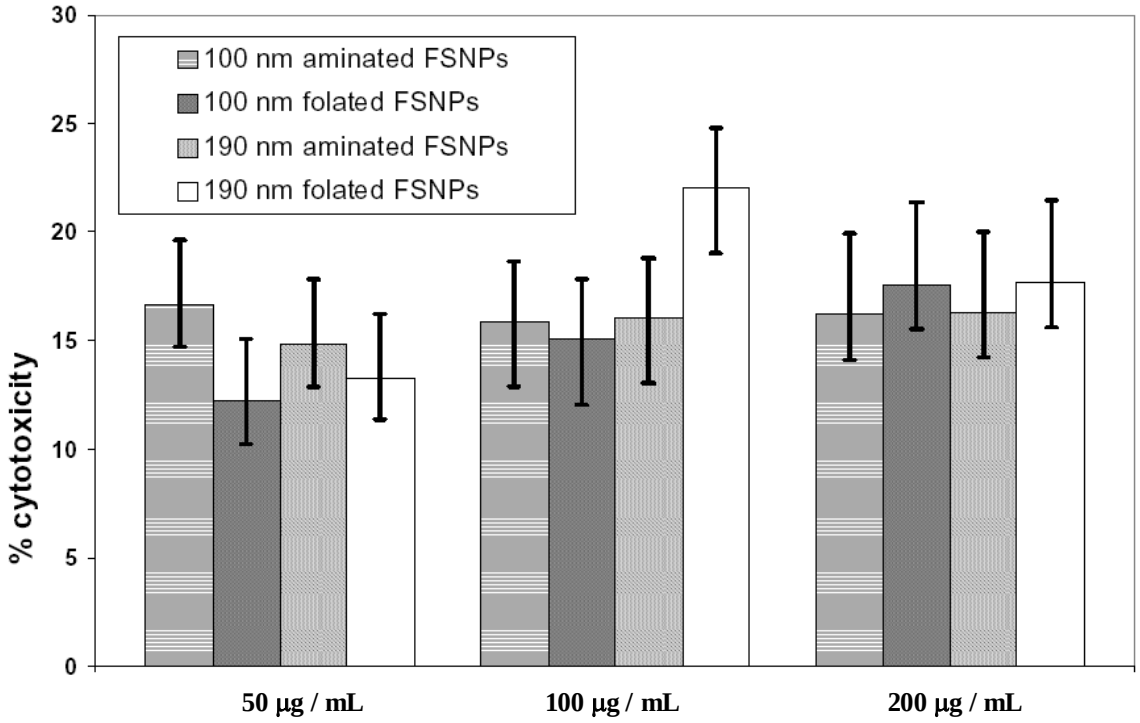

Figure 4-9. Percentage cytotoxicity of 100 nm and 190 nm aminated and folated FSNPs that were not preconditioned in media and incubated in A549 cells for 2 hours.

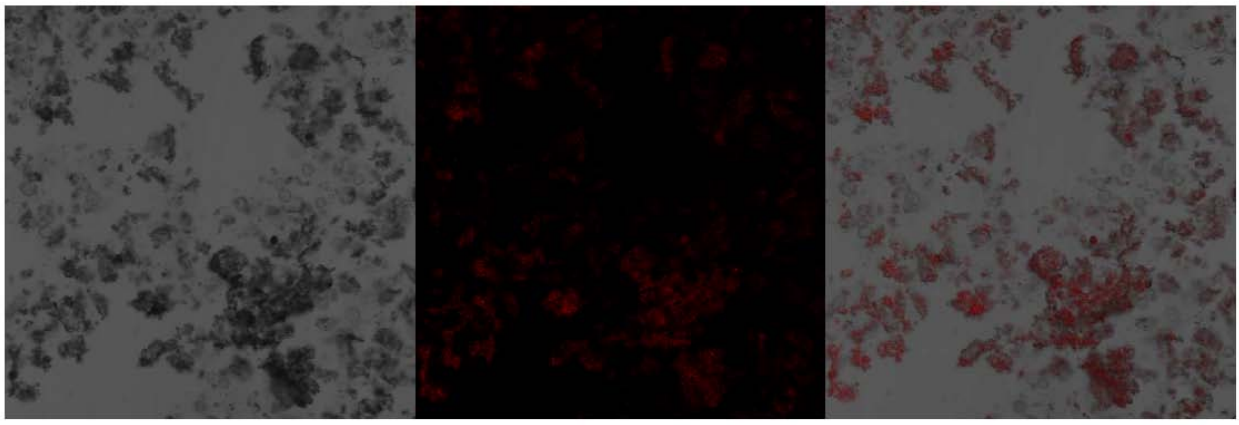

Figure 4-10. Laser scanning confocal microscopic images of A549 cells incubated with QDSG nanoparticles at 200 μg/mL for 24 hours in (a) transmission, (b) fluorescence and (c) combined transmission and fluorescence modes.

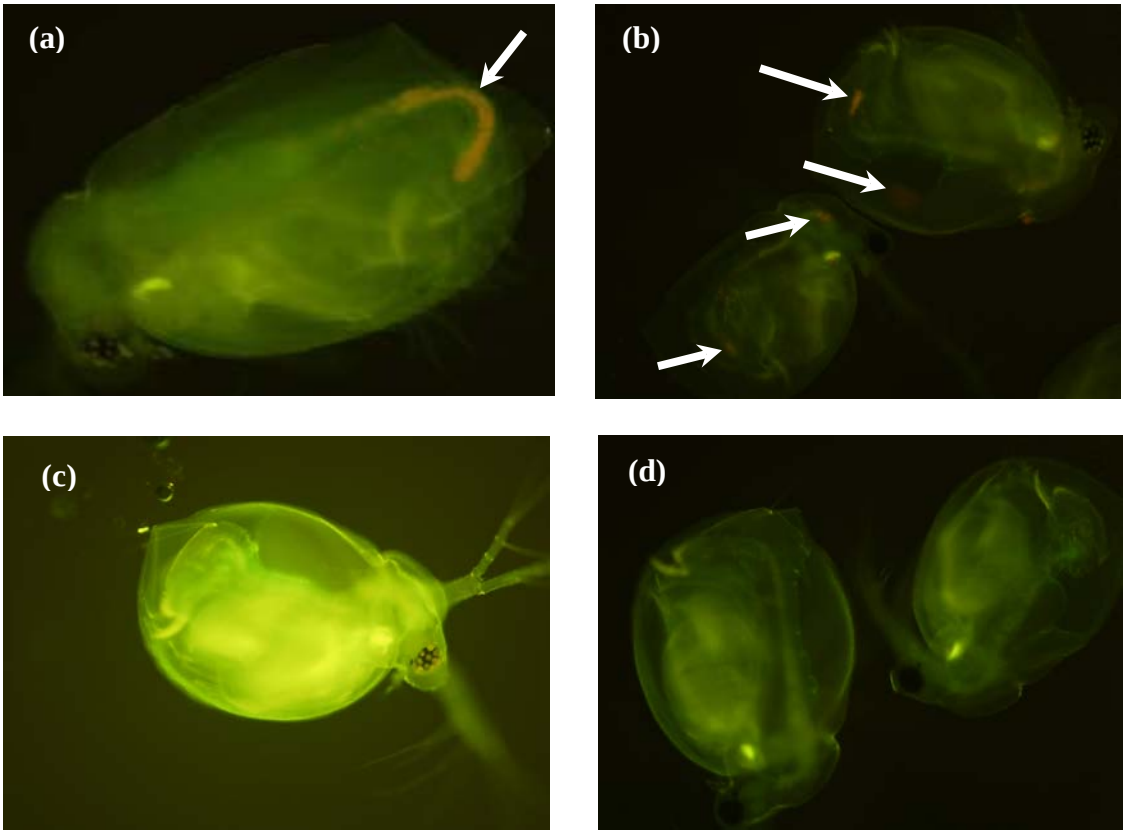

Figure 4-11. QDSG NPs in daphnia. (a) and (b) QDSG NPs uptaken by daphnia after 24 hours as observed with an orange coloration in the gastrointestinal tract. The arrows in (a) and (b) point to QDSG NPs. (c) and (d) Control daphnia with no NPs.

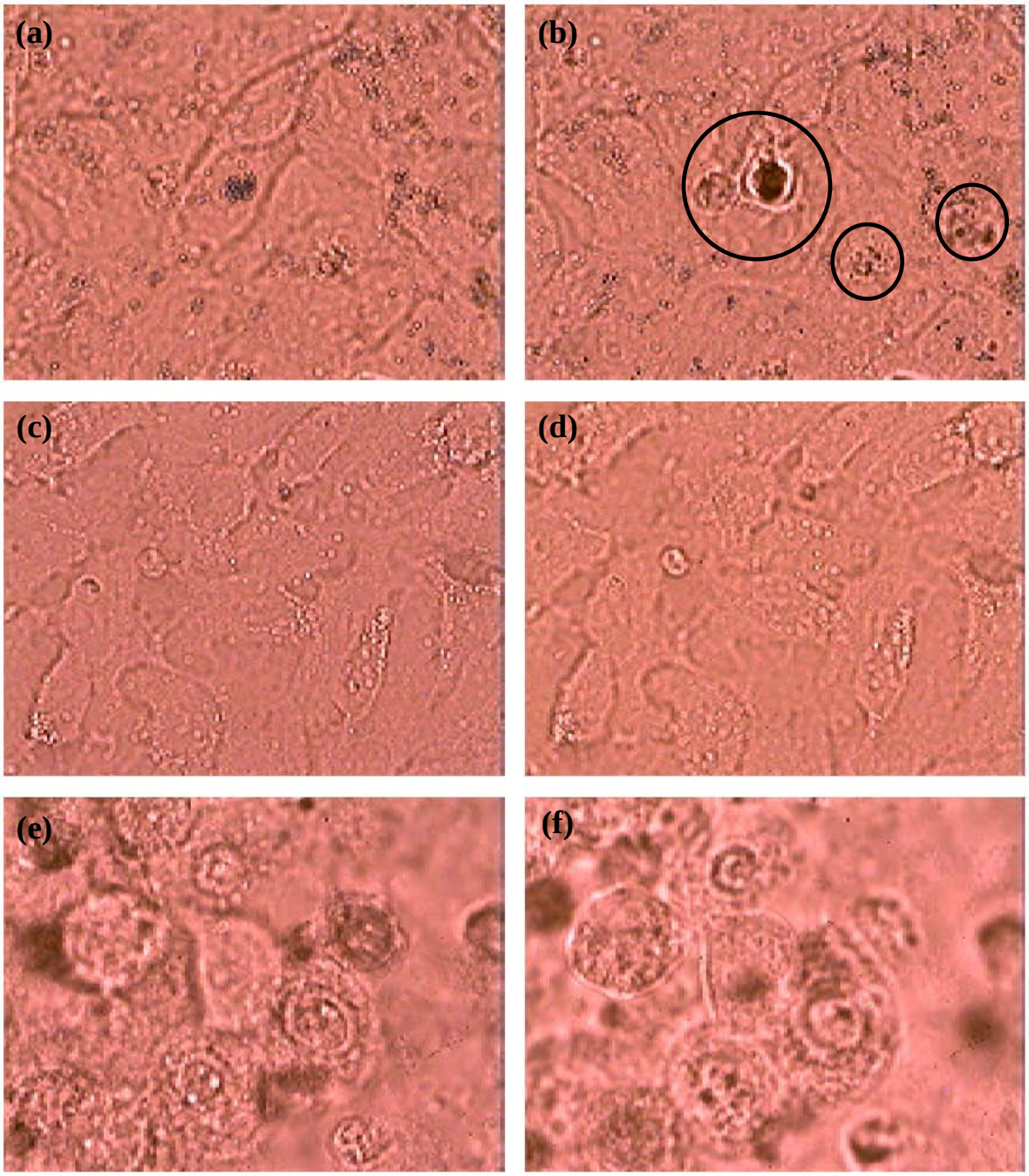

Figure 4-12. Hyperthermic characteristics of nanoparticles in A549 cells incubated for 24 hours and exposed to laser at 785 nm, using QDSG nanoparticles (a) before and (b) after exposure, using QDS nanoparticles (c) before and (d) after exposure and using control cells with no nanoparticles (e) before and (f) after exposure.

CHAPTER 5
PARTICOKINETIC STUDY OF NANOPARTICLES IN RAT BLOOD

There have been numerous in vitro and in vivo studies on the toxicity outcome of quantum dots (QDs). However, inconsistencies regarding various issues like nanoparticle (NP) dosimetry, routes and duration of exposure and choice of animal models exist in many of these *in vivo* studies (Alexis *et al.* 2008, Harper *et al.* 2008, He *et al.* 2008, Huang *et al.* 2008, Jain *et al.* 2008, Khan *et al.* 2005, Li & Huang 2008, Semmler-Behnke *et al.* 2008, Sonavane *et al.* 2008, Yang *et al.* 2007). Similarly, uncertainties in particle concentrations used for dosing cells, state of agglomeration and effects of surface functionalizing the nanoparticles (NPs) are some of the challenges encountered for the *in vitro* studies (Teeguarden *et al.* 2007). Moreover, most of these studies do not provide reliable correlation between the physicochemical properties to the NP disposition (Committee 2004). In this study, a systematic investigation of the blood clearance behavior of NPs in rat was carried out using analytical detection technique. It is anticipated that results from this present study will clarify and eliminate the discrepancies in the literature relating to the effect of material composition and surface charge on the blood clearance behavior of NPs. The goal was to develop a predictable and reliable methodology to elucidate the clearance behavior from the half-life values of the NPs. The final section describes a preliminary protein adsorption study to visually observe the adsorbed proteins on the various NPs. It was conducted using one-dimensional gel electrophoresis using QDS, QDSG and gold NPs with three surface charges: positive, negative and near neutral.

5.1 Experiments with Nanoparticles (NPs) in Rat Model

5.1.1 Nanoparticles (NPs) used for Animal Study

The synthesis and characterization procedures of the NPs used for the animal studies have been discussed in details in Chapter 3. Briefly, five NPs belonging to two different classes -

gold and quantum dot based NPs were used for the rat blood clearance studies. The five different NPs were: 1) bare gold NPs, G- (negatively charged surface), 2) amine-modified gold NPs, G+ (positively charged surface), 3) pegylated gold NPs, GP (near neutral surface charge), 4) silica coated CdS: Mn/ZnS quantum dots (QDS) and 5) gold speckled silica coated CdS: Mn/ZnS quantum dots (QDSG).

As per established practice (Teeguarden *et al.* 2007), a preliminary one-compartmental model was first developed using half-life ($t_{½}$) data of various NP systems reported in the literature (Alexis *et al.* 2008, Banerjee *et al.* 2002, Guo *et al.* 2007, He *et al.* 2008, Lee *et al.* 2007, Li & Huang 2008, Liu *et al.* 2008, Sonavane *et al.* 2008, Wang *et al.* 2004, Yang *et al.* 2007). This model was then used to study the effect of various NP parameters (percentage composition of constituent element, particle concentration and rat weight) on blood clearance and half-life behavior in rat blood. An optimal dose of NPs to be injected into the rats was selected and the model was then modified using experimental data from analytical detection of the blood samples collected from the animal study. The half-life value of each NP was calculated from the one-compartmental model to further refine the model necessary to determine the particokinetic behavior of the NPs in rat blood.

5.1.2 Dosing the Rats

Twenty two Sprague-Dawley rats were purchased from Charles River Laboratories International Inc, (Wilmington, MA) and acclimated for one week in the animal facility at (Teeguarden 2008). All animal treatments and experimental protocol for this study was subjected to the review and approval from the Institutional Animal Care and Use Committee (IACUC). Therefore, the animals were handled according to standard animal husbandry practices and given humane treatments with regard to alleviation of suffering during the entire animal study. The

animals were housed in facilities having less than 12 hours of light/dark cycle, temperature-controlled to room temperature with ad libitum water and food availability.

Fifteen rats were used as experimental animals and dosed with NPs and seven were used as control animals. The experimental rats were labeled 1 to 15, with three rats dedicated to be dosed with each NP. Two of the three rats for each NP were housed in a metabolism cage, in order to facilitate the collection of urine and feces at pre-determined time-points while the third rat was housed in a normal animal cage. The control rats were labeled 16 to 22 and blood samples from the control rats were used to prepare the spiked samples to generate the reference curves for the animal study.

All animals were provided by the supplier with surgically implanted cannulae tubes made of polyurethane (PU) attached to the jugular vein of the rats. All five NPs, as dispersed in biological media, were injected intravenously through the cannulae tubes into the jugular vein of the rats over two minutes. For the rats inside the metabolism cages (first two rats for each NP), dosing was done through the PU tube and drawing of blood was carried out through an eight inch long polyethylene (PE) tube attached to the cannulae of the rats. For the third rat for each NP, kept in a normal animal cage, dosing as well as drawing out blood was conducted through the PU tube provided by the suppliers.

At the start of the experiment, the rats were weighed on a laboratory scale and noted to weigh between 240 and 275 grams (Table 5-1). The mass of NPs used for dosing the rats were calculated such that a rat weighing 225 grams was dosed with approximately 0.5 mg (0.5 mL stock solution of NP at 1000 μg/mL in 0.45% bacteriostatic solution) of each NP solution by intravenous injection through the surgically implanted PU cannulae tubes attached to the jugular vein. The syringes used for dosing the NPs were pre- and post-weighed in order to ascertain the

exact dose of NPs delivered to each individual rat (Table 5-1). Similarly, the glass tubes used for blood collection and storage were pre- and post-weighed to determine the exact mass of blood collected from each animal (Table 5-2).

Blood samples of approximately 400 μL volume was drawn from each of the 15 rats just prior to dosing i.e. at time-point 0 minutes, using the pre-heparinized syringes and luers and placed in pre-heparinized borosilicate glass tubes. Similarly, post dosing, 400 μL of blood was drawn out from the rats at every pre-determined time-point of 5, 15, 30, 60, 180, 360 and 1440 minutes. Serial sacrifices of the animals were conducted using carbon dioxide atmosphere at the end of the study i.e. after 1440 minutes (24 hours) following dosing of the rats. Tissue samples, including liver, lungs, kidneys, heart, spleen, brain, muscles and fat were collected after the sacrifice. Urine and feces were collected from 2 of the 3 rats dosed with each NP i.e. the rats placed in the metabolism cages. All tissues, blood plasma, urine and feces were labeled and stored in freezers at -80°C for future analysis. The carcass of all animals were labeled and stored in freezers at -80°C for possible further investigations.

The blood samples collected from the rats at different time-points were analyzed for gold (molecular weight = 196.97) in rats that were dosed with G-, GP and G+ NPs. Rats dosed with QDS and QDSG were analyzed for cadmium (molecular weight = 112.41). All analyses of blood samples were conducted at standard conditions (room temperature and pressure) utilizing inductively coupled plasma mass spectroscopy (ICP MS) techniques.

5.1.3 Nanoparticle (NP) Dispersion in Dosing Solution

Gold NPs have been shown to exhibit variations in color with a change in size (Jiang *et al.* 2004b). During the process of NP administration into the rats, it was noticed that the stock solution of gold NPs on contact with biological media displayed a gradual change in color from

dark red to bluish-red, purple and finally formation of black precipitates that settled down in a clear solution, These visual observations indicated the formation of gold NP agglomerates in the bacteriostatic solution used as the biological media.

In order, to study the effect of the different dispersion media (blood-plasma, heparin lock flush solution and bacteriostatic solution), a stock solution of gold NPs was prepared at a concentration of 1000 μg/mL in de-ionized water. The stock solution was then added in increasing amounts (with infinitesimal increments) to different vials containing blood-plasma, heparin and bacteriostatic solutions respectively and visually observed for any changes in color of the solution. Generally, heparin lock flush solution (Emergency Medical Products Inc, Waukesha, WI) is used in an animal study to prevent blood coagulation while 0.9% bacteriostatic solution (Med-Tech Resource Inc., Eugene, OR) is used as a buffer to maintain a pH 7.4 in the rat blood after dosing the animal with NPs.

It was observed that the addition of blood turned the color of the stock solution to dark red. Thereafter, it was difficult to visualize any observable color changes in the red colored gold NPs that can be attributed to the formation of agglomerates in the presence of blood. An addition of an equal amount of 100% (by mass) heparin solution (or more) to gold NP solution changed its color from red to bluish-red, purple and finally after ten minutes led to the formation of black precipitates in a clear solution. For example, an addition of 0.5 mL heparin solution or more to 0.5 mL gold NP solution resulted in the described color changes of the solution. Finally, addition of bacteriostatic solution to gold colloids at a ratio of 7:10 led to the agglomeration of the negatively charged colloidal gold NPs. For example, an addition of 0.35 mL of bacteriostatic solution or more to 0.5 mL of gold colloids led to the afore-mentioned color changes. This simple experiment, using visual inspection, provided an insight into the maximum amount and

concentration of heparin lock flush solution and bacteriostatic solution that could be used to disperse the particles to prepare the stock solution.

As per the IACUC protocols (Teeguarden 2008) at the national laboratory, the acceptable range for composition of the bacteriostatic solution (buffer) for an animal study was between 0.3 to 0.9%. However, it was impossible to disperse the NPs in the 0.9% bacteriostatic solution, which is the preferred biological media for animal studies. There was an immediate change in color of the gold NP stock solution in the 0.9% bacteriostatic solution which indicated the formation of micron-sized aggregates. Formation of aggregates was avoided by reducing the electrolytic concentration of the media used for dispersion to 0.45% bacteriostatic solution. The present study, although nearing the lower electrolytic limit, was valid. The stock solution of NPs for the animal study was prepared in 0.45% bacteriostatic solution with trace quantities of heparin in it to emulate the conclusions from the observations of the above study. The results of the visual observations from this study are summarized in Table 5-3.

The bare gold (G-) and pegylated gold (GP) NP samples remained dispersed in 0.45% bacteriostatic solution at their primary particle sizes for 24 hours. The positively charged gold NPs, QDS and QDSG NPs remained dispersed for 12 hours only. The actual dosing solutions of the five NPs for the animal study were prepared the previous night, eight hours before injection into the rats in the morning.

5.1.4 Analysis Protocol

As mentioned above, 400 μL of actual blood samples were collected from the fifteen experimental rats at different time points. The blood was collected in pre-heparinized disposable borosilicate glass culture tubes 16 x 150 mm (Fisher Scientific, Pittsburg, PA). The blood samples were treated with 2 mL of concentrated (70%) nitric acid (Sigma-Aldrich, St. Louis,

MO) to digest all organic components present in the samples. The mixture of blood, NPs and acid in the glass tube was then heated in a dry bath using aluminum blocks at 125℃ for 15 minutes. The bath was then cooled to 110℃, followed by the addition of 1.6 mL of pure aqua regia (Hydrochloric Acid: Nitric Acid = 3:1) into the glass tubes to allow acid digestion of gold and quantum dot NPs. Further heating was continued for 15 minutes before the samples were evaluated for completeness of digestion. The high effective concentration of aqua regia (40%) and nitric acid (50%) used was sufficient to completely digest all NPs. The glass tubes were then removed from the dry bath, allowed to cool to room temperature and the contents were filtered through Acrodisc 0.45 μm PTFE syringe filters (Acrodisc: Catalog Number 4219, Pall Life Sciences, Ann Arbor, MI) to remove all tissue debris from the samples. Considering complete digestion of all NPs, the possibility of any loss of analyte during passage through the filters was negligible. This was verified from the background level signals for gold and cadmium detection in samples prepared by scraping and digesting the filters (post-filtration of NPs) and analyzed using the ICP MS. Post-filtration, the acid-digested blood samples from the animal study were then stored into 15 mL polystyrene centrifuge tubes for further dilution and analysis using ICP MS. In summary, the following acid-digested protocol was used for the subsequent studies.

- Addition of 1.5 mL concentrated HNO3 (70%) to the blood-plasma samples in glass tubes samples are heated in aluminum blocks in a dry bath at 125℃ for 15 minutes
- The samples should be completely digested and clear at this point with no tissue remaining, if not, the temperature of the dry bath is carefully increased to 140℃ and heating is continued for another 15 minutes.
- The dry bath is now cooled to 110℃ and the tubes are removed and allowed to cool
- Addition of 0.5 mL hydrogen peroxide (30%) to the samples and the glass tube is put back into the dry bath at 110℃ and digestion is continued for another 60 minutes to ensure complete digestion of all biological molecules in the samples.

- Next 1 mL of aqua regia (HNO3: HCl = 1:3) is added and the samples are put back into dry bath at 110°C and heating is continued for another 15 minutes.
- Samples are filtered through a 0.45 micron and put into 15mL polystyrene centrifuge tubes.
- Samples are stored in 15 mL centrifuge tubes for future analysis.

5.1.5 Analysis of Blood Samples

An Agilent 7500CE series ICP MS (Agilent Technologies, Inc, Santa Clara, CA) with an octapole reaction system (ORS) was used for analytical detection of gold and cadmium in blood samples in the present study. The theoretical detection limit of an ICP MS for gold and cadmium was reported (Lewen *et al.* 2004) to be 1 and 3 nanograms per liter respectively. Generally, nanograms per liter is more commonly expressed as parts per trillion (ppt) for analytical detection techniques. However, it is to be noted that the reported detection limits have been determined using elemental standards in dilute aqueous solutions with an expressed 98% confidence level. However, detection limits inside the biological matrix was suspected to be much lower due to the presence of high backgrounds and have to be individually determined for the samples and the particular analyte in the matrix in question.

The ORS technology of the Agilent 7500 CE series ICP MS uses helium (He) collision mode for the predictable removal of all matrix interferences and allows full-scan semi quantitative analysis. Moreover, there is optional hydrogen (H_2) and argon (Ar) reaction modes for the sensitive (single digit ppt) detection limits for various additional elements. The analytical technique employed in the present study utilized the argon mode for detecting gold and the helium mode for detecting cadmium for the quantum dot NPs respectively.

Two separate standard reference curves were generated using known (spiked) samples of gold and QD NPs respectively. The first set of gold spiked samples consisted of increasing gold concentration of 0, 1, 2, 4, 8, 16, 32, 64 and 128 parts per billion in control rat blood. The second

set of samples generated using known amounts of QDS NPs contained increasing cadmium concentration of 0, 1, 2, 4, 8, 16, 32, 64, 128 and 256 parts per billion in control rat blood. All samples were prepared in triplicates and the average values of the three readings obtained from the ICP MS was used to generate the standard curve. The standard deviations of the three readings along with the value of R^2 of the linear line gave an indication to the accuracy of the curve fit for the standard curve. The reference curves were used to quantify the amount of gold and QD-cored NPs present in the blood samples. Finally, a 'concentration - time profile' curve was generated for each of the five NPs. This curve along with equations in the one-compartmental model was used to calculate the half-life value of each NP in rat blood. More details of this procedure are given later in this chapter.

5.1.6 One Compartmental Model

A common approach, especially used by researchers in the pharmaceutical field is to develop pharmacokinetic models that can describe the time-dependent distribution and disposition of a substance in a living system. Towards a medicinal end-point, these models are used to estimate an optimum drug dosage and schedule protocol. For the industrial end-point, such models help to characterize the toxins and assess the transport and metabolism characteristics of the substance *in vivo*.

Various pharmacokinetic models consider the animal body as a system of compartments. The rate of transfer of the drug between one compartment to another and the rate of elimination from the various compartments is assumed to follow first-order or linear kinetics. The one compartmental model, which is the simplest model, presumes that the whole body is a single homogenous unit for 'kinetics' considerations. The one compartmental model has been shown to be especially relevant for the pharmacokinetic analysis of drugs that can distribute extremely rapidly throughout the body. The blood plasma or serum is almost invariably the anatomical

reference for the one compartmental model. It assumes that the rate of change of drug concentration in the blood plasma quantitatively reflects the rate of change in drug concentration throughout the body.

Investigators (Teeguarden *et al.* 2007) have shown that similar studies for NPs using one-compartmental models can be conducted. Accordingly, a one compartmental model was developed in this research, to assess the clearance of NPs from rat blood. These results are anticipated to provide some insight to NP clearance from the blood without the considerations of other competitive and complicated processes like tissue uptake and presence of opsonins, which may be incorporated into subsequent research studies.

First Order Kinetics. In the one compartmental model, the NPs, following intravenous injection into the body, distribute rapidly and are eliminated according to first-order kinetics i.e. the rate of particle loss from the body is given by:

$$\frac{dX}{dt} = -KX \tag{5-1}$$

where X is the mass of the particles in the body at time t after injection and K is the first-order (elimination) rate constant for the NP (negative sign implies that the NP mass in the body reduces with time).

In order to describe the time course of the NPs after injection into the body, Equation 5-1 can be integrated to obtain

$$X = X_0 \exp(-Kt) \tag{5-2}$$

where X_0 is the initial mass of the particles. Applying natural logarithm on both sides of Equation 5-2

$$\ln X = \ln X_0 - Kt \tag{5-3}$$

Converting Equation 5-3 in terms of Log results in

$$\log X = \log X_0 - \frac{Kt}{2.303} \tag{5-4}$$

The relationships expressed by Equations 5-3 and 5-4 can be written in terms of the concentration of the particles per unit volume of blood (instead of mass of particles) as follows.

$$C_t = C_0 \exp(-kt) \tag{5-5}$$

$$\log C = \log C_0 - \frac{kt}{2.303} \tag{5-6}$$

where C_0 is the initial NP concentration in blood immediately after injection, that is at t = 0, C_t is concentration after time t and k is the first order rate constant for concentration-time relationship.

Equation 5.6 indicates that a plot of log C versus t is a linear curve for the assumed first order kinetics. C_0 can be obtained by the extrapolation of the log$C$ versus t plot to time zero. This value of C_0 is used in calculating the apparent volume of distribution, V given by the relationship

$$V = \frac{X_0}{C_0} \tag{5-7}$$

The slope of the line generated from Equation 5-6 is equal to -k/2.303 and the value of k is obtained from the value of this slope. Alternatively, setting C = C0/2 and t = $t_{1/2}$ gives another relationship between the (elimination) rate constant k and half-life $t_{1/2}$ as

$$t_{1/2} = \frac{0.693}{k} \tag{5-8}$$

where $t_{1/2}$ is the biological half-life of the NPs in the rat blood. The biological half-life of any substance is defined as the time it takes to lose half of its activity i.e. expressed by a drop in concentration to half its initial value. An important aspect of a first-order process is that the $t_{1/2}$ is independent of the initial concentration of the substance. Equations 5-1 to 5-8 were used for

developing the one-compartmental model The model was initially used to calculate the particle concentration of the dosing solutions at 1000 μg/mL for the animal study to ensure detectability on the ICP MS. Relevant information (composition, surface area, density) for each NP was used as input parameters for the model to calculate the half-life of the NPs. For example, the relevant particle information for the QDSG NPs is listed in Table 5-4.

5.2 Establishing the Protocols for Animal Experiments

Before conducting the actual animal experiments, it was necessary to develop protocols for analytically detecting the analytes (gold and cadmium) in the blood sample collected after NP injection into the rats. During the process of establishing the protocol, the effect of a number of different variables on the experimental data was encountered. This section describes the effect of the different variables and the optimized protocol established for the animal study.

5.2.1 Effect of Background from Aqua Regia

Preliminary observations from the ICP MS demonstrated that high concentrations of aqua-regia in solutions present a background signal even without any presence of gold in the solution. Therefore, it was necessary to determine an upper limit of the aqua-regia concentration below which the background effect was insignificant. In order to minimize the background signal from aqua regia, the effect of varying concentration of aqua regia on the ICP MS readings was studied. A series of spiked samples having concentrations of aqua regia 0, 0.078, 0.156, 0.313, 0.625, 1.25, 2.5, 5 and 10% of the as prepared aqua regia concentration (1:3 HCl:HNO_3) were prepared. An increasing ICP MS background signal (detecting for gold) as a function of increasing aqua regia concentration for samples dispersed in water when no NPs were present can be seen in Figure 5-1. It can be observed that for aqua regia concentrations of 0.625% and above, there is a background contribution to the instrument signal due to the high concentration of acid. Moreover, above concentrations of 1.5% it was observed that the background effects far

supercede the signal intensity of gold solutions containing 32 ppb of gold. Therefore, the aqua regia concentration used for digesting the samples was maintained at 5% and below for all subsequent studies.

5.2.2 Effect of Background from Other Components

The experiment in the preceding section was conducted with aqua regia in water (matrix). A similar experiment was conducted with aqua regia in a matrix that would imitate the experimental conditions of the animal study. This matrix contains control rat blood, nitric acid and water. First, six glass test tubes were each filled with 1.0 mL of control rat blood and 1.0 mL of nitric acid. To these 6 test tubes 1 mL of 0%, 1%, 2%, 3%, 4%, 5% and 6.25% of aqua regia were added. The volume of the solution in each glass tube was then increased to 10 mL by the addition of 7 mL of water to each tube. This results in an effective concentration of aqua regia in the test tubes of 0%, 0.1%, 0.2%, 0.3%, 0.4%, 0.5% and 0.625%, respectively. The results from ICP MS analysis of these solutions are shown in Figure 5-1. It can be observed that the background reading is constant over the range of 0% to 0.625% aqua regia concentration. This trend is similar to the above experiment of aqua regia in water. However, the magnitude of background signal is uniformly higher in the second case. It could be easily inferred that this background is due to the other constituents of the matrix-blood and nitric acid.

It is imperative to reduce the background effect of blood and nitric acid to a minimum value, which can be accomplished by diluting the above solutions with water. It was found that diluting the above solution in blood and nitric acid matrix containing 0.5% aqua regia by 4 times with water reduced the background signal to the levels observed with pure water. In all subsequent experiments prior to the animal study, the blood samples were digested using 5% aqua regia, followed by dilution to forty times with de-ionized water before analysis to reduce background effects and generate best results.

5.2.3 Digestion of Nanoparticles (NPs)

Experiments were carried out using a series of spiked samples containing a constant amount of 50 ppb (a central point in the reference curves) of gold NPs in blood. These NPs were digested by adding the following concentrations of aqua regia: 0, 0.78, 1.56, 3.13 and 6.25% and continued heating in an aluminum block at 125°C in the dry bath for 15 minutes. Thereafter, the samples were diluted by ten times with de-ionized water to reduce the aqua regia concentration to less than 0.625% before being analyzed in the ICP MS. The concentration of gold as a function of aqua regia concentration is shown in Figures 5-2. It can be seen that the curve increases initially and then flattens in the region of 3% to 6.25% aqua regia concentration. At concentrations lower than 3%, the particles were not digested completely and the undigested particles were not analyzed by the ICP MS resulting in a lower concentration. The fact that the curve flattens out in the 3% to 6.25% region indicates that the particles have been completely digested.

The effect of increasing aqua regia concentration on samples in acid and blood as the matrix are compared in Figure 5-2. Moreover, similar to previous observations (Figure 5-1) there was a noticeable higher background effect even for samples with gold NPs in the presence of blood as compared to water at higher aqua regia concentrations. The cumulative effects of all the above findings are shown in Figure 5-3. The blue line in the background shows the effect of increasing aqua regia concentration on the background while the red line shows the extent of NP digestion with increasing aqua regia concentration.

5.2.4 Deposition of Nanoparticles (NPs) on Cannulae Tubes

It has been previously mentioned that the dosing of rats was carried out by injecting the NPs through the cannulae tubes made of PU. However, to draw the blood out, the rats in the metabolism cages had an 8 inch PE tube attached to the already existing PU tubes. It was found,

during preliminary studies, that the particle concentration in the blood drawn through the PE tubes was consistently lower than the particle concentration in the blood drawn through only the PU tubes. In order to quantify possible loss of gold or QD NPs through adsorption onto the PE or PU tube surface during intravenous injection and blood collection, two experiments were conducted.

The rats were provided by the supplier with PU cannulae tubes, 3 inches in length, 0.025 inches internal diameter and dead volume of 0.05 mL, surgically attached to the jugular veins. Additionally, for the two rats placed in the metabolism cages, PE tubes, 8 inches in length, 0.023 inches internal diameter and dead volume of 0.1 mL, were attached to facilitate the drawing of blood collection through the metabolism cages. For each NP, only one of the 3 rats was placed outside the metabolism cage.

Stock solutions for all five NPs were prepared in bacteriostatic solution, sonicated for 15 minutes and subsequently vortexed for five minutes and then added to control blood collected from rats prior to the experiments to bring the final concentration to 1000 μg/mL in blood. Four 15 mL centrifuge tubes for each NP were pre-weighed and kept aside. Sample PU tubes having 0.025 inches internal diameter and 3 inches in length were pre-weighed and 500 μL NP dosing solution is passed through the tubes using a syringe. The exiting solution from the tube is collected in the first pre-weighed 15 mL centrifuge tube, Tube A, which is then weighed to calculate the mass of sample. The PU tube is also re-weighed after rushing the sample through it. Thereafter, 500 μL phosphate buffered saline (PBS) solution is then passed through the tube and collected in the second pre-weighed centrifuge tube, Tube B, which is again weighed to calculate the mass of dead volume + PBS solution. The PU tube is also re-weighed to calculate the mass of PBS solution remaining back in it. Then, 500 μL of 5% aqua regia is passed through the tube.

The exiting solution from the tube is collected in the third pre-weighed centrifuge tube, Tube C, which is again weighed as before along with the PU tube. For the gold NPs, a final 500 μL of 5% aqua regia was passed through the tube and for the QD-based NPs, this final step was carried out with 2% nitric acid. The exiting solution from the tube is collected in the fourth pre-weighed centrifuge tube, Tube D, which is again weighed as before along with the PU tube. All sample collected in Tubes A to D were then digested using 1 mL of 5% aqua regia and heated at 125 ℃ for 15 minutes. This was followed by addition of 1 mL of 2% nitric acid and heated at 110 ℃ for 15 minutes. The samples were then dialyzed through 0.45 μm filters and the volume of the samples is brought to 10 mL by adding de-ionized water. The samples were then analytically quantified for gold and cadmium using the ICP MS.

(a) Using Polyurethane Tubes. The above experiment was first conducted using PU cannulae tubes and the results are given in Table 5-5. The amount of analyte detected by the ICP MS in Tube B for all 5 NPs after PBS rinse was less than 10%. It is important to note that the dead volume of the PU cannulae tube is 0.05 mL which is 10% of the total volume injected. Therefore, it can be concluded that a total amount of NP loss of les than 10% after dosing, which was recovered by the PBS rinse, is within the expected margin. The amount of analyte detected in tube C, after the first 0.5% Aqua Regia rinse was less than 2% for all the NPs and the amount of analyte detected in tube D after the last rinse with 0.5% Aqua Regia for all NPs was less than 1%. This confirmed a minimal adsorption of NPs from both the gold and the quantum dot solution inside the PU cannulae tube during dosing the rats.

(b) Using Polyethylene (PE) Tubes**.** A similar experiment was conducted using PE cannulae tubes, similar to the ones used for drawing blood from the rats in the metabolism cages in the animal study. Three pieces of PE tubings (8 inches in length, 0.023 inches internal diameter and

dead volume = 0.05 mL) were used for each NP dosing solution. The experiment was conducted in a way to imitate the process of drawing blood from rats in metabolism cages to analyze for any possibility of NP adsorption on the PE tube material. The results from the experiment conducted using the PE tubes are shown in Table 5-6. Contrary to the previous experiment using PU tube, in this case the loss of NPs due to adsorption on the PE tube was substantial for all particles except for GP. The total amount of NP loss after dosing as recovered by the PBS rinse was greater than 30%. The dead volume of the PE tube was 0.075 mL which is 15% of the total volume. Thus the NP loss due to adsorption on the PE tube was much higher than the expected margin of dead volume. The amount of analyte detected in Tube C, after the first 0.5% Aqua Regia rinse was greater than 8 % for all the NPs and the amount of analyte detected in Tube D after the last rinse with 0.5% Aqua Regia for all NPs was greater than 2%. This experiment confirmed that PE cannot be used as a cannulae tube material for further animal studies, as there would be NP loss during dosing and blood draw due to NP adsorption on the surface of the tube.

The observations from the experiment agreed with the results of the animal studies as shown for the QDSG NPs in Table 5-7. A high value of each analyte (gold and cadmium) was detected in Rat 3 placed in the normal cage and not attached to the PE tube as against a much lower value of the analyte in the blood of Rats 1 and 2 in the metabolism cages. Moreover, the discrepancy in the value for Rat 3 kept in the normal cage was only observed for the blood samples drawn out at the 5 minute time-point. The differences in the analyte detected between the three rats reduced remarkably for the 15 minute time-point. Finally, there was negligible difference for blood samples drawn at and after the 30 minute time-point for all three rats. It can be explained that the available sites on the PE tube were partially covered by the adsorbing NPs after the blood draw at the 5 minute time-point and completely covered after the blood draw at

the 15 minute time-point. Thereafter, the adsorption sight could have been saturated and hence no variations were observed in the detected analyte for blood drawn after the 15 minute time-period. These observations were similar for the other three NPs, namely QDS, G+ and G- NPs.

For GP NPs, no significant differences were observed between Rat 3 and Rats 1 and 2 at all time points. GP NPs are known to have stealth characteristics due to the presence of polyehtyleneglycol (PEG) that projects hydroxyl functional groups on the surface of the NPs. These functional groups make the NPs hydrophilic in nature and thus the proteins in the physiological environment do not get adsorbed onto the particle surface. However, this is not the case for the other four NPs and, thus, a distinctly different behavior can be observed in the remaining for NPs when compared to GP. Therefore, it can be surmised that surface functionality of the NPs is a crucial factor in determining the adsorption of NPs on the PE surface.

5.3 Results from Blood Clearance Study

In the following sections the results of the rat blood clearance study will be presented. The stock solutions were prepared with NPs dispersed in bacteriostatic solutions at varying concentration in such a way that the final NP concentration was 1000 μg/mL in 0.45% bacteriostatic solution. The stoichiometric calculations for preparing the dosing solutions of each NP at the target concentration of 1000 μg/mL are shown in Table 5-8. The blood samples containing the NPs were digested, analyzed and the half-life values were finally calculated.

5.3.1 Using Silica Coated Quantum Dots Nanoparticles (QDS NPs)

As per dispersion protocol established in Section 5.1.3, stock solutions of silica coated quantum dot (QDS) NPs at a particle concentration of 1000 μg/mL in bacteriostatic solution was prepared. The solution was vortexed (Vortex Genie 2, A. Daigger and Company, Vernon Hills, IL) and sonicated (Branson 1510, Kell-Strom, Wethersfield, CT) respectively for five minutes

for better NP dispersion. 500 μL of QDS in 0.45 % bacteriostatic solution was administered into the cannulae tube of three rats (labeled 13–15) and the solution was rinsed up and down to ensure that all QDS NPs in the dose including the dead volume had been injected into the rat blood. Subsequently, 400 μL of blood was drawn from each rat at the pre-determined time-points, collected in pre-weighed glass tubes and acid digested with the established digestion protocol described before.

The concentrated QDS samples had the following ratios: blood-plasma: H_2O_2: nitric acid: aqua regia = 4: 5: 15: 16 (total volume of 4 mL). 300 μL of the above-mentioned concentrated QDS samples was mixed with 2.7 mL nanopure de-ionized water and vortexed and sonicated for 15 minutes respectively for homogenization. The diluted samples (C/10 of the actual concentration of the acid digested samples) were now ready to be analyzed for cadmium on the ICP MS in the helium gas mode. A reference curve of cadmium was generated using spiked samples of QDS NPs containing 0–256 ppb of cadmium and digested using the same acid composition and ratios used for the pilot study blood samples. The reference curve for cadmium was first generated (Figure 5-4), followed by blood sample analysis using the same instrument settings.

Cadmium was detected and quantified in the blood samples by the ICP MS analysis, from which the actual amount of NPs present in the blood at the time of draw is back calculated using the percentage composition values of cadmium in the QDS NPs and the sample dilutions made before the analysis. A graph of particle concentration in blood versus time profile was plotted for the QDS NPS (Figure 5-5) and the half-life was calculated using the one-compartmental model. The half-life of the QDS NPs was found to be 12.5 ± 9.7 minutes.

5.3.2 Using Gold Speckled Quantum Dot Nanoparticles (QDSG NPs)

The QDSG samples were treated exactly in the same way as the QDS samples mentioned above in Section 5.3.1 for particle and blood digestion. The samples were analyzed for cadmium as the quantity of gold in the specks was extremely low (Cd =21.4%, Au = 4.39% by weight). The reference curve generated for Cadmium is shown in Figure 5-6 while the PK data of the QDSG samples as obtained from the ICP MS from cadmium quantification and back calculations (to make up for dilutions) are plotted in Figure 5-7. QDSG NPs were determined to have a half-life of 14 $\pm$ 6.5 minutes which was similar to the value for QDS NPs.

5.3.3 Using Bare Gold Nanoparticles (G- NPs)

For the gold based NPs, ICP MS analysis was done to detect gold as an analyte. The acid digestion protocol for the NPs was exactly the same as the one used for the silica coated quantum dot (QDS) samples (Section 5.3.1). 300 μL of the G+ samples was mixed with 2.7 mL nanopure de-ionized water (C/10 of the actual concentration of the acid digested samples) and vortexed and sonicated for 15 minutes respectively to homogenize the samples. The diluted samples were then analyzed for gold on the ICP MS in the normal argon gas mode. A reference curve (similar to Figure 5-8) of gold was generated using spiked samples of bare gold NPs containing 0–128 ppb of gold that were digested using the same acid protocol used for blood samples from the animal study.

The PK data of the bare gold samples showed the presence of a very low amount of gold in the blood even at the 5 minute time-point, (similar to Figure 5-9). The level of gold NP concentration level remains unchanged and there is no difference in the gold detected and quantified between blood draw at any of the various time points mentioned before.

5.3.4 Using Aminated Gold Nanoparticles (G+ NPs)

The digestion protocol for G+ NPs was same as described in previous section. The reference curve generated using gold NPs was similar to that shown in Figure 5-8. The PK data of the blood samples containing amine-modified gold NPs was also similar to that shown in Figure 5-9. The G+ and G- NPs had a similar blood clearance behavior and appeared to have been removed even before the first blood draw at the five minute time-point after NP injection into the rats. The half-life values of G+ and G- NPs was < 5 minutes.

5.3.5 Using Pegylated Gold Nanoparticles (GP NPs)

As before, the same protocol for particle and tissue digestion was followed for the pegylated-gold NPs (GP). A reference curve for gold NPs was generated (Figure 5-10). The PK data obtained from the ICP MS from gold quantification is shown in Figure 5-11. The PK data of the blood samples showed significant amount of gold in the blood even after 1440 minutes. The GP NPs had a half-life of 640 $\pm$ 15.5 minutes. The half-life values for all five NPs used for this study are shown in Figure 5-12.

5.4 Differential Binding of Serum Proteins to Nanoparticles (NPs)

Recently, it has been reported (Cedervall *et al.* 2007, Lundqvist *et al.* 2008, Lynch *et al.* 2007, Lynch & Dawson 2008) that when particles enter the physiological environment, they are immediately covered by proteins that play a critical role in determining biodistribution, clearance and inflammatory processes. As mentioned before, many such proteins known as opsonins can facilitate particle recognition and trigger phagocytosis by the cells of the reticuloendothelial system (RES) leading to particle removal from the blood often within seconds. This may be followed by either a relatively benign response or stimulation of the inflammatory system that can eventually lead to various particle-induced diseases. In order to assess the biocompatibility of NPs, it is important to understand the proteins that bind to the surface of the NPs. The

determination of the proteins that bind (Dutta *et al.* 2007) to the particle surface can be achieved using one-dimensional (1-d) and two-dimensional (2-d) gel electrophoresis and isotope-coded affinity tags (ICAT). Various investigators have reported the used of 2-d electrophoresis of adsorbed proteins to characterize the pattern protein-NP binding and the ICAT technique to identify and quantify human serum proteins adsorbed onto particles (Wasdo *et al.* 2008). Most of these techniques are extremely complex and are beyond the scope of this dissertation. Therefore, the 1-d gel electrophoresis process was selected to get a preliminary idea of the molecular weight of the proteins that bind to the surface of the QDS, QDSG and the gold NPs dispersed in rat serum. The results of the 1-d gel electrophoresis are shown in Figure 5.12.

Stock solutions for QDS and QDSG NPs were prepared according to published protocols (Wasdo *et al.* 2008), 100 mgs of QDS, QDSG, G+, G- and GP NPs were placed in 50 mL centrifuge tubes along with 1 mL of PBS. The tubes are sonicated and vortexed for 5 minutes respectively and the NP suspensions of QDS and QDSG were transferred to the reservoir of 300 mL 0.22 μm polysulfone centrifuge filters (Whatman Catalog No. 6610-7169). The spin filters were centrifuged down using a swinging bucket centrifuge at 42 X g for 30 minutes, till the entire PBS solution had passed completely through the filter. The NPs were trapped inside the filter reservoir to form a column of approximately 5 mm in height. A 0.5 mL aliquot of pooled rat serum (Innovative Research, Novi, MI) was transferred to the NP column and the spin filter was centrifuged at 100 X g for 30 minutes until the serum had completely passed through the filter. After the first pass, the serum filtrate was recovered and made to pass through the column for a second time. The column was subsequently rinsed four times with PBS to remove all residual serum. Following this, the NPs were taken to a 1.5 mL centrifuge tube using three 0.5

mL volumes of PBS. The particles were then pelleted by centrifuging at 4000 X g and the supernatant was discarded.

As the G+, G- and GP NPs were reasonably well dispersed and stable in water, they could not be retained in the 0.22 μm centrifuge filters. In order to make the NP column, the gold NPs were taken in a 1.5 mL centrifuge tube, and centrifuged at 8000 X g, and the supernatant was carefully discarded. The pelleted NPs were rinsed by resuspending them in PBS, re-centrifugating at 8000 X g, and discarding the supernatant. This process is repeated for four times, followed by the addition of 0.5 mL filtered pooled serum to the NPs, and final re-suspension of the NPs in the serum by vortexing. The centrifuge tubes are placed on a shaker (Innova 2000 oscillating platform shaker) and agitated for 30 minutes at 200 rpm. Following this, the tube was centrifuged at 8000 X g, and the supernatant was discarded. The NPs were suspended in 0.5 mL of fresh PBS and centrifuged again at 8000 X g, and the supernatant was discarded. This rinsing is repeated four times to a point that there should be no more protein left in the supernatant, as verified by using the bichrinninc acid (BCA) protein assay.

For protein desorption, all NPs are resuspended in 0.3 mL of 1% sodium dodecyl sulphate (SDS) in 0.1 M tris buffer, pH 8.5 and sonicated and vortexed for 5 minutes respectively after the final rinse. Following this, the NPs are centrifuged down at 8000 X g for 30 minutes and the supernatant was transferred to another fresh 1.5 mL with an automatic pippetter. Acidified acetone was added to the supernatant and the tube was left undisturbed for – 20ºC. The precipitated proteins were centrifuged and removed and washed with 1 mL of acetone and stored at – 80ºC, until using it for loading the gels to conducting the 1-d gel electrophoresis. Thereafter, the gels were loaded with the protein ladder, QDS, G+, G- and QDSG NPs as shown in Figure 5.13. The set up was left undisturbed for the next 8 hours until the completion of electrophoresis.

Finally, the gels were removed from the set up, scanned and analyzed. It is observed from Figure 5.13, that a comparatively higher amount of proteins are located in lanes (c) and (d) that were loaded with samples containing adsorbed proteins on G+ and G- NPs respectively. A significantly lesser quantity of proteins were observed in lanes containing the QDS and QDSG NPs as seen in lanes (b) and (d). The amount of adsorbed proteins samples containing GP was not sufficient for being introduced into any lane during 1-d gel electrophoresis. These results from the 1-d gel experiment on varying protein adsorption on the surface of NPs appear to corroborate the results of half-life behavior of the NPs obtained from the blood clearance studies.

5.5 Discussions

The half-life behavior of GP NPs was completely different from the other two gold NPs and the QDS and QDSG NPs. This confirms the effect of pegylation reported in literature for various NPs (Chapter 1). In Chapter 3, it was reported that pegylation of the surface of bare gold NPs resulted in a reduction of surface charge to near neutral values. This indicated that the PEG functional group was successfully attached to the surface of the gold NPs. The large half-life value of GP NPs when viewed in the context of the small half-life values of G+ and G- clearly indicates that the GP NPs' clearance from the rat blood stream was significantly delayed. This behavior can be attributed to the fact that PEG modification of the particle surface that have been shown to reduce the non-specific binding of particles to the blood proteins (opsonins), which is the main mechanism for the partitioning of NPs out of the blood (Moghimi & Hunter 2001, Moghimi & Szebeni 2003, Owens & Peppas 2006). This imparts stealth properties to the GP NPs that help them to evade blood clearance for a much longer time, whereas, the G+ and G- NPs are removed from the blood possibly due to the combined processes of rapid opsonization followed by phagocytosis.

It was also found that the half-life values of QDSG and QDS NPs in the rat blood are similar. This implies that the gold speckles added to the surface of the QDS NPs do not significantly change the biological response of these particles in blood. As observed in Chapter 3, the addition of gold speckles did not significantly change the surface charge of the QDS NPs, as compared to QDSG NPs. Thus, even though the bare gold NPs (G-) were rapidly cleared from the rat blood stream, this same response could not be observed in the case of gold speckled surface of the QDSG NPs. Therefore, the blood clearance behavior of QDSG NPs was more comparable to the QDS NPs than that of gold NPs. The composition of the QDSG NPs consisted of 27.4 % cadmium sulphide, 16.8 % zinc sulphide, 4.39% gold and the remaining being silica. Therefore, it was not a surprise that the effect of the quantum dot core was more significant than gold in determining the particokinetic behavior of QDSG NPs in rat blood. It was interesting to observe that even though G+ and G- NPs have a large positive and a large negative surface charge values, respectively, they both were cleared very rapidly from the blood stream.

One of the trends that can be observed from the half-life values of all the five NPs is that the particles with a large surface charge (either positive or negative) are removed rapidly from the blood stream when compared to the particles with surface charge values close to zero (GP, QDSG and QDS). This clearly confirms the hypothesis of this research effort, that the particle surface can be altered to tailor engineered NPs for specific bioimaging applications.

The half-life results obtained from the animal study corroborated the findings of the protein adsorption study using 1-d gel electrophoresis. The amount and molecular weights of the different proteins that adsorbed on the surface of NPs could be visiually observed from the gel in Figure 5.13. It was noticed that GP could not be loaded into the lanes of the gel due to insufficient quantity of adsorbed proteins in the samples. In the animal study, it was noticed that

the half-life value of GP was very high due to its delayed blood clearance, probably due to the inability of the opsonin proteins to adsorb and initiate the process of phagocytosis. The adsorbed proteins for G+ and G- NPs were observed to be very high (Figure 5.13), which corroborated the animal study data showing an extremely fast clearance from rat blood. Finally, QDS and QDSG had an intermediate amount of adsorbed proteins, and a blood clearance rate that was higher than G+ and G- but far lesser than GP.

One of the major conclusions from this chapter is that protein adsorption appears to play a crucial role in regulating the blood clearance behavior of the NPs. The physicochemical parameters of NPs (particle size, shape and surface charge and chemistry) have a secondary and indirect effect on the biological activity. The primary effect can be attributed to the adsorbed proteins that contribute towards the blood partitioning behavior. Regarding the indirect effect of the physicochemical parameters, generally, it is known that opsonization of NPs with hydrophobic groups on the surface occur more quickly than NPs with hydrophilic surface groups like PEG due to enhanced adsorbability of blood serum proteins on the surfaces (Carstensen *et al.* 1992, Muller *et al.* 1992, Norman *et al.* 1992). The actual role of the adsorbed proteins in governing the activity can be explained only after identification, followed by monitoring any conformational or chemical changes in the protein structure. This would involve sophisticated proteomic research and detailed analysis which is included as a future recommended work.

Table 5-1. Actual dose of nanoparticles administered to each rat

Animal Study			Volume (ml)	Dose Weights (grams)		
Group	Rat #	Rat Weight (gms)	Dosing solution	Pre-dose Syringe	Post-dose Syringe	Delivered dose
G +	1	243.8	0.54	3.095	2.574	0.521
G +	2	261.6	0.58	3.181	2.592	0.588
G +	3	251.9	0.56	3.153	2.585	0.568
G -	4	251.3	0.56	3.149	2.589	0.560
G -	5	255.7	0.57	3.162	2.595	0.567
G -	6	274.8	0.61	3.218	2.599	0.620
GP	7	257.8	0.57	3.163	2.538	0.625
GP	8	264.6	0.59	3.180	2.570	0.61
GP	9	267.1	0.59	3.205	2.616	0.589
QDS	10	255.1	0.57	3.201	2.626	0.574
QDS	11	274.8	0.61	3.157	2.573	0.584
QDS	12	259.2	0.58	3.151	2.551	0.600
QDSG	13	253	0.56	3.193	2.622	0.571
QDSG	14	242.7	0.54	3.119	2.590	0.529
QDSG	15	273.9	0.61	3.234	2.613	0.621

Table 5-2. Amount (mass) of blood collected from rats dosed with nanoparticles at pre-determined time-points (0, 5, 15, 30, 60, 180, 360 and 1440 minutes)

		0 minutes			5 minutes			15 minutes		
Group	Rat #	Tare Wt	Vial + Sample	Wt	Tare Wt	Vial + Sample	Wt	Tare Wt	Vial + Sample	Wt
G +	1	9.405	9.936	0.531	9.497	9.879	0.382	9.510	9.945	0.434
G +	2	9.512	9.964	0.452	9.603	10.044	0.441	9.503	9.964	0.460
G +	3	9.554	9.965	0.411	9.579	10.038	0.460	9.546	9.922	0.375
G -	4	9.509	9.9530	0.444	9.631	9.999	0.367	9.521	9.947	0.426
G -	5	9.494	9.954	0.459	9.601	10.038	0.436	9.462	9.922	0.461
G -	6	9.515	9.980	0.466	9.538	9.967	0.430	9.592	10.041	0.448
GP	7	9.504	9.912	0.415	9.477	9.912	0.439	9.560	9.968	0.408
GP	8	9.505	9.911	0.406	9.562	10.038	0.476	9.610	10.070	0.458
GP	9	9.590	9.910	0.320	9.456	10.003	0.4573	9.542	10.005	0.463
QDS	10	9.475	9.990	0.515	9.521	9.946	0.425	9.578	9.963	0.386
QDS	11	9.587	9.851	0.264	9.462	9.926	0.464	9.475	9.953	0.478
QDS	12	9.965	10.131	0.476	9.511	9.971	0.460	9.588	10.044	0.456
QDSG	13	9.520	9.960	0.437	9.466	9.893	0.427	9.520	9.9648	0.445
QDSG	14	9.459	9.962	0.413	9.503	9.924	0.421	9.500	9.951	0.456
QDSG	15	9.489	9.911	0.422	9.546	10.002	0.457	9.523	9.984	0.461

Table 5-2 Continued.

		30 minutes			60 minutes			180 minutes		
Group	Rat #	Tare Wt	Vial + Sample	Wt	Tare Wt	Vial + Sample	Wt	Tare Wt	Vial + Sample	Wt
G +	1	9.525	9.961	0.436	9.522	9.948	0.426	9.485	9.940	0.455
G +	2	9.597	10.060	0.462	9.505	9.967	0.462	9.488	9.996	0.510
G +	3	9.571	10.025	0.454	9.451	9.961	0.412	9.552	10.013	0.461
G -	4	9.490	9.900	0.411	9.474	9.920	0.446	9.572	9.973	0.401
G -	5	9.576	10.014	0.438	9.634	10.105	0.470	9.610	10.080	0.470
G -	6	9.505	9.923	0.418	9.574	10.095	0.520	9.666	10.097	0.430
GP	7	9.583	9.965	0.383	9.370	9.985	0.588	9.545	9.970	0.425
GP	8	9.506	10.021	0.516	9.513	9.873	0.360	9.528	9.940	0.466
GP	9	9.536	9.995	0.4590	9.620	10.111	0.493	9.527	9.987	0.460
QDS	10	9.541	10.186	0.644	9.476	9.924	0.448	9.566	10.007	0.441
QDS	11	9.558	10.014	0.456	9.452	9.930	0.479	9.530	10.100	0.570
QDS	12	9.502	9.955	0.453	9.523	9.999	0.477	9.511	10.033	0.523
QDSG	13	9.637	10.098	0.462	9.598	10.083	0.485	9.476	9.958	0.482
QDSG	14	9.474	9.922	0.448	9.531	9.985	0.455	9.483	9.985	0.502
QDSG	15	9.516	10.008	0.492	9.408	9.908	0.500	9.473	9.926	0.453

Table 5-2 Continued.

		360 minutes			1440 minutes		
Group	Rat #	Tare Wt	Vial + Sample	Wt	Tare Wt	Vial + Sample	Wt
G +	1	9.537	9.981	0.445	9.483	9.969	0.486
G +	2	9.449	9.887	0.438	9.600	10.136	0.536
G +	3	9.493	9.982	0.489	9.520	10.006	0.486
G -	4	9.937	9.866	0.489	9.507	10.023	0.516
G -	5	9.490	9.998	0.507	9.578	10.094	0.516
G -	6	9.530	10.010	0.481	9.522	10.000	0.478
GP	7	9.558	10.019	0.461	9.603	10.077	0.474
GP	8	9.496	10.053	0.557	9.502	10.012	0.511
GP	9	9.528	10.027	0.499	9.499	10.004	0.505
QDS	10	9.548	10.046	0.498	9.530	10.079	0.549
QDS	11	9.530	10.069	0.538	9.555	10.012	0.456
QDS	12	9.460	9.963	0.504	9.465	9.940	0.475
QDSG	13	9.473	9.976	0.503	9.518	10.038	0.521
QDSG	14	9.511	10.048	0.537	9.451	9.905	0.453
QDSG	15	9.510	9.991	0.481	9.541	10.017	0.476

Table 5-3. Observations from dispersion study

NP Solution	NP Concentration (microgm/ml)	Volume of NPs (ml)	Dispersion Media	Amount of Dispersant Media (ml)	Visual Observation after 2 minutes	Visual Observation after 30 minutes
Gold Colloids	1000	2	Blood	0.25	No visible change	No visible change
		2		0.5	No visible change	No visible change
		2		1	No visible change	No visible change
		0.5		0.5	No visible change	No visible change
Gold Colloids	1000	2	Heparin	0.2	No visible change	No visible change
		2		0.25	No visible change	No visible change
		2		1	Pale blue color	Darker but pale blue color
		2		2	Dark purple color	Black precipitates in Clear Solution
		0.5		0.5	Dark purple color	Black precipitates in Clear Solution
Gold Colloids	1000	0.5	Bacteriostatic Solution (0.45%)	0.05	No visible change	No visible change
		0.5		0.1	No visible change	No visible change
		0.5		0.15	No visible change	No visible change
		0.5		0.25	Red color gets darker	Dark red color
		0.5		0.3	Pale Purple color	Pale Purple Solution
		0.5		0.35	Dark purple color	Black precipitates in Clear Solution

Table 5-4. Details of nanoparticles

NP System	Bare Gold
NPs / Volume	10 mg/m^3
Density	19.3 gm/cm^3

Particle Diameter (mm)	Surface Area (mm)^2	Particle Volume (mm)^3	Particle Volume (cm)^3	Mass per Particle (gm)	Mass per Particle (mg)	Specific Surface Area (mm)^2/mg	Particle Surface Area (mm)^2/(cm)^3	Particle Number (m^{-3})	Particle Number (cm^{-3})
0.010	3.142E-04	5.233E-07	5.233E-19	1.010E-17	1.010E-23	3.110E+19	6.003E+14	9.901E+23	9.901E+17
0.015	7.069E-04	1.766E-06	1.766E-18	3.409E-17	3.409E-23	2.074E+19	4.002E+14	2.934E+23	2.934E+17
0.020	1.257E-03	4.187E-06	4.187E-18	8.080E-17	8.080E-23	1.555E+19	3.002E+14	1.238E+23	1.238E+17

NP System	Silica
NPs / Volume	10 mg/m^3
Density	2.2 gm/cm^3

Particle Diameter (mm)	Surface Area (mm)^2	Particle Volume (mm)^3	Particle Volume (cm)^3	Mass per Particle (g)	Mass per Particle (mg)	Specific Surface Area (mm)^2/mg	Particle Surface Area (mm)^2/(cm)^3	Particle Number (m^{-3})	Particle Number (cm^{-3})
0.001	3.142E-06	5.233E-10	5.233E-22	1.151E-21	1.151E-27	2.729E+21	6.003E+15	8.686E+27	8.686E+21
0.015	7.069E-04	1.766E-06	1.766E-18	3.886E-18	3.886E-24	1.819E+20	4.002E+14	2.574E+24	2.574E+18
0.002	1.257E-05	4.187E-09	4.187E-21	9.211E-21	9.211E-27	1.364E+21	3.002E+15	1.086E+27	1.086E+21

Table 5-5. Nanoparticle deposition on polyurethane (PU) cannulae tube

Nanoparticle Details	Samples in Tubes	% Analyte in Sample 1	% Analyte in Sample 2
GP	Tube A	91.85	87.58
	Tube B	7.5	10.64
	Tube C	0.35	1.32
	Tube D	0.30	0.46
	Control Particles	100	100
G+	Tube A	91.78	94.94
	Tube B	7. 97	4.87
	Tube C	0.19	0.11
	Tube D	0.06	0.08
	Control Particles	100	100
G–	Tube A	95.26	93.41
	Tube B	4.60	6.36
	Tube C	0.11	0.19
	Tube D	0.04	0.05
	Control Particles	100	100
QDSG	Tube A	93.40	95.21
	Tube B	5.56	4.66
	Tube C	0.62	0.10
	Tube D	0.43	0.03
	Control Particles	100.00	100
QDS	Tube A	97.42	95.65
	Tube B	2.57	4.26
	Tube C	0.07	0.09
	Tube D	0.01	0.01
	Control Particles	100	100

Table 5-6. Nanoparticle deposition on polyethylene (PE) cannulae tube

Nanoparticle Details	Samples in Tubes	% Analyte in Sample 1	% Analyte in Sample 2
GP	Tube A	93.61	91.44
	Tube B	2.35	3.625
	Tube C	2.48	3.33
	Tube D	1.57	1.6
	Control Particles	100	100
G+	Tube A	57.06	58.05
	Tube B	31.43	31.49
	Tube C	8.75	7.33
	Tube D	2.76	3.13
	Control Particles	100	100
G–	Tube A	55.96	54.00
	Tube B	32.43	33.04
	Tube C	6.85	7.33
	Tube D	4.76	5.63
	Control Particles	100	100
QDSG	Tube A	49.31	48.50
	Tube B	36.3	33.29
	Tube C	8.58	11.12
	Tube D	5.81	7.09
	Control Particles	100	100
QDS	Tube A	50.03	48.50
	Tube B	35.89	38.53
	Tube C	9.58	8.12
	Tube D	4.50	4.85
	Control Particles	100	100

Table 5-7. Quantitative data of analytical detection of blood samples collected from rats

Details of Sample	QDSG in Rat Blood		
	Detected Quantity of Analyte		
Time-point (minutes)	First Rat	Second Rat	Third Rat
0	0.4059	0.6587	0.4612
1440	2.175	1.357	1.61
360	3.533	4.821	2.281
180	1.498	5.188	3.147
60	1.372	1.593	1.634
30	3.292	2.464	4.376
15	5.096	6.125	**13.95**
5	29.93	22.46	**81.4**

Details of Sample	QDS in Rat Blood		
	Detected Quantity of Analyte		
Time-point (minutes)	First Rat	Second Rat	Third Rat
0	0.746	0.164	0.159
1440	8.223	4.686	3.966
360	8.135	7.626	8.011
180	2.599	4.206	2.714
60	1.833	0.471	2.137
30	0.827	3.9	1.965
15	4.45	6.576	**14.95**
5	27.25	33.99	**81.85**

Details of Sample	GP in Rat Blood		
	Detected Quantity of Analyte		
Time-point (minutes)	First Rat	Second Rat	Third Rat
0	-0.2112	-0.8834	0.7144
1440	6.795	2.867	4.221
360	32.06	33.25	32.39
180	34.08	29.37	31.97
60	39.25	30.77	38.6
30	43.55	30.6	43.86
15	37.81	36.22	42.83
5	38.95	38.22	43.51

Table 5-8. Preparation of nanoparticle stock solution

Particle Details	Stock Concentration (mg/ml)	Stock Volume (ml)	Stock Mass (mg)	Target Volume (ml)	Target Concentration (mg/ml)	Stock Volume (ml)	Bacteriostatic Solution Volume (ml)	Volume of Water (ml)	Dosing Volume (ml)	Dosing Mass (mg)
Bare Gold (G-)	1.2	500	600	10	1	8.33	1.67	7.82	500	500
Gold – PEG (GP)	1.2	60	72	10	1	8.33	1.67	7.82	500	500
Aminated Gold (G+)	1.2	500	600	10	1	8.33	1.67	7.82	500	500
QD-Silica –Amine (QDS)	3.5	150	525	10	1	2.86	7.14	2.34	500	500
QD-Silica-Amine-Au (QDSG)	4	100	400	10	1	2.50	7.50	1.98	500	500

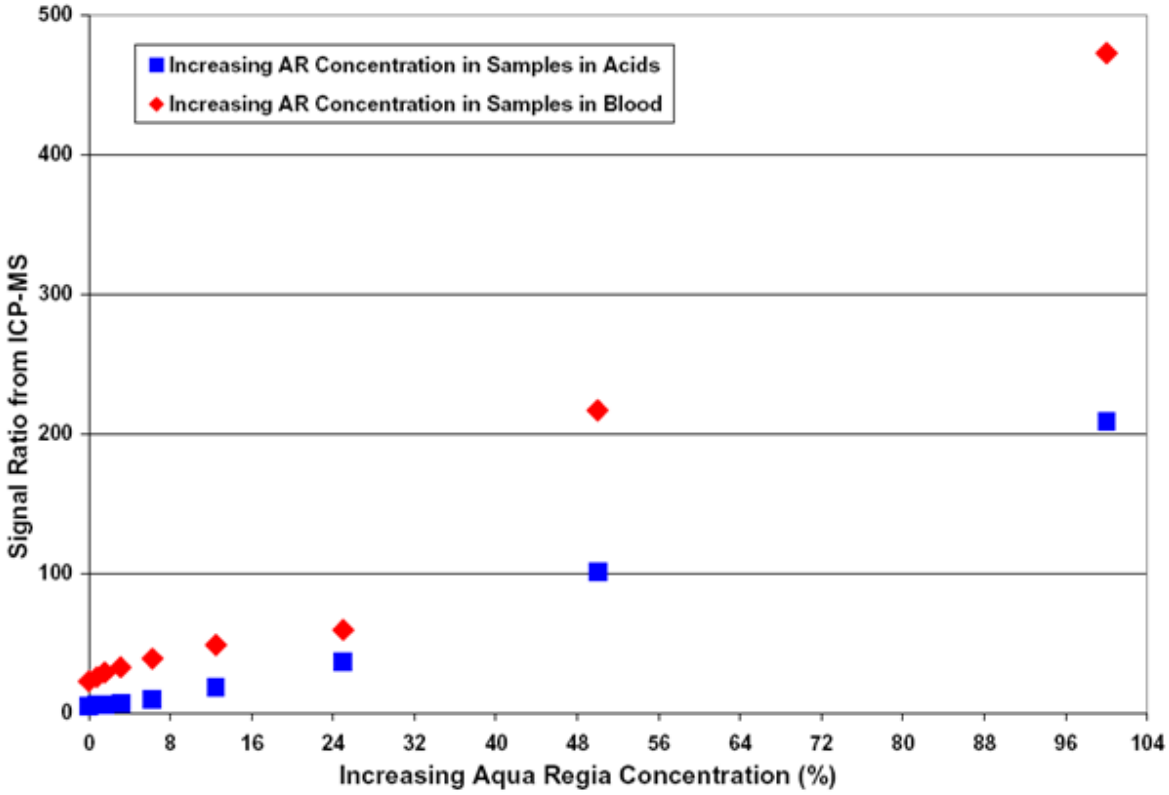

Figure 5-1. Effect of increasing the aqua regia concentration in digested samples with no nanoparticles in acid matrix (marked in blue squares) and in blood matrix (marked in red diamonds).

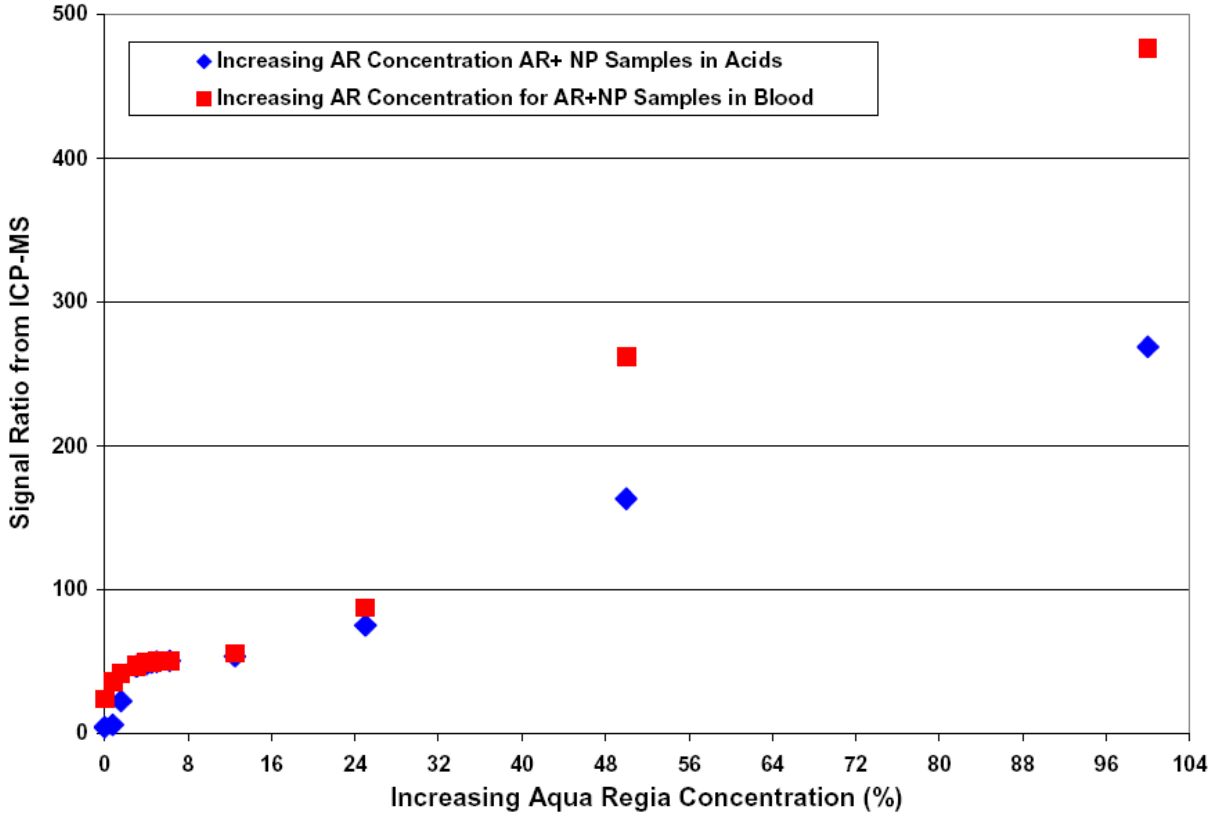

Figure 5-2. Effect of increasing the aqua regia concentration with gold nanoparticles in digested samples (marked in blue diamonds) in acid matrix and (marked in red squares) in blood matrix.

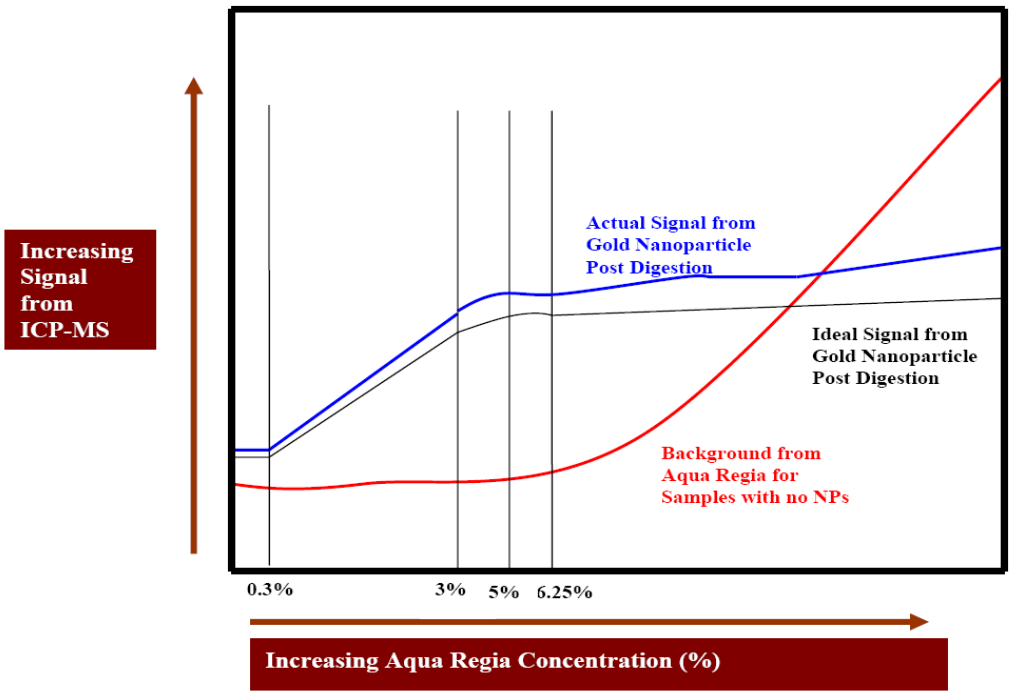

Figure 5-3. Effect of increasing aqua regia concentration on the background signal (blue) and completion of nanoparticle digestion (red)

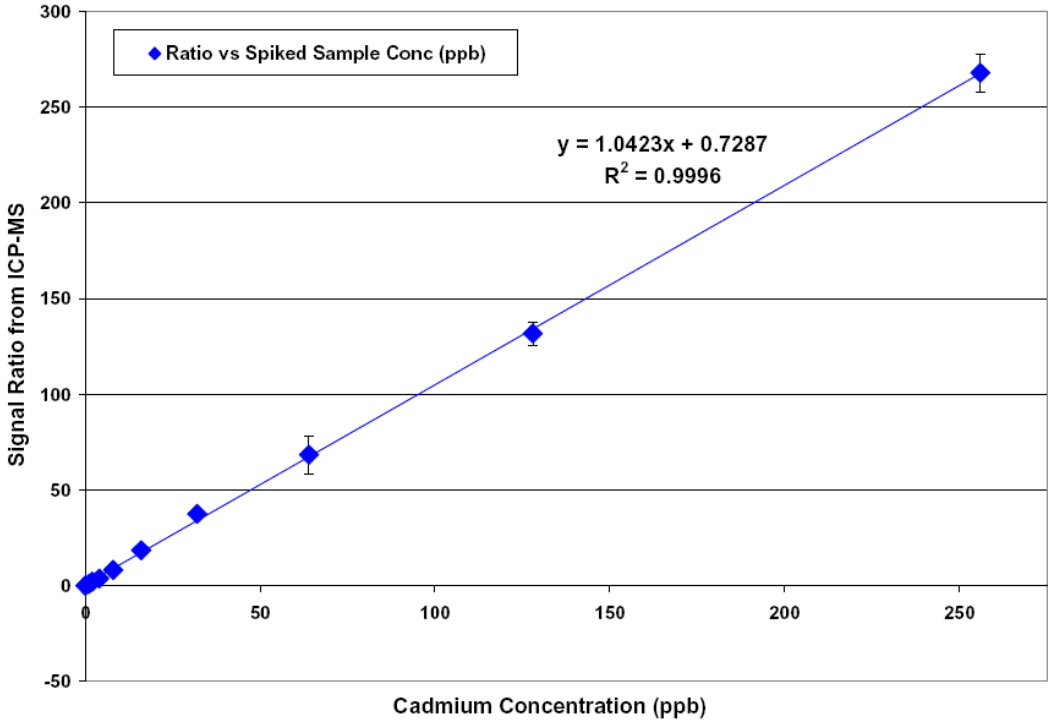

Figure 5-4. Standard curve for cadmium generated using spiked samples of QDS nanoparticles

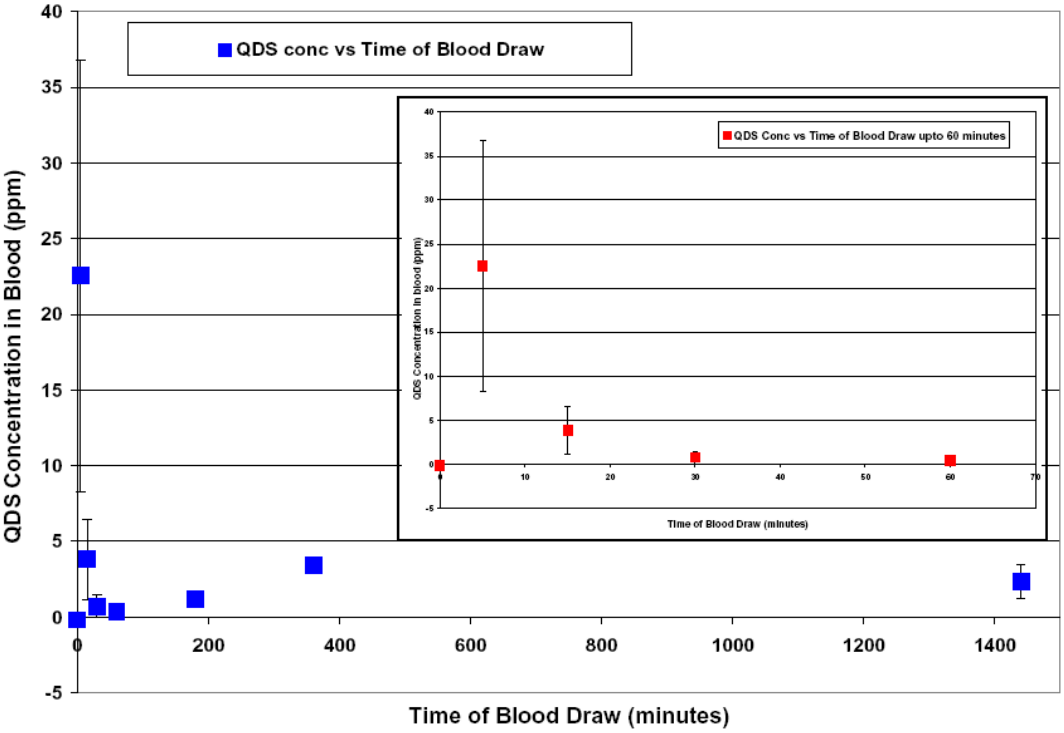

Figure 5-5. Particle concentration of QDS nanoparticles in blood versus time of draw; inset shows data plotted up to 60 minutes to magnify the datapoints near the axes

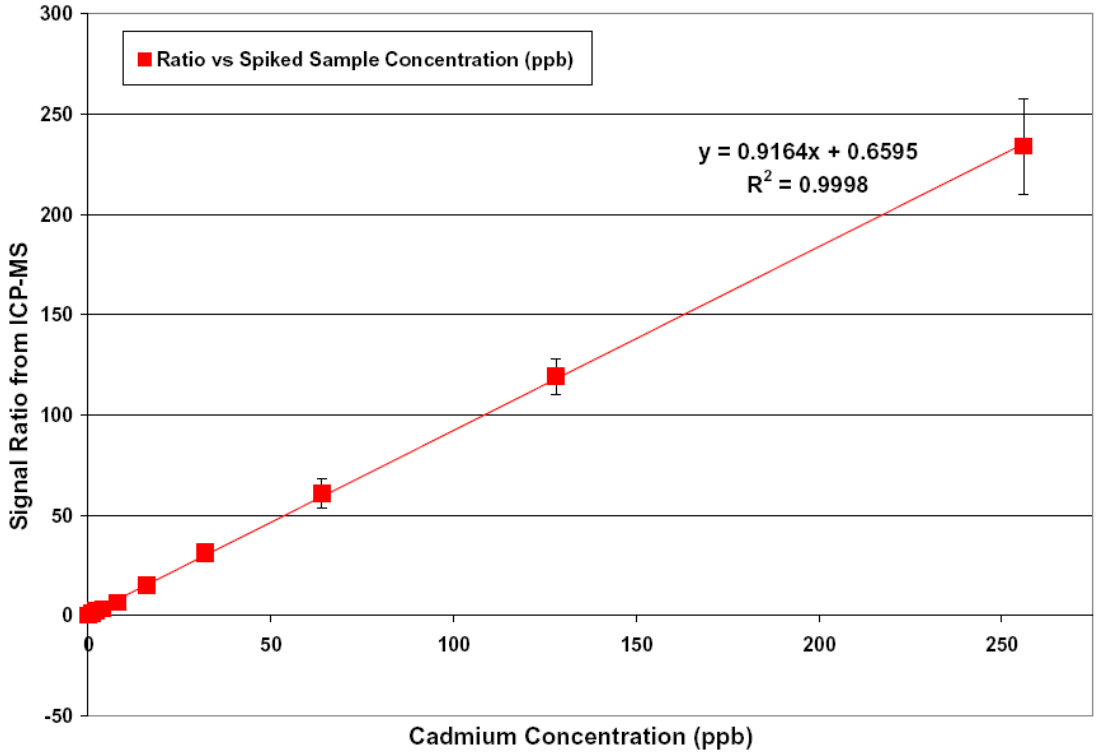

Figure 5-6. Standard curve for cadmium generated using spiked samples of QDSG nanoparticles

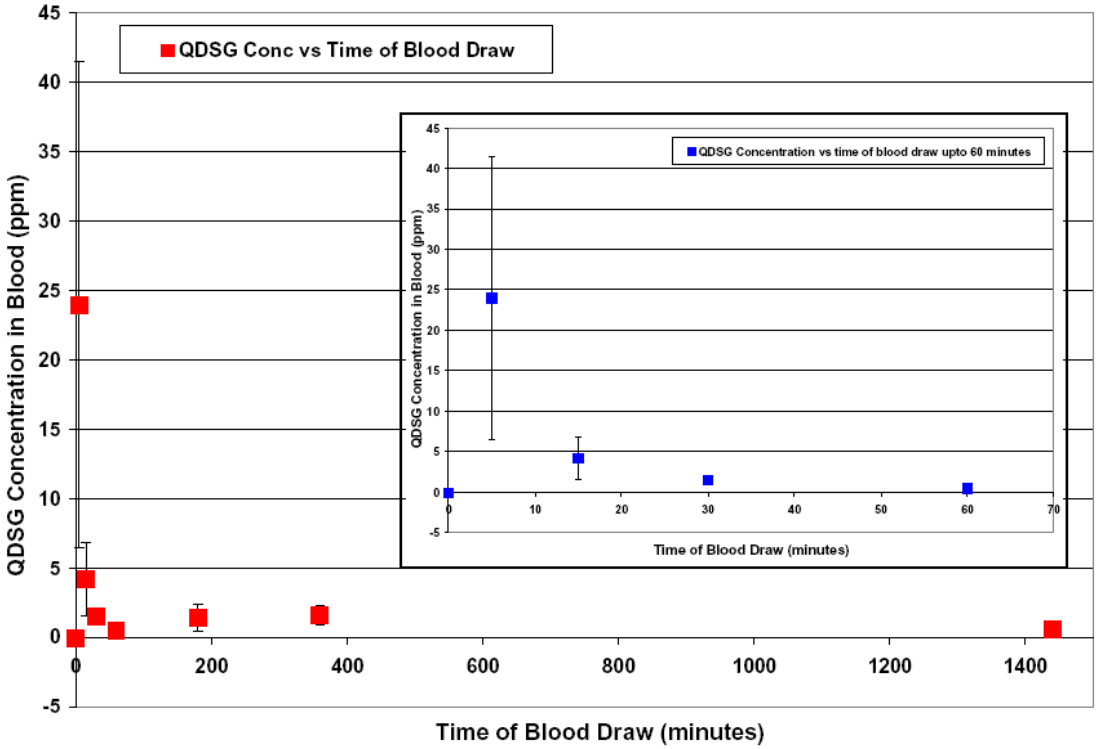

Figure 5-7. Particle concentration of QDSG nanoparticles in blood versus time of draw; inset shows data plotted up to 60 minutes to magnify the datapoints near the axes

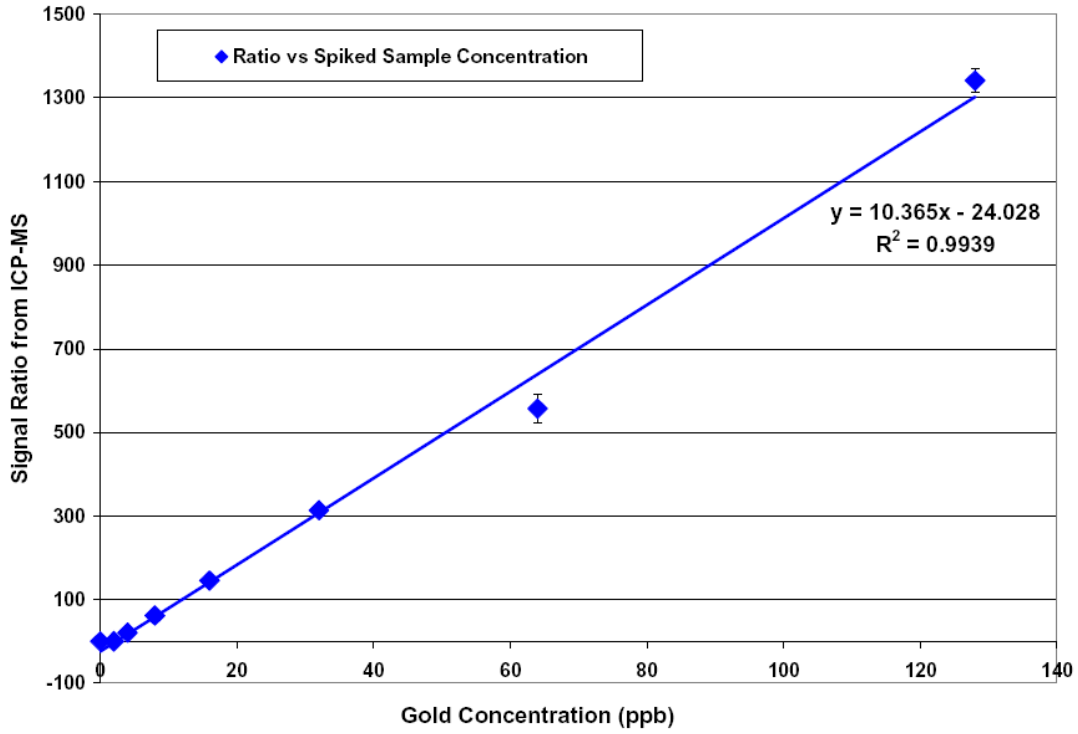

Figure 5-8. Standard curve of gold generated using spiked samples of G+ nanoparticles

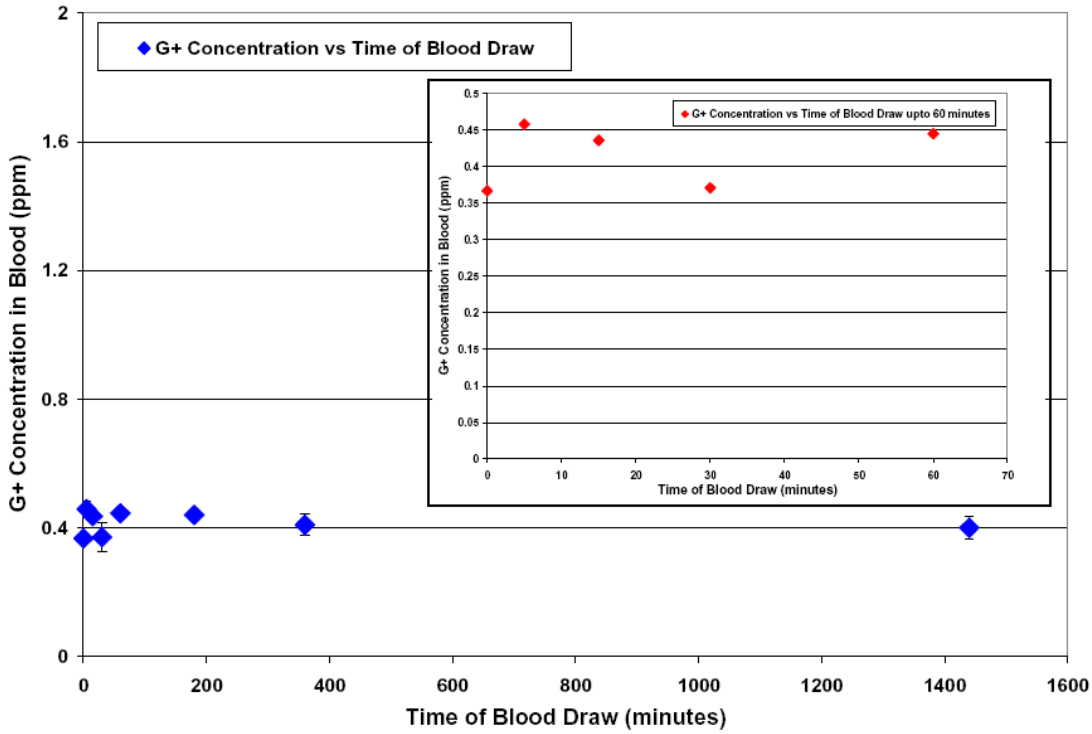

Figure 5-9. Particle concentration of G+ nanoparticles in blood versus time of draw; inset shows data plotted up to 60 minutes to magnify the datapoints near the axes

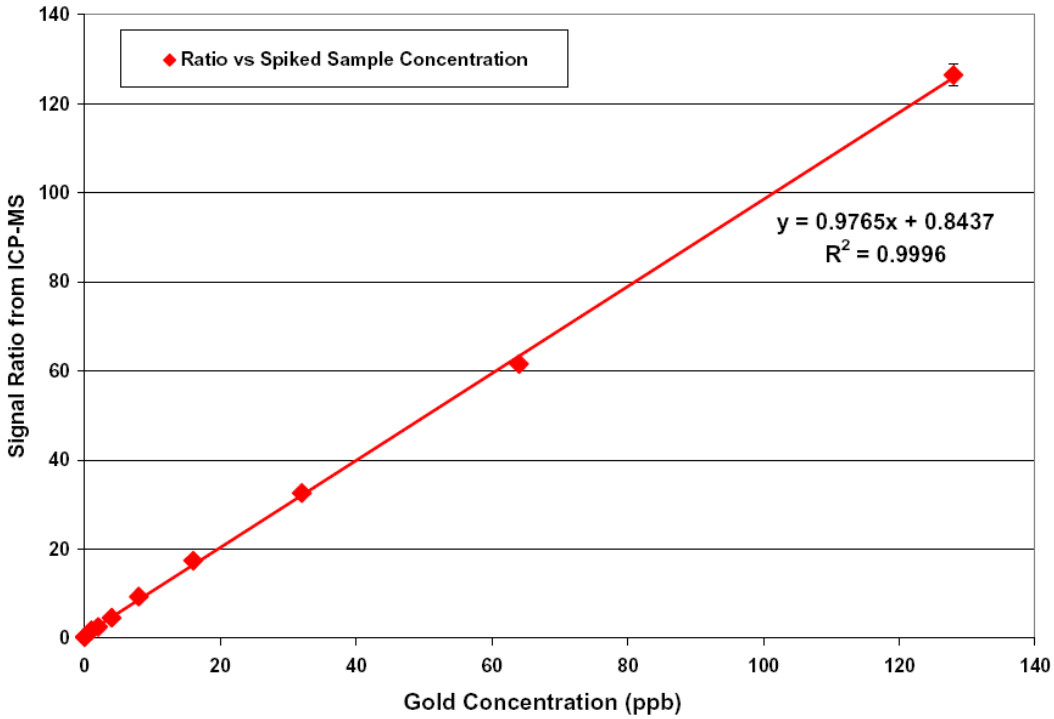

Figure 5-10. Standard curve for gold generated using spiked samples of GP nanoparticles

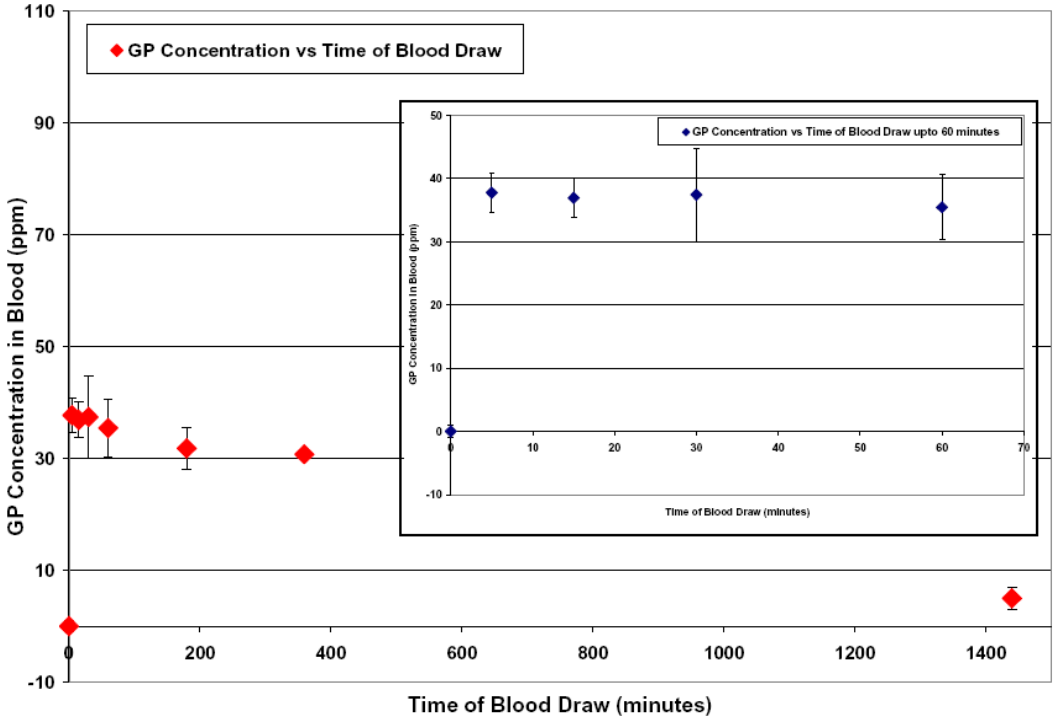

Figure 5-11. Particle concentration of GP nanoparticles in blood versus time of draw; inset shows data plotted up to 60 minutes to magnify the datapoints near the axes

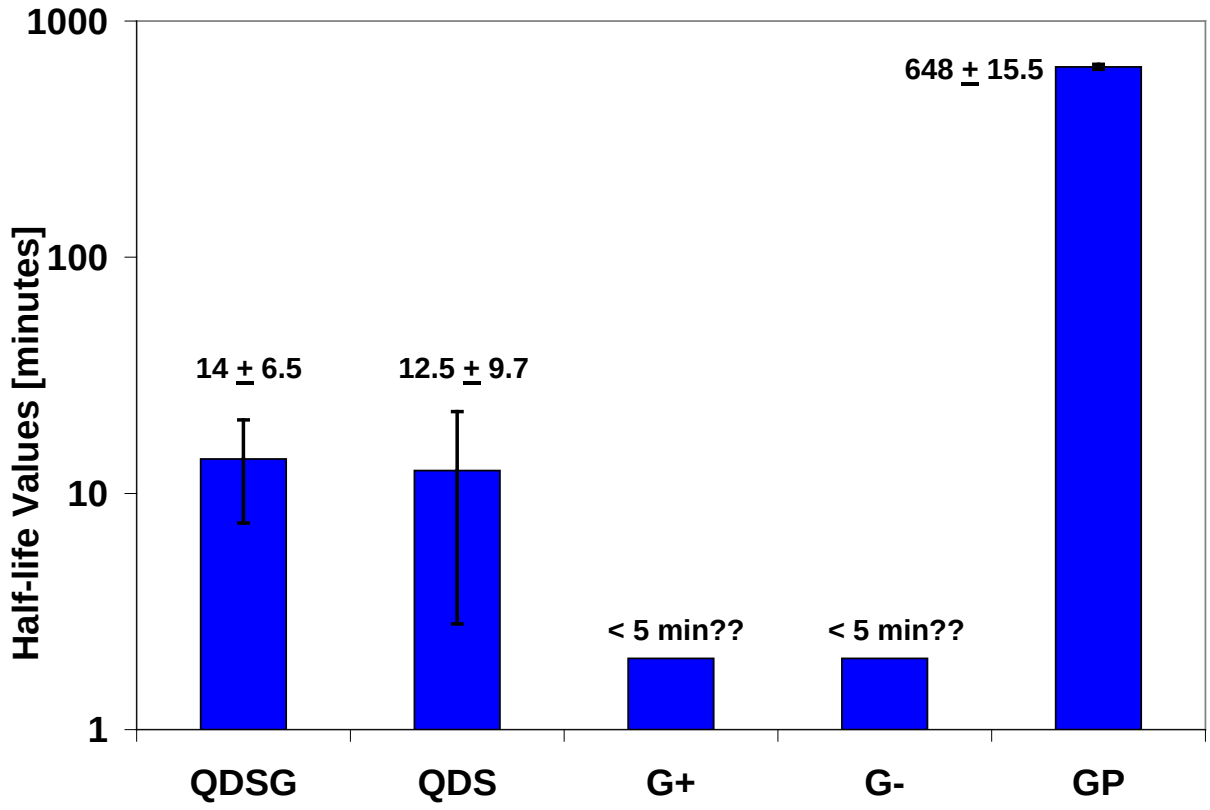

Figure 5-12. Histogram showing the half-life values of QDSG, QDS, G+, G- and GP NPs

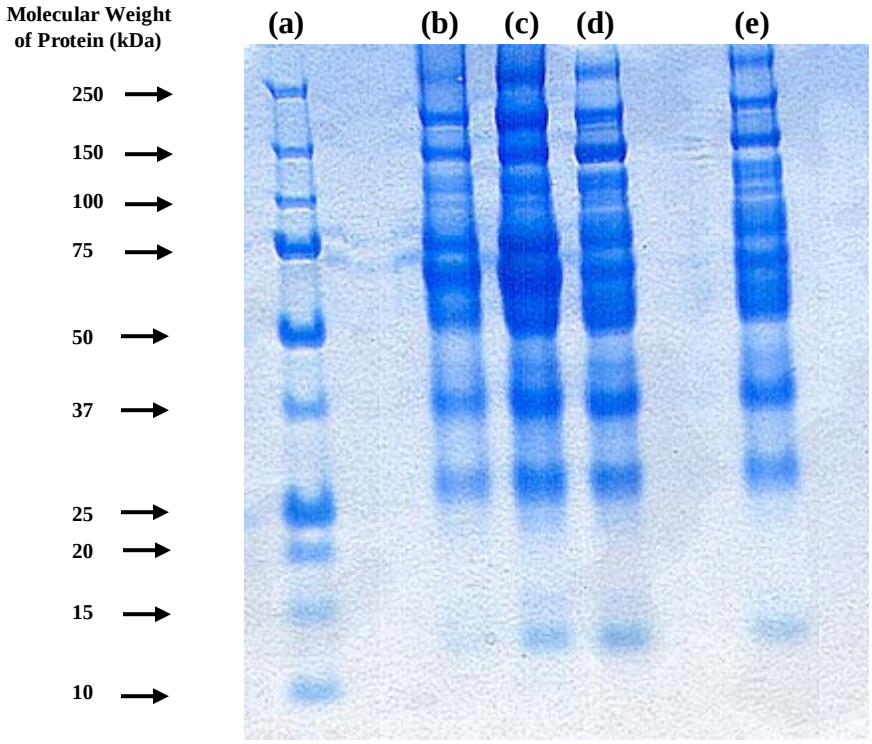

Figure 5-13. Results from the one-dimensional gel electrophoresis experiment on differential protein binding on the nanoparticles The samples in the lanes are as follows (a) ladder (with protein molecular weight bands (b) QDS (c) G+ (d) G- (e) QDSG NPs

CHAPTER 6
CONCLUSIONS AND SUGGESTIONS FOR FUTURE WORK

6.1 Conclusions

Nanoparticle (NP)-based contrast agents have initiated a whole new class of robust nano-sized (between 1 and 100 nm) particulate materials that have been shown to have immense potential for bioimaging applications. Some of the major advantages of the NP-based contrast agents being improved sensitivity, enhanced brightness and photostability with a small size (approximately 2 to 3 orders of magnitude smaller than the cells), making them suitable for use as contrast agents inside the cells. However, till date there exists no clinical contrast agent with an added therapeutic functionality in the structure. There is a significant clinical need for the development of NPs with in-built imaging and therapeutic functionalities, for early cancer detection and therapeutic applications. Furthermore, in order to establish a contrast agent, it is crucial to understand the various factors that influence NP uptake *in vitro* and biodistribution behavior *in vivo*.

A suite of novel engineered NP systems for bioimaging and therapeutic applications were developed for this present study and the influence of certain physicochemical parameters of the NPs like particle size, material composition, surface charge and chemistry on the cellular uptake and blood clearance behavior was investigated. The different NPs developed for this research effort include: 100 nm and 190 nm fluorescent silica nanoparticles (FSNPs), 15 nm silica coated quantum dots (QDS) and gold speckled silica coated quantum dots (QDSG) and 15 nm gold NPs with three different surface charge and functionalization. The particles were synthesized using reverse-microemulsion and/or sol gel techniques and characterized for particle size, shape, surface charge absorbance and fluorescence spectroscopy.

The effect of particle size, time of incubation, particle concentration and surface functionality on the cellular uptake was studied using the 100 and 190 nm FSNPs. The effect of two different FSNP-surface functionalizations, folate conjugation and amine modification was studied using A549 cells. Uptake studies using confocal microscopy (qualitative) and protein assay (semi-quantitative) techniques showed that the cellular uptake increased with increasing particle size and concentration. There was no significant effect of increasing the incubation time on the cellular uptake. The folated FSNPs were uptaken more aggressively by the A549 cells than the aminated FSNPs. The cellular uptake for the 100 nm aminated NPs was observed to be anomalously low as compared to the other FSNPs. This anomaly was explained from results of particle size measurements of NPs dispersed in cell media. It was found that the 100 nm FSNPs agglomerated in the cell media to have a size range between 40 nm and 20 microns. Similarly, the size range of the 190 nm FSNPs in cell media was 2 to 200 microns. Increased settling and cell-NP interactions due to agglomeration in the cell media for the larger sized FSNPs, along with an increase in the possibility of phagocytosis could lead to increased uptake behavior. Cell viability studies of the FSNPs were conducted using lactate dehydrogenase (LDH) assay in A549 cells. The maximum percentage cytotoxicity value for FSNPs that were pre-conditioned with cell media, prior to their incubation, was found to be less than 8% whereas for FSNPs that were not pre-conditioned in cell media, it was approximately 20%. The decrease in cytotoxicity upon pre-conditioning was attributed to protein adsorption on the particle surface that influences the biological activity inside the cells.

In order to investigate the effect of material composition and surface functionality of the NPs on the blood clearance behavior, rats were dosed with pre-determined amounts of QDSG, QDS and gold NPs. Gold NPs with three different surface charges: bare gold G- (negative),

amine-modified gold G+, (positive) and pegylated-gold GP (neutral) NPs were synthesized to study the effect of surface charge. The QDSG, QDS and bare gold NPs were used to study the effect of material composition on their partitioning in blood.

The synthesis protocol for QDSG was optimized for fluorescence and absorbance properties. It was observed that an excess of gold speckles on the QDSG surface "quenched" the QD-core fluorescence property. The amount of gold speckles on the NP surface and the thickness of the silica shell were optimized to obtain good fluorescent and absorbance properties. Bioimaging capability of QDSG was demonstrated in A549 cells and daphnia. The fluorescence from the QD core was utilized for imaging, and hyperthermic property of gold speckles on QDSG was demonstrated using A549 cells.

The biodistribution studies of gold and quantum dot based NPs were conducted in rat blood. An acid digestion protocol using an optimized amount of aqua regia (5%) and nitric acid (2%) was established to ensure complete particle digestion with minimum background from the matrix. A one-compartmental model was generated using equations from first-order kinetics and was employed to calculate the particle concentration for dosing the rats. Stock solutions of NPs were prepared at 1 mg/mL and dispersed in 0.45% bacteriostatic solution for dosing the rats for the blood clearance study. The rats were intravenous injected with NPs through the surgically attached cannulae tubes and samples of blood were collected at various time points. The blood samples were acid digested and analyzed for gold and cadmium using Inductively Coupled Plasma-Mass Spectroscopy. A particle concentration – time profile graph was generated from the analytical data. This graph along with the one-compartmental model was used to calculate the half-life values of the NPs in rat blood. The half-life values for the various NPs were determined to be: 12.5±9.7, 14±6.5 and 640±15.5 minutes for QDS, QDSG and GP NPs were respectively.

The G+ and G- NPs were cleared very fast and no significant amount of gold could be detected in the blood samples collected at the five minute time-point. It was concluded that the half-life values for G+ and G- NPs in rat blood were less than five minutes. QDSG and QDS NPs with relatively small surface charges of 6.3 ± 2.9 mV and 4.1 ± 1.7 mV respectively were cleared slower as compared to G+ and G- NPs with surface charges of 24 ± 5.8 mV and - 34.5 ± 7.8 mV respectively. The PEG groups on GP (5 ± 1.9 mV) led to delayed clearance with a large half-life value of more than 600 minutes.

In order to further investigate the trends of half-life of NPs in blood, one-dimensional gel electrophoresis preliminary protein adsorption studies were conducted. It showed a significantly high amount of adsorbed proteins on the G+ and G- NP surface, followed by moderate amount of proteins on the QDS and QDSG NP surface, and negligible amount on the GP surface. This trend of adsorbed proteins on the NP surface correlated directly with the results from the blood clearance study and half-life of NPs in rat blood.

It is known that when particles enter the physiological environment, they are likely to be covered by proteins that exist in the blood. Many of these proteins, also known as opsonin proteins, when adsorbed on the NP surface, can render the NP to be visible to the phagocytic cells and trigger their phagocytosis (process of engulfing the NP and attempting to destroy or remove the particle from the bloodstream). The opsonin proteins are continuously present inside the blood and are believed to come into contact with NPs typically as a result of random Brownian motion. However, once the proteins are close enough to the NP surface, several other attractive forces including the van der Waals, electrostatic, ionic and hydrophilic/hydrophobic interactions are involved for opsonin protein binding on the NP surface (Moghimi & Szebeni 2003, Owens & Peppas 2006). The adsorbed proteins play a crucial role in phagocytosis, since

the phagocytes do not recognize the NPs or any other foreign material, without the presence of the opsonin proteins attached to the NP surface. The last step in the clearance process, following ingestion of the NPs into the phagocytes is the secretion of various enzymes and 'oxidative-reactive' chemical like nitric oxide, hydrogen peroxide and superoxides to break down the phagocytosed NPs. Non-biodegradeable materials cannot be removed by this process, and depending on their relative size and molecular weights shall be removed either by the renal system or uptaken and stored in one of the organs of the reticuloendothelial system. The tissue uptake of the NPs can be investigated through biodistribution studies in relevant tissues inside living systems.

6.2 Suggestions for Future Work

The biodistribution of QDSG, QDS and gold NPs in rats should be carried out by quantifying the particle content in liver, spleen, lung and kidney. The effect of material composition and surface functionalization on tissue uptake and determination of half-life values for the NPs in various tissues would enable the development of a computational model similar to a physiologically based pharmacokinetic (PBPK) model. This would help establish the complete particokinetic behavior of the NPs in the animal environment.

One of the major conclusions of this research effort is that the adsorped proteins on the NP surface can influence the biological activity in the physiological environment. For the current research work, a preliminary protein adsorption study using one-dimensional gel electrophoresis was conducted in this regard. More detailed proteomic studies will help to better understand the exact mechanism of interaction between the cells and NPs. This understanding will help to tailor the NPs to mitigate the toxicological effects of NPs and help in targeted bioimaging and therapeutic applications.

Most importantly, robust characterization protocols have to be developed in order to investigate the physicochemical parameter of NPs inside the biological environment. The biological responses are related to the physicochemical parameters of the NPs as encountered by the cells *invitro* or *in vivo*. Nanoparticle characterization in blood still remains a challenge and a robust methodology to accurately investigate the physicochemical parameters of NPs in blood has to be developed. The state of agglomeration of the NPs in the physiological environment will provide an insight to the actual effect of particle size distribution on NP toxicity.

In future, different methods for surface functionalization of QDSG NPs should be explored. Further, the surface of the NPs could be bioconjugated with folic acid or other biomolecules to selectively target cancer cells. This concept was demonstrated using folated FSNPs to selectively target cancer cells for this research work.

LIST OF REFERENCES

Akerman ME, Chan WCW, Laakkonen P, Bhatia SN, Ruoslahti E. 2002. Nanocrystal targeting in vivo. *Proceedings of the National Academy of Sciences of the United States of America* 99: 12617-21

Alexis F, Pridgen E, Molnar LK, Farokhzad OC. 2008. Factors affecting the clearance and biodistribution of polymeric nanoparticles. *Molecular Pharmaceutics* 5: 505-15

Antony AC. 1992. The Biological Chemistry of Folate Receptors. *Blood* 79: 2807-20

Bajpai SK, Mohan YM, Bajpai M, Tankhiwale R, Thomas V. 2007. Synthesis of polymer stabilized silver and gold nanostructures. *Journal Of Nanoscience And Nanotechnology* 7: 2994-3010

Banerjee T, Mitra S, Singh AK, Sharma RK, Maitra A. 2002. Preparation, characterization and biodistribution of ultrafine chitosan nanoparticles. *International Journal of Pharmaceutics* 243: 93-105

Barnes CA, Elsaesser A, Arkusz J, Smok A, Palus J, *et al.*. 2008. Reproducible Comet assay of amorphous silica nanoparticles detects no genotoxicity. *Nano Letters* 8: 3069-74

Ben-Ari ET. 2003. Nanoscale quantum dots hold promise for cancer applications. *Journal of the National Cancer Institute* 95: 502-4

Bhushan B. 2007. *Springer Handbook of Nanotechnology*: Springer

Blodgett K, Langmuir I. 1932. Accommodation coefficient of hydrogen, a sensitive detector of surface films. *PHYSICAL REVIEW* 40: 78-104

Blodgett K, Langmuir I, Volume: S. 1932. A film which adsorbs atomic H and does not adsorb H-2. *JOURNAL OF THE AMERICAN CHEMICAL SOCIETY* 54: 3781-2

Borm P, Klaessig FC, Landry TD, Moudgil B, Pauluhn J, *et al.*. 2006. Research strategies for safety evaluation of nanomaterials, Part V: Role of dissolution in biological fate and effects of nanoscale particles. *Toxicological Sciences* 90: 23-32

Bornhop DJ, Contag CH, Licha K, Murphy CJ. 2001. Advances in contrast agents, reporters, and detection. *Journal of Biomedical Optics* 6: 106-10

Bremer C, Ntziachristos V, Weissleder R. 2003. Optical-based molecular imaging: contrast agents and potential medical applications. *European Radiology* 13: 231-43

Brigger I, Dubernet C, Couvreur P. 2002. Nanoparticles in cancer therapy and diagnosis. *Advanced Drug Delivery Reviews* 54: 631-51

Bright RM, Walter DG, Musick MD, Jackson MA, Allison KJ, Natan MJ. 1996. Chemical and electrochemical Ag deposition onto preformed Au colloid monolayers: Approaches to uniformly-sized surface features with Ag-like optical properties. *Langmuir* 12: 810-7

Brown DM, Stone V, Findlay P, MacNee W, Donaldson K. 2000. Increased inflammation and intracellular calcium caused by ultrafine carbon black is independent of transition metals or other soluble components. *Occupational and Environmental Medicine* 57: 685-91

Brown SC, Kamal M, Nasreen N, Baumuratov A, Sharma P, *et al.*. 2007. Influence of shape, adhesion and simulated lung mechanics on amorphous silica nanoparticle toxicity. *Advanced Powder Technology* 18: 69-79

Bruchez M, Moronne M, Gin P, Weiss S, Alivisatos AP. 1998. Semiconductor nanocrystals as fluorescent biological labels. *Science* 281: 2013-6

Carstensen H, Muller RH, Muller BW. 1992. Particle-Size, Surface Hydrophobicity And Interaction With Serum Of Parenteral Fat Emulsions And Model-Drug Carriers As Parameters Related To Res Uptake. *Clinical Nutrition* 11: 289-97

Cauvel A, Brunel D, DiRenzo F, Garrone E, Fubini B. 1997. Hydrophobic and hydrophilic behavior of micelle-templated mesoporous silica. *Langmuir* 13: 2773-8

Cedervall T, Lynch I, Lindman S, Berggard T, Thulin E, *et al.*. 2007. Understanding the nanoparticle-protein corona using methods to quantify exchange rates and affinities of proteins for nanoparticles. *Proceedings of the National Academy of Sciences of the United States of America* 104: 2050-5

Champion JA, Mitragotri S. 2006. Role of target geometry in phagocytosis. *Proceedings of the National Academy of Sciences of the United States of America* 103: 4930-4

Chan WCW, Nie SM. 1998. Quantum dot bioconjugates for ultrasensitive nonisotopic detection. *Science* 281: 2016-8

Chithrani BD, Chan WCW. 2007. Elucidating the mechanism of cellular uptake and removal of protein-coated gold nanoparticles of different sizes and shapes. *Nano Letters* 7: 1542-50

Chithrani BD, Ghazani AA, Chan WCW. 2006. Determining the size and shape dependence of gold nanoparticle uptake into mammalian cells. *Nano Letters* 6: 662-8

Cho SJ, Maysinger D, Jain M, Roder B, Hackbarth S, Winnik FM. 2007. Long-term exposure to CdTe quantum dots causes functional impairments in live cells. *Langmuir* 23: 1974-80

Cohen ML. 2001. Nanotubes, nanoscience, and nanotechnology. *Materials Science & Engineering C-Biomimetic And Supramolecular Systems* 15: 1-11

Committee. 2004. *Final Report: Nanotoxicology Workshop*, University of Florida, Gainesville, FL

Copland JA, Eghtedari M, Popov VL, Kotov N, Mamedova N, *et al.*. 2004. Bioconjugated gold nanoparticles as a molecular based contrast agent: Implications for imaging of deep tumors using optoacoustic tomography. *Molecular Imaging and Biology* 6: 341-9

Craighead JE. 1988. Diseases Associated with Exposure to Silica and Nonfibrous Silicate Minerals. *Archives of Pathology & Laboratory Medicine* 112: 673-720

Craighead JE. 1992. Do silica and asbestos cause lung cancer? *Arch Pathol Lab Med* 116: 16-20

Cullen RT, Tran CL, Buchanan D, Davis JMC, Searl A, *et al.*. 2000. Inhalation of poorly soluble particles. I. Differences in inflammatory response and clearance during exposure. *Inhalation Toxicology* 12: 1089-111

Dabbousi BO, RodriguezViejo J, Mikulec FV, Heine JR, Mattoussi H, *et al.*. 1997. (CdSe)ZnS core-shell quantum dots: Synthesis and characterization of a size series of highly luminescent nanocrystallites. *Journal of Physical Chemistry B* 101: 9463-75

Das M, Patil S, Bhargava N, Kang JF, Riedel LM, *et al.*. 2007. Auto-catalytic ceria nanoparticles offer neuroprotection to adult rat spinal cord neurons. *Biomaterials* 28: 1918-25

De M, Ghosh PS, Rotello VM. 2008. Applications of Nanoparticles in Biology. *Advanced Materials* 20: 4225-41

Decker SP. 2006. Current and emerging applications involving nanoscale fillers and minerals. In *Functional Fillers And Nanoscale Minerals: New Markets/New Horizons*, ed. JJ Kellar: Society of Mining Engineers

Del Campo A, Sen T, Lellouche JP, Bruce IJ. 2005. Multifunctional magnetite and silica-magnetite nanoparticles: Synthesis, surface activation and applications in life sciences. *Journal of Magnetism and Magnetic Materials* 293: 33-40

Derfus AM, Chan WCW, Bhatia SN. 2004a. Intracellular delivery of quantum dots for live cell labeling and organelle tracking. *Advanced Materials* 16: 961-+

Derfus AM, Chan WCW, Bhatia SN. 2004b. Probing the cytotoxicity of semiconductor quantum dots. *Nano Letters* 4: 11-8

Derjaguin BV, Abrikosova, II, Lifshitz EM. 1992. Direct Measurement Of Molecular Attraction Between Solids Separated By A Narrow Gap (Reprinted From Quart Rev, Vol 10, Pg 295-329, 1956). *Progress In Surface Science* 40: 83-117

Diagaradjane P, Shetty A, Wang J, Schwartz J, Park HC, *et al.*. 2008. Modulation of in vivo tumor radiation response via vascular-focused hyperthermia-characterizing gold nanoshells as integrated anti-hypoxic and localized vascular disrupting agents. *International Journal of Radiation Oncology Biology Physics* 72: S64-S

Ding LH, Stilwell J, Zhang TT, Elboudwarej O, Jiang HJ, *et al.*. 2005. Molecular characterization of the cytotoxic mechanism of multiwall carbon nanotubes and nano-onions on human skin fibroblast. *Nano Letters* 5: 2448-64

Dobrovolskaia MA, Aggarwal P, Hall JB, McNeil SE. 2008. Preclinical studies to understand nanoparticle interaction with the immune system and its potential effects on nanoparticle biodistribution. *Molecular Pharmaceutics* 5: 487-95

Donaldson K, Borm PJA. 1998. The quartz hazard: A variable entity. *Annals of Occupational Hygiene* 42: 287-94

Donaldson K, Stone V, Tran CL, Kreyling W, Borm PJA. 2004. Nanotoxicology. *Occupational and Environmental Medicine* 61: 727-8

Drexler E. 1987. *Engines of Creation: The Coming Era of Nanotechnology*. New York: Anchor Books Edition

Driscoll KE, Carter JM, Howard BW, Hassenbein DG, Pepelko W, *et al.*. 1996. Pulmonary inflammatory, chemokine, and mutagenic responses in rats after subchronic inhalation of carbon black. *Toxicology and Applied Pharmacology* 136: 372-80

Driscoll KE, Guthrie GD. 1997. *Crystalline Silica and Silicosis*. New York: Elsevier. 373-91 pp.

Dubertret B, Skourides P, Norris DJ, Noireaux V, Brivanlou AH, Libchaber A. 2002. In vivo imaging of quantum dots encapsulated in phospholipid micelles. *Science* 298: 1759-62

Dutta D, Moraga D, Santra S. In Review for Publication. In vitro biocompatibility assessment of folate-conjugated silica nanoparticles. *Materials Science & Engineering C*

Dutta D, Moudgil BM. 2007. Crystalline Silica Particles Mediated Lung Injury. *Kona-Powder and Particle* 25: 76-87

Dutta D, Sundaram SK, Teeguarden JG, Riley BJ, Fifield LS, *et al.*. 2007. Adsorbed proteins influence the biological activity and molecular targeting of nanomaterials. *Toxicological Sciences* 100: 303-15

Eichelbaum M, Schmidt BE, Ibrahim H, Rademann K. 2007. Three-photon-induced luminescence of gold nanoparticles embedded in and located on the surface of glassy nanolayers. *Nanotechnology* 18

Eijkel JCT, van den Berg A. 2006. The promise of nanotechnology for separation devices - from a top-down approach to nature-inspired separation devices. *Electrophoresis* 27: 677-85

El-Sayed IH, Huang XH, El-Sayed MA. 2005. Surface plasmon resonance scattering and absorption of anti-EGFR antibody conjugated gold nanoparticles in cancer diagnostics: Applications in oral cancer. *Nano Letters* 5: 829-34

Elghanian R, Storhoff JJ, Mucic RC, Letsinger RL, Mirkin CA. 1997. Selective colorimetric detection of polynucleotides based on the distance-dependent optical properties of gold nanoparticles. *Science* 277: 1078-81

Espinosa-Mansilla A, Duran-Meras I, Salinas F. 1998. High-performance liquid chromatographic fluorometric determination of glyoxal, methylglyoxal, and diacetyl in urine by prederivatization to pteridinic rings. *Analytical Biochemistry* 255: 263-73

Evans CO, Reddy P, Brat DJ, O'Neill EB, Craige B, *et al*.. 2003. Differential expression of folate receptor in pituitary adenomas. *Cancer Research* 63: 4218-24

Fang XH, Liu XJ, Schuster S, Tan WH. 1999. Designing a novel molecular beacon for surface-immobilized DNA hybridization studies. *Journal of the American Chemical Society* 121: 2921-2

Ferin J, Oberdorster G, Penney DP, Soderholm SC, Gelein R, Piper HC. 1990. Increased Pulmonary Toxicity of Ultrafine Particles.1. Particle Clearance, Translocation, Morphology. *Journal of Aerosol Science* 21: 381-4

Ferrari M. 2005. Cancer nanotechnology: Opportunities and challenges. *Nature Reviews Cancer* 5: 161-71

Feynman R. 1959. Plenty of Room at the Bottom. ed. APS meeting. Caltech

Finney LA, O'Halloran TV. 2003. Transition metal speciation in the cell: Insights from the chemistry of metal ion receptors. *Science* 300: 931-6

Franklin WA, Waintrub M, Edwards D, Christensen K, Prendegrast P, *et al*.. 1994. New Anti-Lung-Cancer Antibody Cluster-12 Reacts With Human Folate Receptors Present On Adenocarcinoma. *International Journal Of Cancer*: 89-95

Frost RL, Cejka J, Weier ML, Martens W. 2006. Molecular structure of the uranyl silicates - a Raman spectroscopic study. *Journal of Raman Spectroscopy* 37: 538-51

Fubini B. 1997. Surface reactivity in the pathogenic response to particulates. *Environmental Health Perspectives* 105: 1013-20

Gao XH, Cui YY, Levenson RM, Chung LWK, Nie SM. 2004. In vivo cancer targeting and imaging with semiconductor quantum dots. *Nature Biotechnology* 22: 969-76

Gao XH, Nie SM. 2003. Molecular profiling of single cells and tissue specimens with quantum dots. *Trends in Biotechnology* 21: 371-3

Gao XH, Yang LL, Petros JA, Marshal FF, Simons JW, Nie SM. 2005. In vivo molecular and cellular imaging with quantum dots. *Current Opinion in Biotechnology* 16: 63-72

Geoghegan WD, Ackerman GA. 1976. Electron-Microscopic Study Of Concanavalin-A (Con A) And Wheat-Germ Agglutinin (Wga) Binding On Mouse Peritoneal Cells Using Colloidal Gold As An Indirect Marker. *Journal Of The Reticuloendothelial Society* 20: A1-A

Geoghegan WD, Scillian JJ, Ackerman GA. 1978. Detection Of Human Lymphocytes-B By Both Light And Electron-Microscopy Utilizing Colloidal Gold Labeled Anti-Immunoglobulin. *Immunological Communications* 7: 1-12

Godt J, Scheidig F, Grosse-Siestrup C, Esche V, Brandenburg P, *et al.*. 2006. The toxicity of cadmium and resulting hazards for human health. *J Occup Med Toxicol* 1: 22

Goodsell DS. 2004. *Nanobiotechnology: Lessons from Nature*: Wiley-Liss

Govorov AO, Richardson HH. 2007. Generating heat with metal nanoparticles. *Nano Today* 2: 30-38

Govorov AO, Zhang W, Skeini T, Richardson H, Lee J, Kotov NA. 2006. Gold nanoparticle ensembles as heaters and actuators: melting and collective plasmon resonances. *Nanoscale Research Letters* 1: 84-90

Green M, Howman E. 2005. Semiconductor quantum dots and free radical induced DNA nicking. *Chemical Communications*: 121-3

Grodzinski P, Silver M, Molnar LK. 2006. Nanotechnology for cancer diagnostics: promises and challenges. *Expert Review Of Molecular Diagnostics* 6: 307-18

Grzelczak M, Perez-Juste J, Mulvaney P, Liz-Marzan LM. 2008. Shape control in gold nanoparticle synthesis. *Chemical Society Reviews* 37: 1783-91

Guo JX, Zhang X, Li QN, Li WX. 2007. Biodistribution of functionalized multiwall carbon nanotubes in mice. *Nuclear Medicine and Biology* 34: 579-83

Guo SJ, Wang EK. 2007. Synthesis and electrochemical applications of gold nanoparticles. *Analytica Chimica Acta* 598: 181-92

Hamoir J, Nemmar A, Halloy D, Wirth D, Vincke G, *et al.*. 2003. Effect of polystyrene particles on lung microvascular permeability in isolated perfused rabbit lungs: role of size and surface properties. *Toxicology and Applied Pharmacology* 190: 278-85

Hardman R. 2006. A toxicologic review of quantum dots: Toxicity depends on physicochemical and environmental factors. *Environmental Health Perspectives* 114: 165-72

Harper S, Usenko C, Hutchison JE, Maddux BLS, Tanguay RL. 2008. In vivo biodistribution and toxicity depends on nanomaterial composition, size, surface functionalisation and route of exposure. *Journal Of Experimental Nanoscience* 3: 195-206

Haugland RP. 2003. *Handbook of fluorescent probes and research products*. Eugene, OR

He XX, Duan JH, Wang KM, Tan WH, Lin X, He CM. 2004. A novel fluorescent label based on organic dye-doped silica nanoparticles for HepG liver cancer cell recognition. *Journal of Nanoscience and Nanotechnology* 4: 585-9

He XX, Nie HL, Wang KM, Tan WH, Wu X, Zhang PF. 2008. In Vivo Study of Biodistribution and Urinary Excretion of Surface-Modified Silica Nanoparticles. *Analytical Chemistry* 80: 9597-603

He XX, Wang KM, Tan WH, Li J, Yang XH, *et al.*. 2002. Photostable luminescent nanoparticles as biological label for cell recognition of system lupus erythematosus patients. *Journal of Nanoscience and Nanotechnology* 2: 317-20

Hett A. 2004. *Nanotechnology. Small matter, many unknowns.*, Swiss Reinsurance Company, Zurich

Hiremath SRR, Hota A. 1999. Nanoparticles as drug delivery systems. *Indian Journal of Pharmaceutical Sciences* 61: 69-75

Hirsch LR, Stafford RJ, Bankson JA, Sershen SR, Rivera B, *et al.*. 2003. Nanoshell-mediated near-infrared thermal therapy of tumors under magnetic resonance guidance. *Proceedings of the National Academy of Sciences of the United States of America* 100: 13549-54

Holm BA, Bergey EJ, De T, Rodman DJ, Kapoor R, *et al.*. 2002. Nanotechnology in biomedical applications. *Molecular Crystals and Liquid Crystals* 374: 589-98

Hood JD, Bednarski M, Frausto R, Guccione S, Reisfeld RA, *et al.*. 2002. Tumor regression by targeted gene delivery to the neovasculature. *Science* 296: 2404-7

Hoshino A, Fujioka K, Oku T, Suga M, Sasaki YF, *et al.*. 2004a. Physicochemical properties and cellular toxicity of nanocrystal quantum dots depend on their surface modification. *Nano Letters* 4: 2163-9

Hoshino A, Hanaki K, Suzuki K, Yamamoto K. 2004b. Applications of T-lymphoma labeled with fluorescent quantum dots to cell tracing markers in mouse body. *Biochemical and Biophysical Research Communications* 314: 46-53

Hu M, Wang X, Hartland GV, Salgueirino-Maceira V, Liz-Marzan LM. 2003. Heat dissipation in gold-silica core-shell nanoparticles. *Chemical Physics Letters* 372: 767-72

Huang XH, El-Sayed IH, Qian W, El-Sayed MA. 2006. Cancer cell imaging and photothermal therapy in the near-infrared region by using gold nanorods. *Journal of the American Chemical Society* 128: 2115-20

Huang XL, Zhang B, Ren L, Ye SF, Sun LP, *et al.*. 2008. In vivo toxic studies and biodistribution of near infrared sensitive Au-Au2S nanoparticles as potential drug delivery carriers. *Journal of Materials Science-Materials In Medicine* 19: 2581-8

Huff TB, Hansen MN, Zhao Y, Cheng JX, Wei A. 2007a. Controlling the cellular uptake of gold nanorods. *Langmuir* 23: 1596-9

Huff TB, Tong L, Zhao Y, Hansen MN, Cheng JX, Wei A. 2007b. Hyperthermic effects of gold nanorods on tumor cells. *Nanomedicine* 2: 125-32

Huo Q, Worden JG. 2007. Monofunctional gold nanoparticles: synthesis and applications. *Journal Of Nanoparticle Research* 9: 1013-25

IARC M. 1997. *IARC Monograph on the Evaluation of the Carcinogenic Risk of Chemicals to Humans: Silica, some silicates, coal dust and para-aramid fibrils*. Geneva: IARC Press

Ivanitsky GR, Medvinsky AB, Deev AA, Tsyganov MA. 1998. From Maxwell's Demon to the self-organization of mass transfer processes in living systems. *Uspekhi Fizicheskikh Nauk* 168: 1221-33

Jain TK, Reddy MK, Morales MA, Leslie-Pelecky DL, Labhasetwar V. 2008. Biodistribution, clearance, and biocompatibility of iron oxide magnetic nanoparticles in rats. *Molecular Pharmaceutics* 5: 316-27

Jakobs S, Subramaniam V, Schonle A, Jovin TM, Hell SW. 2000. EGFP and DsRed expressing cultures of Escherichia coli imaged by confocal, two-photon and fluorescence lifetime microscopy. *FEBS Letters* 479: 131-5

Jiang W, Papa E, Fischer H, Mardyani S, Chan WCW. 2004a. Semiconductor quantum dots as contrast agents for whole animal imaging. *Trends in Biotechnology* 22: 607-9

Jiang ZL, Pan HC, Yuan WE. 2004b. Change color effect and spectral properties of gold nanoparticle-cationic surfactants system. *Chemical Research In Chinese Universities* 20: 523-8

Juang JY, Bogy DB. 2005. Nanotechnology advances and applications in information storage. *Microsystem Technologies-Micro-And Nanosystems-Information Storage And Processing Systems* 11: 950-7

Karakoti AS, Hench LL, Seal S. 2006. The potential toxicity of nanomaterials - The role of surfaces. *Jom* 58: 77-82

Khan MK, Nigavekar SS, Minc LD, Kariapper MST, Nair BM, *et al.*. 2005. In vivo biodistribution of dendrimers and dendrimer nanocomposites - Implications for cancer imaging and therapy. *Technology In Cancer Research & Treatment* 4: 603-13

Kim DK, Jo YS, Dobson J, Haj AE, Muhammed M. 2006. *Nanomaterials for the controlled release of anti-cancer agent: Nanomaterials for Cancer Therapy*: Wiley-VCH

Kirchner C, Liedl T, Kudera S, Pellegrino T, Javier AM, *et al.*. 2005. Cytotoxicity of colloidal CdSe and CdSe/ZnS nanoparticles. *Nano Letters* 5: 331-8

Klostranec JM, Chan WCW. 2006. Quantum dots in biological and biomedical research: Recent progress and present challenges. *Advanced Materials* 18: 1953-64

Kobayashi H, Hama Y, Koyama Y, Choyke PL, Asanuma D, *et al.*. 2008. In vivo real-time monitoring of cancer cell viability using a molecularly targeted pH-activatable fluorescent imaging probe. *Proceedings of the American Association for Cancer Research Annual Meeting* 49: 1077

Köhler M, Fritzsche W. 2007. *Nanotechnology: An Introduction to Nanostructuring Techniques*. Federal Republic of Germany: Wiley-VCH

Langmuir I, Blodgett K. 1935. Regarding some new methods for the investigation of monomolecular layers. *Kolloid-Zeitschrift* 73: 257-63

Leamon CP, Low PS. 1991. Delivery Of Macromolecules Into Living Cells - A Method That Exploits Folate Receptor Endocytosis. *Proceedings Of The National Academy Of Sciences Of The United States Of America* 88: 5572-6

Leatherdale CA, Woo W-K, Mikulec FV, Bawendi MG. On the absorption cross section of CdSe nanocrystal quantum dots. *Journal of Physical Chemistry B* 106: 7619-22

Lee HA, Imran M, Monteiro-Riviere NA, Colvin VL, Yu WW, Rivlere JE. 2007. Biodistribution of quantum dot nanoparticles in perfused skin: Evidence of coating dependency and periodicity in arterial extraction. *Nano Letters* 7: 2865-70

Levine EM, Robbins EB. 1970. Differential Temperature Sensitivity Of Normal And Cancer Cells In Culture. *Journal Of Cellular Physiology* 76: 373-&

Levy L, Sahoo Y, Kim KS, Bergey EJ, Prasad PN. 2002. Nanochemistry: Synthesis and characterization of multifunctional nanoclinics for biological applications. *Chemistry of Materials* 14: 3715-21

Lewen N, Mathew S, Schenkenberger M, Raglione T. 2004. A rapid ICP MS screen for heavy metals in pharmaceutical compounds. *Journal of Pharmaceutical and Biomedical Analysis* 35: 739

Li SD, Huang L. 2008. Pharmacokinetics and biodistribution of nanoparticles. *Molecular Pharmaceutics* 5: 496-504

Licha K, Olbrich C. 2005. Optical imaging in drug discovery and diagnostic applications. *Advanced Drug Delivery Reviews* 57: 1087-108

Licha K, Riefke B, Ebert B, Grotzinger C. 2002. Cyanine dyes as contrast agents in biomedical optical imaging. *Academic Radiology* 9: S320-S2

Limbach LK, Li YC, Grass RN, Brunner TJ, Hintermann MA, *et al.*. 2005. Oxide nanoparticle uptake in human lung fibroblasts: Effects of particle size, agglomeration, and diffusion at low concentrations. *Environmental Science & Technology* 39: 9370-6

Liu MX, Li HF, Luo G, Liu QF, Wang YM. 2008. Pharmacokinetics and biodistribution of surface modification polymeric nanoparticles. *Archives of Pharmacal Research* 31: 547-54

Liu P, Zhang A, Xu Y, Xu LX. 2005. Study of non-uniform nanoparticle liposome extravasation in tumour. *International Journal of Hyperthermia* 21: 259-70

Loo C, Hirsch L, Lee MH, Chang E, West J, *et al.*. 2005a. Gold nanoshell bioconjugates for molecular imaging in living cells. *Optics Letters* 30: 1012-4

Loo C, Lin A, Hirsch L, Lee MH, Barton J, *et al.*. 2004. Nanoshell-enabled photonics-based imaging and therapy of cancer. *Technology in Cancer Research & Treatment* 3: 33-40

Loo C, Lowery A, Halas N, West J, Drezek R. 2005b. Immunotargeted nanoshells for integrated cancer imaging and therapy. *Nano Letters* 5: 709-11

Lovern SB, Owen HA, Klaper R. 2008. Electron microscopy of gold nanoparticle intake in the gut of Daphnia magna. *Nanotoxicology* 2: 43-8

Lovric J, Bazzi HS, Cuie Y, Fortin GRA, Winnik FM, Maysinger D. 2005a. Differences in subcellular distribution and toxicity of green and red emitting CdTe quantum dots. *Journal of Molecular Medicine-Jmm* 83: 377-85

Lovric J, Cho SJ, Winnik FM, Maysinger D. 2005b. Unmodified cadmium telluride quantum dots induce reactive oxygen species formation leading to multiple organelle damage and cell death. *Chemistry & Biology* 12: 1227-34

Lundqvist M, Stigler J, Elia G, Lynch I, Cedervall T, Dawson KA. 2008. Nanoparticle size and surface properties determine the protein corona with possible implications for biological impacts. *Proceedings of the National Academy of Sciences of the United States of America* 105: 14265-70

Lynch I, Cedervall T, Lundqvist M, Cabaleiro-Lago C, Linse S, Dawson KA. 2007. The nanoparticle - protein complex as a biological entity; a complex fluids and surface science challenge for the 21st century. *Advances in Colloid and Interface Science* 134-35: 167-74

Lynch I, Dawson KA. 2008. Protein-nanoparticle interactions. *Nano Today* 3: 40-7

Magrez A, Kasas S, Salicio V, Pasquier N, Seo JW, *et al.*. 2006. Cellular toxicity of carbon-based nanomaterials. *Nano Letters* 6: 1121-5

Mann S, Shenton W, Li M, Connolly S, Fitzmaurice D. 2000. Biologically programmed nanoparticle assembly. *Advanced Materials* 12: 147-50

Maye MM, Zheng WX, Leibowitz FL, Ly NK, Zhong CJ. 2000. Heating-induced evolution of thiolate-encapsulated gold nanoparticles: A strategy for size and shape manipulations. *Langmuir* 16: 490-7

Maysinger D, Lovric J, Eisenberg A, Savic R. 2007. Fate of micelles and quantum dots in cells. *European Journal of Pharmaceutics and Biopharmaceutics* 65: 270-81

Medintz IL, Uyeda HT, Goldman ER, Mattoussi H. 2005. Quantum dot bioconjugates for imaging, labelling and sensing. *Nature Materials* 4: 435-46

Michalet X, Pinaud FF, Bentolila LA, Tsay JM, Doose S, *et al.*. 2005. Quantum dots for live cells, in vivo imaging, and diagnostics. *Science* 307: 538-44

Moghimi SM. 2006. The effect of methoxy-PEG chain length and molecular architecture on lymph node targeting of immuno-PEG liposomes. *Biomaterials* 27: 136-44

Moghimi SM, Hunter AC. 2001. Capture of stealth nanoparticles by the body's defences. *Critical Reviews in Therapeutic Drug Carrier Systems* 18: 527-50

Moghimi SM, Szebeni J. 2003. Stealth liposomes and long circulating nanoparticles: critical issues in pharmacokinetics, opsonization and protein-binding properties. *Progress in Lipid Research* 42: 463-78

Mrksich M. 2000. A surface chemistry approach to studying cell adhesion. *Chemical Society Reviews* 29: 267-73

Muller RH, Wallis KH, Troster SD, Kreuter J. 1992. Invitro Characterization Of Poly (Methyl-Methacrylate) Nanoparticles And Correlation To Their Invivo Fate. *Journal Of Controlled Release* 20: 237-46

Murray CB, Norris DJ, Bawendi MG. 1993. Synthesis and Characterization of Nearly Monodisperse Cde (E = S, Se, Te) Semiconductor Nanocrystallites. *Journal of the American Chemical Society* 115: 8706-15

Nardin C, Thoeni S, Widmer J, Winterhalter M, Meier W. 2000. Nanoreactors based on (polymerized) ABA-triblock copolymer vesicles. *Chemical Communications*: 1433-4

Nayak S, Lyon LA. 2005. Soft nanotechnology with soft nanoparticles. *Angewandte Chemie-International Edition* 44: 7686-708

Nel A, Xia T, Madler L, Li N. 2006. Toxic potential of materials at the nanolevel. *Science* 311: 622-7

Niidome T, Yamagata M, Okamoto Y, Akiyama Y, Takahashi H, *et al.*. 2006. PEG-modified gold nanorods with a stealth character for in vivo applications. *Journal of Controlled Release* 114: 343-7

Norman ME, Williams P, Illum L. 1992. Human Serum-Albumin as a Probe for Surface Conditioning (Opsonization) of Block Copolymer-Coated Microspheres. *Biomaterials* 13: 841-9

O'Neal DP, Hirsch LR, Halas NJ, Payne JD, West JL. 2004. Photo-thermal tumor ablation in mice using near infrared-absorbing nanoparticles. *Cancer Letters* 209: 171-6

Oberdorster G. 1993. Lung Dosimetry - Pulmonary Clearance of Inhaled Particles. *Aerosol Science and Technology* 18: 279-89

Oberdorster G. 2000. Toxicology of ultrafine particles: in vivo studies. *Philosophical Transactions of the Royal Society of London Series a-Mathematical Physical and Engineering Sciences* 358: 2719-39

Oberdorster G, Ferin J, Finkelstein G, Wade P, Corson N. 1990. Increased Pulmonary Toxicity of Ultrafine Particles.2. Lung Lavage Studies. *Journal of Aerosol Science* 21: 384-7

Oberdorster G, Ferin J, Gelein R, Soderholm SC, Finkelstein J. 1992. Role of the Alveolar Macrophage in Lung Injury - Studies with Ultrafine Particles. *Environmental Health Perspectives* 97: 193-9

Oberdorster G, Ferin J, Lehnert BE. 1994. Correlation between Particle-Size, in-Vivo Particle Persistence, and Lung Injury. *Environmental Health Perspectives* 102: 173-9

Oberdorster G, Finkelstein J, Ferin J, Godleski J, Chang LY, *et al.*. 1996. Ultrafine particles as a potential environmental health hazard. Studies with model particles. *Chest* 109: 68S-9S

Oberdorster G, Gelein RM, Ferin J, Weiss B. 1995. Association of Particulate Air-Pollution and Acute Mortality - Involvement of Ultrafine Particles. *Inhalation Toxicology* 7: 111-24

Oberdorster G, Maynard A, Donaldson K, Castranova V, Fitzpatrick J, *et al.*. 2005a. Principles for characterizing the potential human health effects from exposure to nanomaterials: elements of a screening strategy. *Part Fibre Toxicol* 2: 8

Oberdorster G, Oberdorster E, Oberdorster J. 2005b. Nanotoxicology: An emerging discipline evolving from studies of ultrafine particles. *Environmental Health Perspectives* 113: 823-39

Oberdorster G, Oberdorster E, Oberdorster J. 2005c. Nanotoxicology: an emerging discipline evolving from studies of ultrafine particles. *Environ Health Perspect* 113: 823-39

Owens DE, Peppas NA. 2006. Opsonization, biodistribution, and pharmacokinetics of polymeric nanoparticles. *International Journal of Pharmaceutics* 307: 93-102

Pan XQ, Lee RJ, Ratnam M. 2004. Penetration into solid tumor tissue of fluorescent latex microspheres: A mimic of liposome particles. *Anticancer Research* 24: 3005-8

Pellegrino T, Kudera S, Liedl T, Javier AM, Manna L, Parak WJ. 2005. On the development of colloidal nanoparticles towards multifunctional structures and their possible use for biological applications. *Small* 1: 48-63

Pepperkok R, Squire A, Geley S, Bastiaens PI. 1999. Simultaneous detection of multiple green fluorescent proteins in live cells by fluorescence lifetime imaging microscopy. *Current Biology: CB* 9: 269-72

Perez-Juste J, Pastoriza-Santos I, Liz-Marzan LM, Mulvaney P. 2005. Gold nanorods: Synthesis, characterization and applications. *Coordination Chemistry Reviews* 249: 1870-901

Peters K, Unger RE, Kirkpatrick CJ, Gatti AM, Monari E. 2004. Effects of nano-scaled particles on endothelial cell function in vitro: Studies on viability, proliferation and inflammation. *Journal Of Materials Science-Materials In Medicine* 15: 321-5

Pissuwan D, Cortie CH, Valenzuela SM, Cortie MB. 2007a. Gold nanosphere-antibody conjugates for hyperthermal therapeutic applications. *Gold Bulletin* 40: 121-9

Pissuwan D, Valenzuela SM, Cortie MB. 2006. Therapeutic possibilities of plasmonically heated gold nanoparticles. *Trends in Biotechnology* 24: 62-7

Pissuwan D, Valenzuela SM, Killingsworth MC, Xu XD, Cortie MB. 2007b. Targeted destruction of murine macrophage cells with bioconjugated gold nanorods. *Journal of Nanoparticle Research* 9: 1109-24

Pissuwan D, Valenzuela SM, Miller CM, Cortie MB. 2007c. A golden bullet? Selective targeting of toxoplasma gondii tachyzoites using anti body-functionalized gold nanorods. *Nano Letters* 7: 3808-12

Pitsillides CM, Joe EK, Wei XB, Anderson RR, Lin CP. 2003. Selective cell targeting with light-absorbing microparticles and nanoparticles. *Biophysical Journal* 84: 4023-32

Poland CA, Duffin R, Kinloch I, Maynard A, Wallace WAH, *et al.*. 2008. Carbon nanotubes introduced into the abdominal cavity of mice show asbestos-like pathogenicity in a pilot study. *Nature Nanotechnology* 3: 423-8

Powers M. 2006. Nanomedicine and nano device pipeline surges 68%. In *Nanomedicine, Device and Diagnostics Report; NanoBiotech News*, pp. 1 -69

Qhobosheane M, Santra S, Zhang P, Tan WH. 2001. Biochemically functionalized silica nanoparticles. *Analyst* 126: 1274-8

Qu L, Peng X. 2002. Control of photoluminescence properties of CdSe nanocrystals in growth. *Journal of the American Chemical Society* 124: 2049-55

Renovanz HD. 1984. Amorphous Silica - Pathogenicity And Toxicity. *Staub Reinhaltung Der Luft* 44: 217-20

Renwick LC, Brown D, Clouter A, Donaldson K. 2004. Increased inflammation and altered macrophage chemotactic responses caused by two ultrafine particle types. *Occupational and Environmental Medicine* 61: 442-7

Renwick LC, Donaldson K, Clouter A. 2001. Impairment of alveolar macrophage phagocytosis by ultrafine particles. *Toxicology and Applied Pharmacology* 172: 119-27

Rhyner MN, Smith AM, Gao XH, Mao H, Yang LL, Nie SM. 2006. Quantum dots and multifunctional nanoparticles: new contrast agents for tumor imaging. *Nanomedicine* 1: 209-17

Richardson HH, Hickman ZN, Govorov AO, Thomas AC, Zhang W, Kordesch ME. 2006. Thermooptical properties of gold nanoparticles embedded in ice: Characterization of heat generation and melting. *Nano Letters* 6: 783-8

Richardson HH, Thomas AC, Carlson MT, Kordesch ME, Govorov AO. 2007. Thermo-optical responses of nanoparticles: Melting of ice and nanocalorimetry approach. *Journal of Electronic Materials* 36: 1587-93

Romig AD. 2004. Nanotechnology: Scientific challenges and societal benefits and risks. *Metallurgical And Materials Transactions A-Physical Metallurgy And Materials Science* 35A: 3641-8

Roser M, Fischer D, Kissel T. 1998. Surface-modified biodegradable albumin nano- and microspheres. II: effect of surface charges on in vitro phagocytosis and biodistribution in rats. *European Journal Of Pharmaceutics And Biopharmaceutics* 46: 255-63

Rosi NL, Mirkin CA. 2005. Nanostructures in biodiagnostics. *Chemical Reviews* 105: 1547-62

Ross JF, Chaudhuri PK, Ratnam M. 1994. Differential Regulation Of Folate Receptor Isoforms In Normal And Malignant-Tissues In-Vivo And In Established Cell-Lines - Physiological And Clinical Implications. *Cancer* 73: 2432-43

Ryman-Rasmussen JP, Riviere JE, Monteiro-Riviere NA. 2006. Penetration of intact skin by quantum dots with diverse physicochemical properties. *Toxicological Sciences* 91: 159-65

Safarik I, Safarikova M. 2002. Magnetic nanoparticles and biosciences. *Monatshefte Fur Chemie* 133: 737-59

Sahoo SK, Labhasetwar V. 2003. Nanotech approaches to delivery and imaging drug. *Drug Discovery Today* 8: 1112-20

Salata OV. 2005. Tools of nanotechnology: Electrospray. *Current Nanoscience* 1: 25-33

Santra S, Bagwe RP, Dutta D, Stanley JT, Walter GA, *et al.*. 2005a. Synthesis and characterization of fluorescent, radio-opaque, and paramagnetic silica nanoparticles for multimodal bioimaging applications. *Advanced Materials* 17: 2165-9

Santra S, Dutta D. 2007. Nanoparticles for Optical Imaging of Cancer. In *Nanotechnologies for the Life Sciences*, ed. C Kumar: Wiley-VCH Verlag GmbH & Co.

Santra S, Dutta D, Walter GA, Moudgil BM. 2005b. Fluorescent nanoparticle probes for cancer imaging. *Technology in Cancer Research & Treatment* 4: 593-602

Santra S, Liesenfeld B, Bertolino C, Dutta D, Cao ZH, *et al.*. 2006. Fluorescence lifetime measurements to determine the core-shell nanostructure of FITC-doped silica nanoparticles: An optical approach to evaluate nanoparticle photostability. *Journal of Luminescence* 117: 75-82

Santra S, Liesenfeld B, Dutta D, Chatel D, Batich CD, *et al.*. 2005c. Folate conjugated fluorescent silica nanoparticles for labeling neoplastic cells. *Journal of Nanoscience and Nanotechnology* 5: 899-904

Santra S, Wang KM, Tapec R, Tan WH. 2001a. Development of novel dye-doped silica nanoparticles for biomarker application. *Journal of Biomedical Optics* 6: 160-6

Santra S, Xu JS, Wang KM, Tan WH. 2004a. Luminescent nanoparticle probes for bioimaging. *Journal of Nanoscience and Nanotechnology* 4: 590-9

Santra S, Yang H, Dutta D, Stanley JT, Holloway PH, *et al.*. 2004b. TAT conjugated, FITC doped silica nanoparticles for bioimaging applications. *Chemical Communications*: 2810-1

Santra S, Yang H, Stanley JT, Holloway PH, Moudgil BM, *et al.*. 2005d. Rapid and effective labeling of brain tissue using TAT-conjugated CdS: Mn/ZnS quantum dots. *Chemical Communications*: 3144-6

Santra S, Yang HS, Holloway PH, Stanley JT, Mericle RA. 2005e. Synthesis of water-dispersible fluorescent, radio-opaque, and paramagnetic CdS: Mn/ZnS quantum dots: A multifunctional probe for bioimaging. *Journal of the American Chemical Society* 127: 1656-7

Santra S, Zhang P, Wang KM, Tapec R, Tan WH. 2001b. Conjugation of biomolecules with luminophore-doped silica nanoparticles for photostable biomarkers. *Analytical Chemistry* 73: 4988-93

Sau TK, Pal A, Jana NR, Wang ZL, Pal T. 2001. Size controlled synthesis of gold nanoparticles using photochemically prepared seed particles. *Journal of Nanoparticle Research* 3: 257-61

Schellenberger EA, Reynolds F, Weissleder R, Josephson L. 2004. Surface-functionalized nanoparticle library yields probes for apoptotic cells. *Chembiochem* 5: 275-9

Schins RPF, Duffin R, Hohr D, Knaapen AM, Shi TM, *et al.*. 2002. Surface modification of quartz inhibits toxicity, particle uptake, and oxidative DNA damage in human lung epithelial cells. *Chemical Research in Toxicology* 15: 1166-73

Schubert D, Dargusch R, Raitano J, Chan SW. 2006. Cerium and yttrium oxide nanoparticles are neuroprotective. *Biochemical and Biophysical Research Communications* 342: 86-91

Semmler-Behnke M, Kreyling WG, Lipka J, Fertsch S, Wenk A, *et al.*. 2008. Biodistribution of 1.4-and 18-nm Gold Particles in Rats. *Small* 4: 2108-11

Sharma P, Brown SC, Walter G, Santra S, Scott E, *et al.*. 2007. Gd nanoparticulates: from magnetic resonance imaging to neutron capture therapy. *Advanced Powder Technology* 18: 663-98

Shiohara A, Hoshino A, Hanaki K, Suzuki K, Yamamoto K. 2004. On the cyto-toxicity caused by quantum dots. *Microbiology and Immunology* 48: 669-75

Shvedova AA, Castranova V, Kisin ER, Schwegler-Berry D, Murray AR, *et al.*. 2003a. Exposure to carbon nanotube material: Assessment of nanotube cytotoxicity using human keratinocyte cells. *Journal of Toxicology and Environmental Health-Part A* 66: 1909-26

Shvedova AA, Kisin ER, Murray AR, Kommineni C, Gunther MR, *et al.*. 2003b. Inflammatory response and free radical formation in skin of B63CF1 mice with diminished levels of glutathione after phenol exposure. *Toxicological Sciences* 72: 378-

Silva GA. 2004. Introduction to nanotechnology and its applications to medicine. *Surgical Neurology* 61: 216-20

Smith AM, Duan HW, Rhyner MN, Ruan G, Nie SM. 2006. A systematic examination of surface coatings on the optical and chemical properties of semiconductor quantum dots. *Physical Chemistry Chemical Physics* 8: 3895-903

Smith PW. 2002. Fluorescence emission-based detection and diagnosis of malignancy. *Journal of Cellular Biochemistry*: 54-9

Sokolov K, Aaron J, Hsu B, Nida D, Gillenwater A, *et al.*. 2003a. Optical systems for In vivo molecular imaging of cancer. *Technology in Cancer Research & Treatment* 2: 491-504

Sokolov K, Follen M, Aaron J, Pavlova I, Malpica A, *et al.*. 2003b. Real-time vital optical imaging of precancer using anti-epidermal growth factor receptor antibodies conjugated to gold nanoparticles. *Cancer Research* 63: 1999-2004

Sonavane G, Tomoda K, Makino K. 2008. Biodistribution of colloidal gold nanoparticles after intravenous administration: Effect of particle size. *Colloids And Surfaces B-Biointerfaces* 66: 274-80

Sonvico F, Dubernet C, Colombo P, Couvreur P. 2005. Metallic colloid nanotechnology, applications in diagnosis and therapeutics. *Current Pharmaceutical Design* 11: 2091-105

Stober W, Fink A, Bohn E. 1968. Controlled Growth of Monodisperse Silica Spheres in Micron Size Range. *Journal of Colloid and Interface Science* 26: 62-&

Stone V, Tuinman M, Vamvakopoulos JE, Shaw J, Brown D, *et al.*. 2000. Increased calcium influx in a monocytic cell line on exposure to ultrafine carbon black. *European Respiratory Journal* 15: 297-303

Stroh M, Zimmer JP, Duda DG, Levchenko TS, Cohen KS, *et al.*. 2005. Quantum dots spectrally distinguish multiple species within the tumor milieu in vivo. *Nature Medicine* 11: 678-82

Stsiapura V, Sukhanova A, Artemyev M, Pluot M, Cohen JHM, *et al*.. 2004. Functionalized nanocrystal-tagged fluorescent polymer beads: synthesis, physicochemical characterization, and immunolabeling application. *Analytical Biochemistry* 334: 257-65

Tan WH, Fang XH, Li J, Liu XJ. 2000. Molecular beacons: A novel DNA probe for nucleic acid and protein studies. *Chemistry-a European Journal* 6: 1107-11

Taniguchi N. 1974. "On the Basic Concept of 'NanoTechnology'". *Proceedings of International Commission on Physics Education*

Tanojo H, Junginger HE, Bodde HE. 1997. Influence of pH on the intensity and stability of the fluorescence of p-aminobenzoic acid in aqueous solutions. *European Journal of Pharmaceutical Sciences* 5: 31-5

Tarnuzzer RW, Colon J, Patil S, Seal S. 2005. Vacancy engineered ceria nanostructures for protection from radiation-induced cellular damage. *Nano Letters* 5: 2573-7

Teeguarden J. 2008. Protocol Review Form Institutional Animal Care and Use Committee. ed. Battelle. Richland, WA

Teeguarden JG, Hinderliter PM, Orr G, Thrall BD, Pounds JG. 2007. Particokinetics in vitro: Dosimetry considerations for in vitro nanoparticle toxicity assessments. *Toxicological Sciences* 95: 300-12

Tomazic-Jezic VJ, Merritt K, Umbreit TH. 2001. Significance of the type and the size of biomaterial particles on phagocytosis and tissue distribution. *Journal of Biomedical Materials Research* 55: 523-9

Tong L, Zhao Y, Huff TB, Hansen MN, Wei A, Cheng JX. 2007. Gold nanorods mediate tumor cell death by compromising membrane integrity. *Advanced Materials* 19: 3136-+

Tran CL, Buchanan D, Cullen RT, Searl A, Jones AD, Donaldson K. 2000a. Inhalation of poorly soluble particles. II. Influence of particle surface area on inflammation and clearance. *Inhalation Toxicology* 12: 1113-26

Tran CL, Buchanan D, Miller BG, Jones AD, Donaldson K. 2000b. Mathematical modeling to predict the responses to poorly soluble particles in rat lungs. *Inhalation Toxicology* 12: 403-9

Wang HF, Wang J, Deng XY, Sun HF, Shi ZJ, *et al.*. 2004. Biodistribution of carbon single-wall carbon nanotubes in mice. *Journal of Nanoscience and Nanotechnology* 4: 1019-24

Wang S, Low PS. 1998. Folate-mediated targeting of antineoplastic drags, imaging agents, and nucleic acids to cancer cells. *Journal of Controlled Release* 53: 39-48

Wang X, Yang LL, Chen Z, Shin DM. 2008. Application of nanotechnology in cancer therapy and imaging. *Ca-a Cancer Journal for Clinicians* 58: 97-110

Wang Z, Levy R, Fernig DG, Brust M. 2005. The peptide route to multifunctional gold nanoparticles. *Bioconjugate Chemistry* 16: 497-500

Warheit DB, Webb TR, Reed KL, Sayes CM, Colvin VL. 2005. Impact of titania and ouartz nanoparticulate exposures on respiratory health: Role of particle size. *Abstracts of Papers of the American Chemical Society* 229: U911-U

Wasdo SC, Barber DS, Denslow ND, Powers KW, Palazuelos M, *et al.*. 2008. Differential binding of serum proteins to nanoparticles. *International Journal of Nanotechnology* 5: 92-115

Weissleder R. 2002. Scaling down imaging: Molecular mapping of cancer in mice. *Nature Reviews Cancer* 2: 11-8

Weissleder R, Tung CH, Mahmood U, Bogdanov A. 1999. In vivo imaging of tumors with protease-activated near-infrared fluorescent probes. *Nature Biotechnology* 17: 375-8

Wilcox D, Dove B, McDavid D, Greer d. 1995. UTHSCSA.

Wu XY, Liu HJ, Liu JQ, Haley KN, Treadway JA, *et al.*. 2003. Immunofluorescent labeling of cancer marker Her2 and other cellular targets with semiconductor quantum dots. *Nature Biotechnology* 21: 41-6

Xia T, Kovochich M, Brant J, Hotze M, Sempf J, *et al.*. 2006. Comparison of the abilities of ambient and manufactured nanoparticles to induce cellular toxicity according to an oxidative stress paradigm. *Nano Letters* 6: 1794-807

Xia T, Kovochich M, Nel AE. 2007. Impairment of mitochondrial function by particulate matter (PM) and their toxic components: implications for PM-induced cardiovascular and lung disease. *Frontiers in Bioscience* 12: 1238-46

Yamamoto N. 2004. Cellular dynamics visualized in live cells in vitro and in vivo by differential dual-color nuclear-cytoplasmic fluorescent-protein expression. *Cancer Res.* 64: 4251

Yang H, Holloway PH. 2004. Efficient and photostable ZnS-Passivated CdS: Mn luminescent nanocrystals. *Advanced Functional Materials* 14: 152-6

Yang HS, Holloway PH, Cunningham G, Schanze KS. 2004a. CdS: Mn nanocrystals passivated by ZnS: Synthesis and luminescent properties. *Journal of Chemical Physics* 121: 10233-40

Yang HS, Holloway PH, Santra S. 2004b. Water-soluble silica-overcoated CdS: Mn/ZnS semiconductor quantum dots. *Journal of Chemical Physics* 121: 7421-6

Yang ST, Guo W, Lin Y, Deng XY, Wang HF, *et al.*. 2007. Biodistribution of pristine single-walled carbon nanotubes in vivo. *Journal of Physical Chemistry C* 111: 17761-4

Yin H, Too HP, Chow GM. 2005. The effects of particle size and surface coating on the cytotoxicity of nickel ferrite. *Biomaterials* 26: 5818-26

Zhang W, Qiao X, Chen J. 2007. Synthesis of silver nanoparticles - Effects of concerned parameters in water/oil microemulsion. *Materials Science And Engineering B-Solid State Materials For Advanced Technology* 142: 1-15

Zhao ZJ, Wakita T, Yasui K. 2003a. Inoculation of plasmids encoding Japanese encephalitis virus PrM-E proteins with colloidal gold elicits a protective immune response in BALB/c mice. *Journal Of Virology* 77: 4248-60

Zhao ZJ, Wakita T, Yasui K. 2003b. Inoculation of plasmids encoding Japanese encephalitis virus PrM-E proteins with colloidal gold elicits a protective immune response in BALB/c mice (vol 77, pg 4248, 2003). *Journal Of Virology* 77: 9107-

Zhu DH, Lennon SP, Peters MH, Finney WC, Singh M. 2006. Brownian diffusion and surface kinetics of liposome and viral particle uptake by human lung cancer cells in-vitro. *Annals Of Biomedical Engineering* 34: 1573-86

Zsigmondy R. 1916. Some remarkable reactions of colloidal gold. *Zeitschrift Fur Elektrochemie Und Angewandte Physikalische Chemie* 22: 102-4

BIOGRAPHICAL SKETCH

Debamitra Dutta was born and brought up in Calcutta, India. She completed her Bachelor of Engineering in Metallurgical Engineering from Bengal Engineering College, Shibpore, India in 1998 and worked as a Product Development Engineer and Export Coordinator in the R&D Division at Indian Aluminum Company Limited, Belur, India for two years. Subsequently, in 2001, she came to the United States to pursue higher education and received her Master of Science degree in Materials Engineering at Washington State University in 2003. She joined the Particle Engineering Research Center at the University of Florida as a Research Scholar in 2004 to work on projects related to the use of multi-functional nanoparticles for biological imaging. In January 2005, she joined the PhD program at the University of Florida in the Department of Materials Science and Engineering and conducted her research to develop nanoparticles for bioimaging and to study their biological responses in vitro and in vivo for her dissertation. While obtaining her PhD, she spent 4 months during the summer of 2006 and 8 months in 2007 – 2008 as a Visiting Scientist at the Pacific Northwest National Laboratory (PNNL), Richland, WA working with scientists in the Fundamental and Computational Sciences Directorate (FCSD) at the laboratory. She obtained her PhD in May 2009 and joined Intel Corporation as a R&D Engineer at Portland.